THE AERODYNAMIC PERFORMANCE OF THE 24 INCH HOUCK CONFIGURATION

THESIS

Michael M. Walker, First Lieutenant, USAF

AFIT/GAE/ENY/07-M30

DEPARTMENT OF THE AIR FORCE
AIR UNIVERSITY

AIR FORCE INSTITUTE OF TECHNOLOGY

Wright-Patterson Air Force Base, Ohio

The views expressed in this thesis are those of the author and do not reflect the official policy or position of the United States Air Force, Department of Defense, or the U.S. Government.

AFIT/GAE/ENY/07-M30

THE AERODYNAMIC PERFORMANCE OF THE 24 INCH HOUCK CONFIGURATION

THESIS

Presented to the Faculty

Department of Aeronautical and Astronautical Engineering

Graduate School of Engineering and Management

Air Force Institute of Technology

Air University

Air Education and Training Command

In Partial Fulfillment of the Requirements for the

Degree of Master of Science in Aeronautical Engineering

Michael M. Walker, B.S.

First Lieutenant, USAF

March 2007

AFIT/GAE/ENY/07-M30

THE AERODYNAMIC PERFORMANCE OF THE 24 INCH HOUCK CONFIGURATION

Michael M. Walker, B.S.

First Lieutenant, USAF

Approved:

_____	_____
Dr. Mark F. Reeder (Thesis Advisor)	Date
_____	_____
Raymond C. Maple, Lt Col, USAF (Member)	Date
_____	_____
Dr. Robert A. Canfield (Member)	Date

Abstract

Fuel efficiency of aircraft is of great importance to the military and private sector. A more efficient wing design for UAVs would lead to improvements in mission support while reducing fuel costs for the Air Force. An experimental investigation of one candidate design, the Houck Aircraft Configuration, has been conducted in the AFIT low speed wind tunnel. This aircraft shares similarities to other joined-wing aircraft, but includes curved flow-guides of varying spanwise camber connecting the upper and lower wingtips. Experimental results show that the addition of flow guides on the 24" Houck Configuration results in a 2.5% reduction in L/D_{max} at Re ≈ 80K and a 0.3% reduction in L/D_{max} at Re ≈ 125K. This trend shows a decrease in the performance gap as the Reynolds number increases from 80K to 125K. It is recommended that additional testing at higher Reynolds numbers be performed to determine if an increase in performance can be shown. The designed flow guides proved to be successful in combining the upper and lower wing-tip vortices into a single vortex. The flow guides alter what would be two smaller compact vortices and instead produce a slightly larger, spread out vortex which follows the curve of the flow guide. Ultimately, evidence of improvements in aerodynamic efficiency will need to be shown before other claims of the design are demonstrated to be fully successful.

Acknowledgments

I would like to express my sincere appreciation to my faculty advisor, Dr. Mark Reeder, for his direction, help, and support throughout the course of this thesis effort. The knowledge and experience is definitely appreciated. I would like to thank my sponsors, Captain Elaine Bryant and Cale Zeune, from the Air Force Research Laboratory, Air Vehicles Directorate for both the support and latitude provided to me in this endeavor. Thanks to Dwight Gehring for his expertise and coordination during the wind tunnel tests. I would also like to thank John Hixenbaugh, Jay Anderson, Dermot Killian, Tim Fry, John Staiger, Aaron Altman, Servane Altman, Charlie Tyler, Chris Gillum, Ron Houck, Colonel Raymond Maple, and Dr. Robert Canfield for their help along the way. Finally, a special thanks to my friends and family for their support and prayers throughout this process.

Michael M. Walker

Table of Contents

Page

Page

List of Figures

Page

Page

Page

Page

Page

List of Tables

Page

Page

List of Symbols

A	axial load force	(lb_f)
AR	aspect ratio	(-)
α	angle of attack	(º)
b	wing span	(in)
β	sideslip angle	(º)
$\bar{c}$	average chord of upper and lower wings	(in^2)
C_D	total drag coefficient	(-)
C_{Di}	induced drag coefficient	(-)
C_{Do}	minimum coefficient of drag	(-)
C_L	lift coefficient	(-)
C_{Lmax}	maximum coefficient of lift	(-)
C_l	roll moment coefficient	(-)
$C_{l\beta}$	lateral static stability	(/ º)
$C_{l\psi}$	effective dihedral	(/ º)
C_m	pitch moment coefficient	(-)
C_n	yaw moment coefficient	(-)
$C_{n\beta}$	directional static stability	(/ º)
$C_{n\psi}$	directional stability	(/ º)
C_Y	coefficient of side force	(-)
$C_{Y\beta}$	sideslip stability derivative	(-)

D_{form}	form drag	(lbs)
$D_{induced}$	induced drag	(lbs)
$D_{interference}$	interference drag	(lbs)
$D_{parasite}$	parasite drag	(lbs)
$D_{skin\ friction}$	skin friction drag	(lbs)
D_{total}	total drag	(lbs)
δ	aileron deflection angle	(°)
δ_b	blockage correction factor	(-)
e	span efficiency factor	(-)
$e\,AR$	effective aspect ratio	(-)
k	ratio of span to tunnel height	(-)
Ke	normalized turbulent kinetic energy	(-)
L/D	lift-to-drag ratio	(-)
L/D_{max}	maximum lift-to-drag ratio	(-)
λ	wind tunnel aspect ratio	(-)
N	normal load force	(lb_f)
P_{baro}	barometric pressure in test room	(psi)
q	dynamic pressure	(in Hg)
ρ	air density	($slug/ft^3$)
Re	Reynolds number	(-)
S	planform area of wing	(in^2)
T_{room}	temperature in test room	(ºF)

u	u-component of velocity in wind axis	(mph, m/s)
u_{rms}	root mean squared of u measurements	(mph, m/s)
v	v-component of velocity in wind axis	(mph, m/s)
v_{rms}	root mean squared of v measurements	(mph, m/s)
V	average wind tunnel velocity	(mph, m/s)
w	w-component of velocity in wind axis	(mph, m/s)
w_{rms}	root mean squared of w measurements	(mph, m/s)
W	aircraft weight	(lbs)
x	x-component of velocity in hot-wire axis	(mph, m/s)
X_{cg}	x location of center of gravity from aircraft nose	(in)
X_{cmb}	x distance from balance moment center to ¼ chord	(in)
y	y-component of velocity in hot-wire axis	(mph, m/s)
ψ	yaw angle	(°)
z	z-component of velocity in hot-wire axis	(mph, m/s)
Z_{cmb}	z distance from balance moment center to ¼ chord	(in)
ω_x	curl or vorticity about x axis	(rad/s)

THE AERODYNAMIC PERFORMANCE OF THE 24 INCH HOUCK CONFIGURATION

I. Introduction

1.1 Background

The Air Force Research Lab has been tasked with testing a novel aircraft wing design, the Houck Lifting Foil (see Figure 1). The Houck Lifting Foil was designed with the purpose of increasing the aerodynamic efficiency of a joined-wing type aircraft. A description of the lifting foil, found in the presently granted United States Patent of the design, follows:

> A lifting foil for an aircraft, a hydrofoil or the like having a pair of courses or wings. Vortex losses due to span-wise fluid flow are substantially reduced by joining the tips of the courses with flow guides configured for jointly terminating the undesired flows. Termination is effected by providing the flow guides with cross-sections cambered for reducing the dynamic pressure of fluid flowing in a span-wise direction across flow guide surfaces (12).

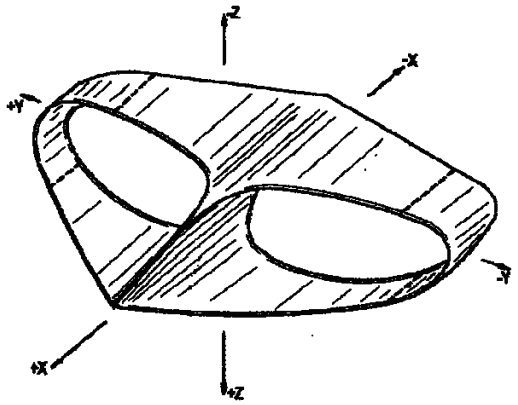

Figure 1: Perspective View of Houck Lifting Foil (reproduced from Reference 12)

The upper and lower wings of the Houck Lifting Foil are connected by specially designed, curved and cambered flow guides (see Figure 2). The curved flow guides were

created to direct the airflow along a desired path. The cambered airfoil sections are placed strategically to try to manipulate the pressure distribution along the surface of the flow guides.

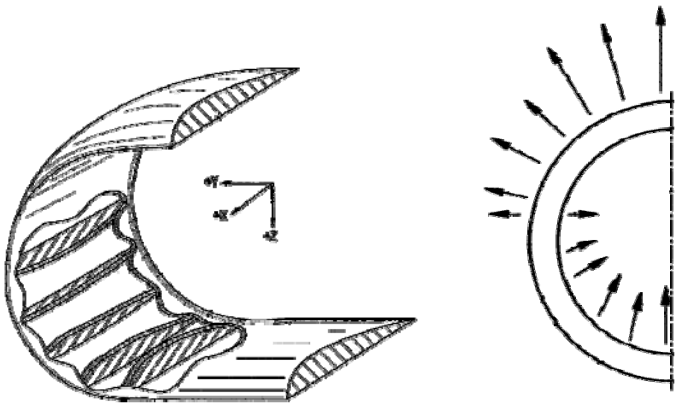

Figure 2: Flow Guides – Varying Camber & Pressure Distribution (reproduced from Reference 12)

The curved design of the flow guides connects the lower and upper wings with the intent of combining the individual wing-tip vortices (of the upper and lower wing) to form a weaker, more spread out vortex (see Figure 3).

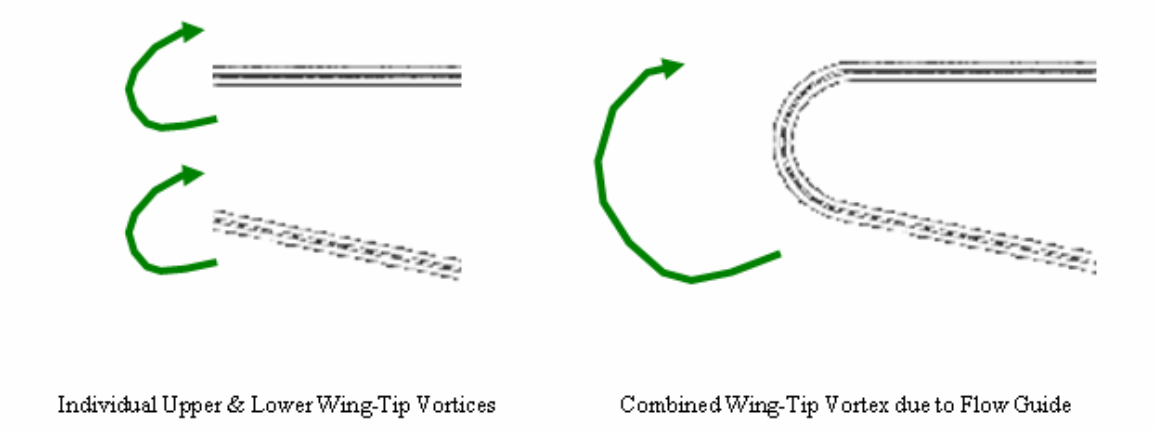

Figure 3: Flow Guide Combining Wing-Tip Vortices

The flow guides are also crafted with varying degrees and orientation of camber in order to try to further manipulate the flow near the wing tips. The cambered airfoil sections that form the flow guides are placed specifically so that the aerodynamic force created by the layout opposes the aerodynamic forces created by the wing-tip vortices (see Figure 4).

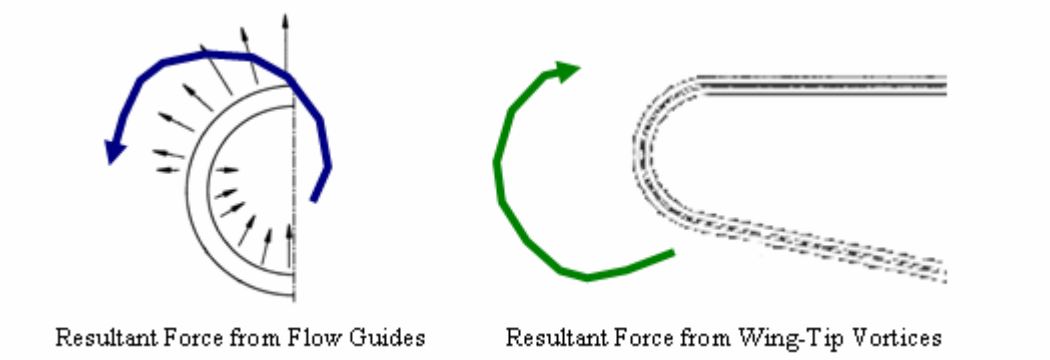

Figure 4: Flow Guide Force Opposing Wing-Tip Vortices

The designer of the Houck Lifting Foil claims increased efficiency through the reduction of span-wise fluid flow over the wings (12). The reduction of wing-tip vortices would result in lower induced drag (drag due to lift). If the decrease in induced drag is greater than the increase in parasite drag (profile drag, skin friction drag, and interference drag) then the total drag will be reduced. If successful, the design could be used for numerous applications where efficiency is valued: fixed wing aircraft, rotary wing aircraft, submarines and hydrofoils (12).

1.2 Research Focus

The purpose of this report is to provide insight into the aerodynamic performance of a specific 24" Houck Configuration, provided by the inventor's company, Iron Hawk

Enterprises LLC. One of the initial steps in the study was to scan in the model built by Iron Hawk for use in setting up a CFD (computational fluid dynamics) mesh. Figure 5 shows an initial computational representation of the 24" Houck Configuration. It is important to note that there is a V-shaped irregularity in the computational side view of the aircraft. This view is used often in the report, but the irregularity does not exist on the actual model and should be ignored.

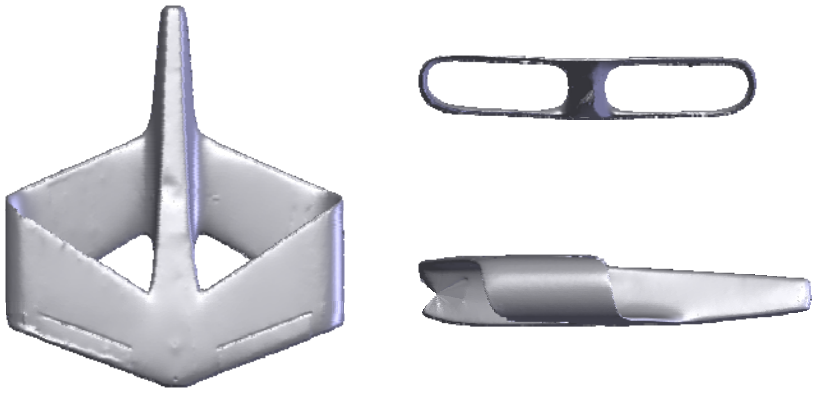

Figure 5: Three-View Representation of 24" Houck Configuration

The model was crafted by Ronald G. Houck II, the holder of U.S. Patent # 7,110,867. The model was then altered (internally only) at AFIT so that it could be fitted on a balance in the low speed wind tunnel. Modifications reduced the overall structural strength of the model because portions of the internal structure had to be hollowed out. In order to achieve aerodynamic analysis of the aircraft, numerous tests were completed in the AFIT low-speed wind tunnel. The results of this report will be used in conjunction with other studies carried out by the Air Force Research Lab, Air Vehicles Directorate, Wright Patterson AFB, Ohio to determine the viability of the Houck Lifting Foil for the United States Air Force (4).

II. Literature Review

2.1 Overview

Numerous past studies have been devoted to devices which are designed to improve aircraft aerodynamics. Studies to improve efficiency have been conducted on both biplanes and joined-wing aircraft. Among the factors which can affect aircraft performance are airfoil camber and the formation of wing-tip vortices. The distribution of the vortex sheet affects the total drag seen by the aircraft, which directly relates to the lift-to-drag efficiency ratio.

2.2 Camber

The chord line of an airfoil is created by drawing a straight line between the leading edge and the trailing edge. The camber line is created by drawing a line from the leading edge to the trailing edge of an airfoil while keeping an equal distance between the top and bottom of the airfoil. Figure 6 shows how camber can affect the lift produced by an airfoil.

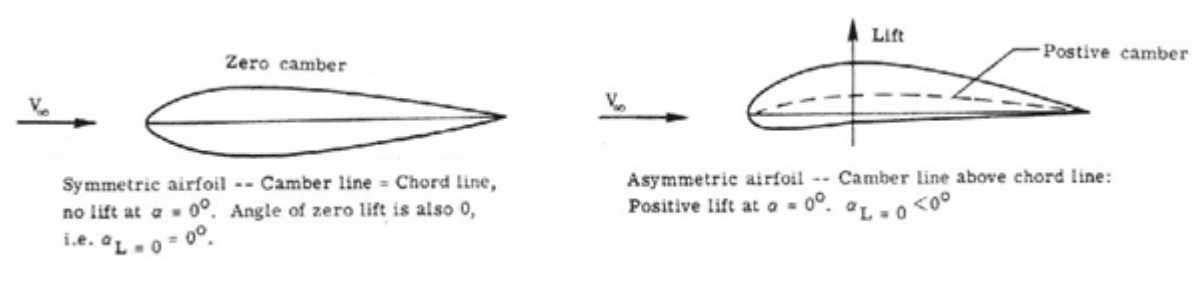

Figure 6: How Camber Works (reproduced from Reference 27)

An airfoil with zero camber creates zero lift at an angle of attack of zero. When positive camber is introduced, positive lift is created at an angle of attack of zero.

2.3 Drag

Drag is the force acting on an aircraft parallel to the free stream velocity. It can be broken up into five major categories: form (pressure) drag, skin friction drag, interference drag, wave drag, and induced drag. Form drag is caused primarily by the turbulent wake behind the aircraft due to pressure differences. Streamlining an aircraft typically helps in the reduction of form drag. Skin friction drag is a result of the interaction between particles of air and the aircraft's surface due to boundary layer growth. A smooth, polished surface often helps in the reduction of skin friction drag. Interference drag is due to interactions between different parts of the aircraft, such as the wing and a fuel tank. Fairing and filleting attachment points can help to smooth the mixing of flow and reduce this type of drag. Wave drag is a form of pressure drag that only comes into consideration in supersonic flight and is not a factor in this low-speed study. The final type of drag that contributes to total aircraft drag is induced drag. Induced drag, also known as drag due to lift, is created primarily by the wing-tip vortices that form as an aircraft creates lift. Also included in induced drag is the incremental change in pressure drag due to lift (change in angle of attack) (27). A breakdown of drag in equation form follows:

$$D_{total} = D_{parasite} + D_{induced} \tag{1}$$

$$D_{parasite} = D_{form} + D_{skin\ friction} + D_{interference} \tag{2}$$

where D_{total} (lbs) is total drag, $D_{parasite}$ (lbs) is parasite drag, $D_{induced}$ (lbs) is induced drag, D_{form} (lbs) is form drag, $D_{skin\ friction}$ (lbs) is skin friction drag, and $D_{interference}$ (lbs) is interference drag.

For a given aircraft weight in steady, level unaccelerated flight, the drag vs. velocity curve helps to determine the most efficient speeds for maximizing range and endurance for a propeller-driven aircraft (see Figure 7).

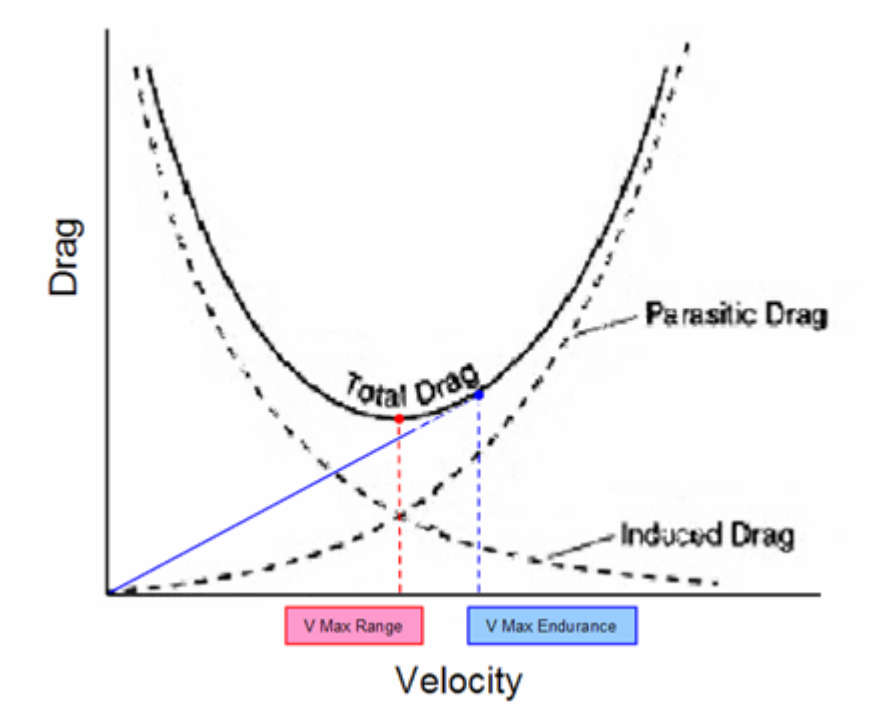

Figure 7: Drag vs. Velocity at a Given Weight for Level Flight (reproduced from Reference 31)

The velocity that will allow the aircraft to maximize its range is the velocity where the total drag is minimized. At this velocity, the lift-to-drag ratio, L/D, is maximized and the induced drag is equal to the parasite drag (31). The velocity for maximum endurance is found by finding the values of drag, *D*, and velocity, *V*, that minimize the ratio of *D*/*V*.

This can be done by drawing a line tangent to the curve through the origin. At this velocity, the ratio of $C_L^{3/2} / C_D$ is maximized and the induced drag is equal to three times the parasite drag (31):

$$C_{D_o} = C_{D_i} \quad \text{at L/D}_{\max} \tag{3}$$

$$3\,C_{D_o} = C_{D_i} \quad \text{at } C_L^{3/2} / C_{D\,\max} \tag{4}$$

where C_{D_o} (-) is the parasite drag coefficient and C_{D_i} (-) is the induced drag coefficient.

2.4 Wing-Tip Vortices

Lift, when created by a wing, results from the net difference in pressure between the upper and lower surface of the wing. If a higher pressure exists below the wing, then positive lift is created. Because aircraft wings are finite in length, the flow over the wings acts in a three-dimensional manner to attempt to reach pressure equilibrium at the tip (see Figure 8).

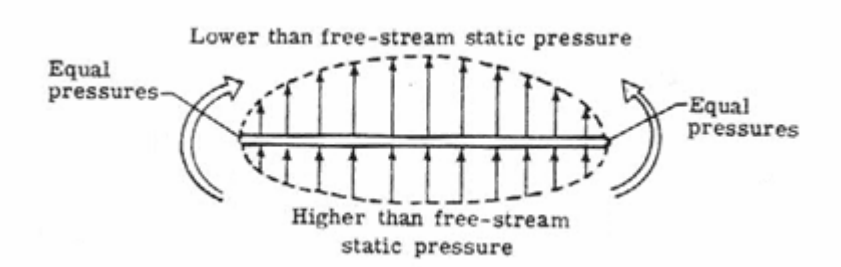

Figure 8: Equalizing Pressure at the Wing Tips (reproduced from Reference 27)

Wing-tip vortices form when high pressure induces a velocity from below a wing, around the wing tip to the lower pressure area above the wing. This movement, combined with the flow of air past the airfoil from the free stream velocity, moves the

circular motion of flow downstream in a spiral pattern. These are called wing tip vortices and can be seen in Figure 9. Vortices are usually located slightly above the wing tip. Velocities are highest at the core of a vortex and can sometimes approach 70% of the free stream velocity (16:304).

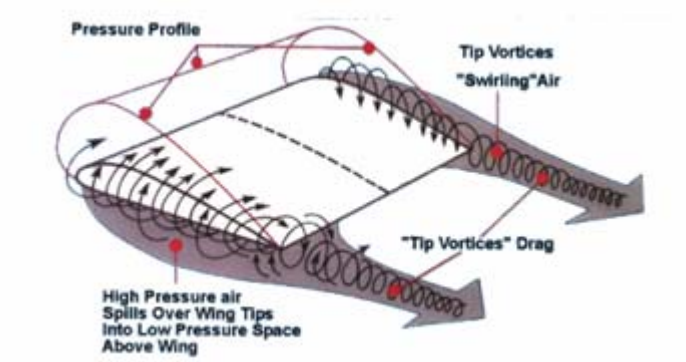

Figure 9: Tip Vortices Spiraling Downstream (reproduced from Reference 27)

The wing-tip vortices cause a downward flow at the trailing edge of the wing. This downward flow, called downwash (see Figure 10), acts strongest near the wing tip while losing strength towards the aircraft body. The downwash has two negative effects on the wing performance. First, it causes the wing to experience a reduced effective angle of attack, therefore reducing the lift. Second, it causes a portion of the lift to act as a drag force. The portion of drag caused by the rotation of the lifting force is referred to as the induced drag, or drag due to lift (2).

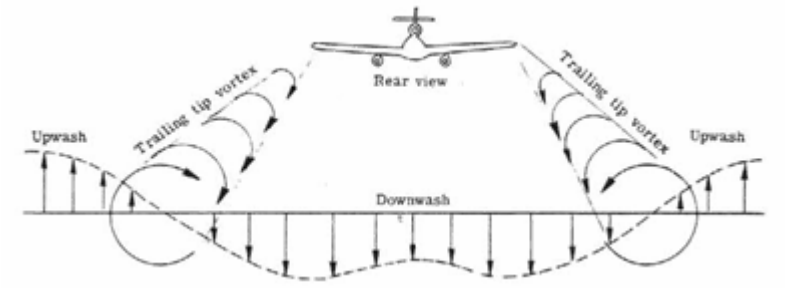

Figure 10: How Downwash is created (reproduced from Reference 27)

Wing-tip vortices "can significantly diminish the aerodynamic performance of a finite wing as opposed to an airfoil" (16:304). For a two-dimensional case (2-D airfoil or wing with infinite span), the induced drag is equal to zero (11:2). However, for a three-dimensional wing or aircraft, induced drag becomes a factor and contributes to the total drag. The induced portion of total drag varies with different flight conditions. Induced drag is more prevalent at slower aircraft speeds. At slow speeds, such as landing or take-off, induced drag can account for up to 75% of the total drag of an aircraft. At higher speeds, such as for cruise, induced drag is generally around 25% of the total aircraft drag (16:304).

2.5 Winglets

"Winglets are aerodynamic components, placed at the tip of a wing to improve its efficiency during cruise" (6). The purpose of the winglet is to spread out the wingtip vortices by introducing a physical constraint to the flow field. Spreading out the wingtip vortices causes a reduction in downwash, and therefore the induced drag (20; 11:1). Properly designed winglets can reduce overall drag, increase lift, provide added stability, increase safety, and improve roll performance.

"Concepts for reducing the strength of the aircraft wing tip vortices have been developed and demonstrated throughout the history of aviation by individuals, companies, and by government agencies including NASA and the Air Force" (16:305). Reducing the induced drag by the addition of wingtips has been researched since the mid 1970's when Dr. Richard Whitcomb at NASA Langley first proposed them (17). They are currently being used on many different aircraft both commercially and militarily. In fact, "data for the Boeing 747-400 indicate that without winglets the aircraft would suffer about 2.5% drag losses, which corresponds to +9.5 tons at take-off" (10).

However, gaining all these advantages with winglets is not a simple task. It is very difficult to properly design a winglet, as there are many design characteristics that have competing influences on the wing. Of all of the advantages that winglets can provide, it is at the cost of an increased cross-sectional and wetted area, both of which cause the profile drag to increase. It is difficult to produce a winglet that decreases the induced drag by more than it increases the profile drag. There are so many variables to consider, that designing an optimized winglet can quickly become complicated (20). Often, a change is made to improve efficiency in one area without consideration of its effects on the other areas of aerodynamics. "An evaluation of effectiveness of various devices for the attenuation of trailing vortices was performed by Kirkman et al. It was found that while many devices show reduction in the maximum swirling velocity in the wake, the effects are typically accompanied by high drag penalties" (16:305). Nonetheless, winglets have, by and large, been accepted as effective fuel-saving aerodynamic devices by both small and large aircraft manufacturers.

2.6 Biplanes

In the early days of aviation, biplanes were commonly used instead of monoplanes because of their advantages given the state of available structural materials. Wings were thin and materials were not as strong or durable as more modern technologies allow. The biplane allows the use of struts and wires to support the upper and lower wing in a box-shaped configuration. The shorter, stronger wings allow for superior maneuverability over monoplanes (important for early fighter aircraft). The dual wing configuration is able to produce more lift than a single wing, but not without added drag from the struts, wires, extra wing surface area, and interference between the upper and lower wing. "In a biplane, the load is not distributed equally between the wings. The presence of one wing will affect the lift characteristics of the other wing" (22:1). Still, for a given wing span, the biplane possesses advantages in aerodynamic efficiency when compared to the monoplane (28:536). For a constrained wing area, however, the monoplane holds the aerodynamic advantage. Other strengths of the biplane design include good load carrying capability, good lift to drag ratio combined with low wing loading, high lift at low speeds, and low-speed maneuverability (1:399).

A biplane, and some of its common terminology, can be seen in Figure 11. Gap, stagger, and angle of decalage are three important parameters when describing a biplane's configuration. The gap is the distance between the upper and lower wings, measured perpendicularly from the chord of the upper wing at the leading edge. The stagger is the distance between the leading edges of the upper and lower wings, measured parallel with the chord of the upper wing. The stagger is positive when the lower wing is

aft of the upper wing (22:2). "The angle of decalage is the acute angle between the chords of the wings of a biplane. The decalage shall be called positive when the lower wing has a smaller angle of attack than the upper wing" (22:2).

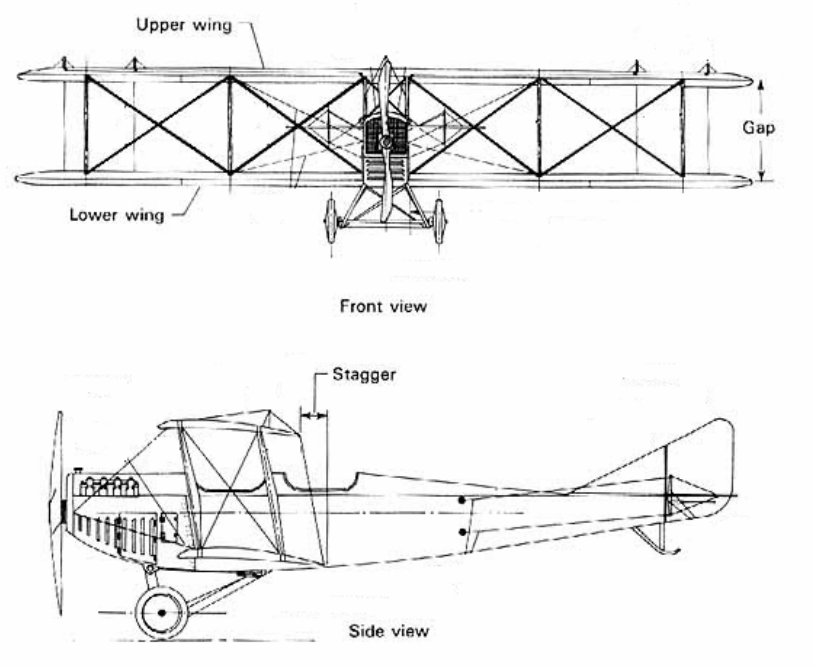

Figure 11: Biplane Terminology (reproduced from Reference 13)

Studies have been done to find optimum configurations for these parameters. Two aerodynamicists, Nenadovitch and Olson, discovered certain combinations of gap, stagger, and decalage for rectangular, untwisted biplane wings that appeared to be optimal values. The optimum values were a gap of 1 chord, a stagger of 0.875 chord, and a decalage angle of -5° (24:6). "Numerical two-dimensional analysis by Rokhsaz confirmed that the combinations determined by Nenadovitch do approach optimum arrangements" (11:2).

Studies have looked into the addition of winglets for the optimized biplane configuration. One 1985 study, a joint effort between NASA Langley Research Center and Pennsylvania State University, used a model consisting of two wings, with NACA 0012 sections, chords of 8" and semi-spans of 20", set up in the optimized configuration. The upper and lower wings were connected to one another at the wing tips by a constant chord NACA 0003 section. A 5% increase in $C_{L\alpha}$ and a 4% increase in C_{Lmax} were gained with the addition of winglets. The advantages of winglets were only seen at values of C_L greater than 0.4. This is because below this value of C_L (at low angles of attack), the decrease in induced drag had not yet overcome the increase in profile drag from the addition of winglets (11:2).

2.7 Joined Wings

For most joined-wing aircraft, the rear wing is attached at its root to the top of the vertical tail or rear of the aircraft. The rear wing then sweeps forward to join the trailing edge of the swept back main wing. "The rear wing is used both for pitch control and as a structural support for the forward wing" (14:897). This wing configuration forms a diamond-like shape in both the top view and front view of the aircraft (30:161). A front view of an example joined-wing can be seen in Figure 12.

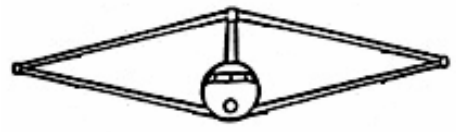

Figure 12: Front View of a Joined-Wing Aircraft (reproduced from Reference 30)

"The main concern of the early biplanes was the large profile drag due to the structural wires that connected the wings. Today, the joined-wing configurations have eliminated the connecting wires" (7:2). As structural strength of materials advanced, monoplanes became more efficient than biplanes. A monoplane's wings could be designed with high aspect ratios, allowing for more efficient flight. But there are still limits to how high the aspect ratios can actually be given the need for maneuverability (with material strength still limiting the design). A joined-wing aircraft allows for the aspect ratio to be increased even more from the monoplane design. Wings on a joined-wing aircraft can be built with smaller chord lengths, thinner airfoils, or longer wingspans because the upper and lower wings are braced to one another, increasing their load bearing capabilities.

Many benefits of optimally loaded joined-wing configurations have been found when compared to other aircraft of the same wingspan. These include the potential of lower structural weight, high stiffness of the wings, good stability and control at both normal flight and stall, suitability for thin airfoils, higher possible aspect ratios, higher efficiency factors, reduced induced drag, reduced wetted area, reduced parasite drag, and reduced total drag (7:2; 14:897-8: 30:161,176).

The chosen design of a joined-wing aircraft depends on its application and goals. Sometimes it may be beneficial to maximize weight savings, minimize induced and parasite drag, or minimize wave drag (thin airfoils for supersonic flight) (30:175). "Joined wings are not always lighter than single wings. Weight will be saved only if the geometric parameters of the joined wing are properly chosen and if the internal wing

structure is optimized" (7:2). When trying to minimize drag (improve efficiency), it is important to consider each flight condition for a given mission. Constraints such as takeoff distance, rate of climb, and landing distance could increase the need for more wing area and offset any possible reduction in drag (14:898).

2.8 Aircraft Efficiency

The lift-to-drag ratio, L/D, is a primary measure of aircraft efficiency. If a propeller driven aircraft is flying at its maximum lift-to-drag ratio, L/D_{max}, then its range is optimized. L/D is usually optimized for given flight conditions (altitude) and desired lift (or aircraft weight for straight and level flight). With this information, a specific combination of velocity and angle of attack will maximize the lift-to-drag ratio. This is the speed and angle of attack that should be flown for the given flight conditions. A history of lift-to-drag ratios for common aircraft can be seen in Table 1. The maximum L/D values range from approximately 8 to 20.

Table 1: Lift-to-Drag Ratios of Historical Aircraft (reproduced from Reference 9)

Type of Aircraft	L/D Ratio
Supersonic Jet Transport (Concorde)	8
Tilt-rotor aircraft	9 to 10
New Supersonic Transport *	15
Oblique Flying Wing *	16 to 17
Subsonic Jet Transport	16 to 18
Bomber B-52	20
* Estimated data	

Subsonic Aircraft	L/D max
Boeing B707-320	19.4
Douglas DC-8	17.9
Airbus A320	17
Boeing 767-200	19
Boeing 747-100	17.7
Douglas DC-10	17.7
Lockeed Tristar	17
Douglas DC-9 (1966)	16.5
Boeing B727-200	16.4
Douglas DC-3 (1935)	14.7
Ford Trimotor (1927)	12
Wright Flyer I (1903)	8.3

A graph showing the historical trend of maximum lift-to-drag ratio for propeller-driven aircraft can be seen in Figure 13. The steep rise in L/D_{max} from 1920 to 1930 is a result of the switch from biplanes to monoplanes (higher aspect ratio) because of the advancement in fabrication materials and the reduction in parasite drag (13). The reduction in parasite drag was due to advancements in aerodynamic design (streamlined design, minimizing interference drag, etc). Not much change took place from 1940 to 1980, but as further advancements in technology have occurred between 1980 and now, the max L/D value has continued to increase ($L/D_{max} \approx 19.4$ for the Boeing 707) (13).

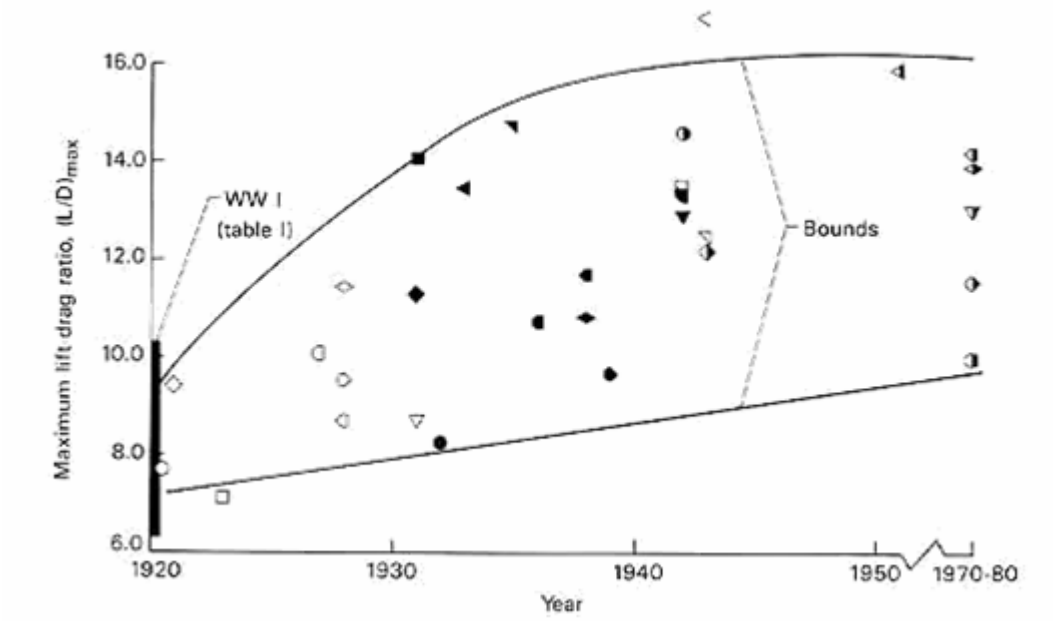

Figure 13: Max Lift-to-Drag Ratio of Propeller-Driven Aircraft (reproduced from Reference 13)

The effective aspect ratio, $e\,AR$, is also used as a measure of efficiency for an aircraft. With information about the lift and induced drag of an aircraft, the effective aspect ratio can be solved for using the equation:

$$C_{D_i} = \frac{C_L^{\,2}}{\pi \cdot e \cdot AR} \qquad (5)$$

where C_{Di} is the induced drag coefficient, C_L is the lift coefficient, e is the span efficiency factor, AR is the aspect ratio, and the combination $e\,AR$ is the effective aspect ratio.

2.9 Hot-Wire Anemometry

A constant temperature anemometer (CTA) is often used to collect fluid velocities. In a CTA, a control algorithm maintains the anemometer wire at a constant temperature. Electric current is supplied to the wire while tracking wire resistance. Air velocity is directly related to the rate of wire heating. The rate at which the heat dissipates off the relatively hot wire, into the surrounding cool air, is dependent on the velocity of the fluid going past the wire. So, as the velocity of the fluid changes, the controller hardware must increase or drop the current supplied to keep the resistance constant. This change in current can be measured and calibrated, so that it can be converted into a fluid velocity (25). Two advantageous reasons for using a CTA are accuracy and high time dependent resolution. The latter reason lends itself to use in collecting and analyzing turbulent flow data (29).

III. Methodology

3.1 Chapter Overview

The 24” Houck Configuration and 3 variations with altered flow guides were tested in the AFIT low-speed wind tunnel using numerous methods for collecting data. The types of data collected in this study include strain-gage balance data, hot-wire anemometry data, and flow visualization using tufts. The methods of reducing data collected by these techniques are covered in this chapter. The results from these tests are also compared with results from other studies. The first study referenced in this report tests the same 24” Houck Configuration using computational fluid dynamics methods (CFD analysis). These tests were performed by AFRL/VA, WPAFB, OH (from 2006 to 2007). The second study referenced for this report was performed by students at the United States Air Force Academy (Fall 2006). The tests done in that study were done on an 18” Houck Configuration and tested in the USAFA Subsonic Wind Tunnel.

3.2 Experimental Equipment

3.2.1 24” Houck Configuration

The model used for this study was the 24” Houck Configuration. It was designed and crafted by Ronald G. Houck II. As part of this research effort, the configuration was scanned using FARO’s Portable Measurement Arm precision measurement instrument. This allowed for a computational replica of the specific 24” Houck Configuration analyzed in this study to be created. The aircraft parameters can be seen in Figure 14. The length of the aircraft is 23.90” and the wingspan is 23.58”. The root chord of the lower (front) wing is 6.10” and starts 7.17” back from the front of the aircraft. The root

chord of the upper (back) wing is 5.02” and starts 19.11” back from the front of the aircraft. The average root chord of the upper and lower wing is 5.56”. The tip chord for both wings is 7.50”. The average chord, $\bar{c}$, is 6.53”. This was found by averaging $\bar{c}_{lower}$ and $\bar{c}_{upper}$. The lower wing has a taper ratio of 1.23 and a leading edge sweep angle of 24º. The upper wing has a taper ratio of 1.49 and a leading edge sweep angle of -31º. If biplane parameters were applied to the 24” Houck Configuration, it would have a gap of $0.5\bar{c}$, a stagger of $1.83\bar{c}$, and a decalage angle of 2º.

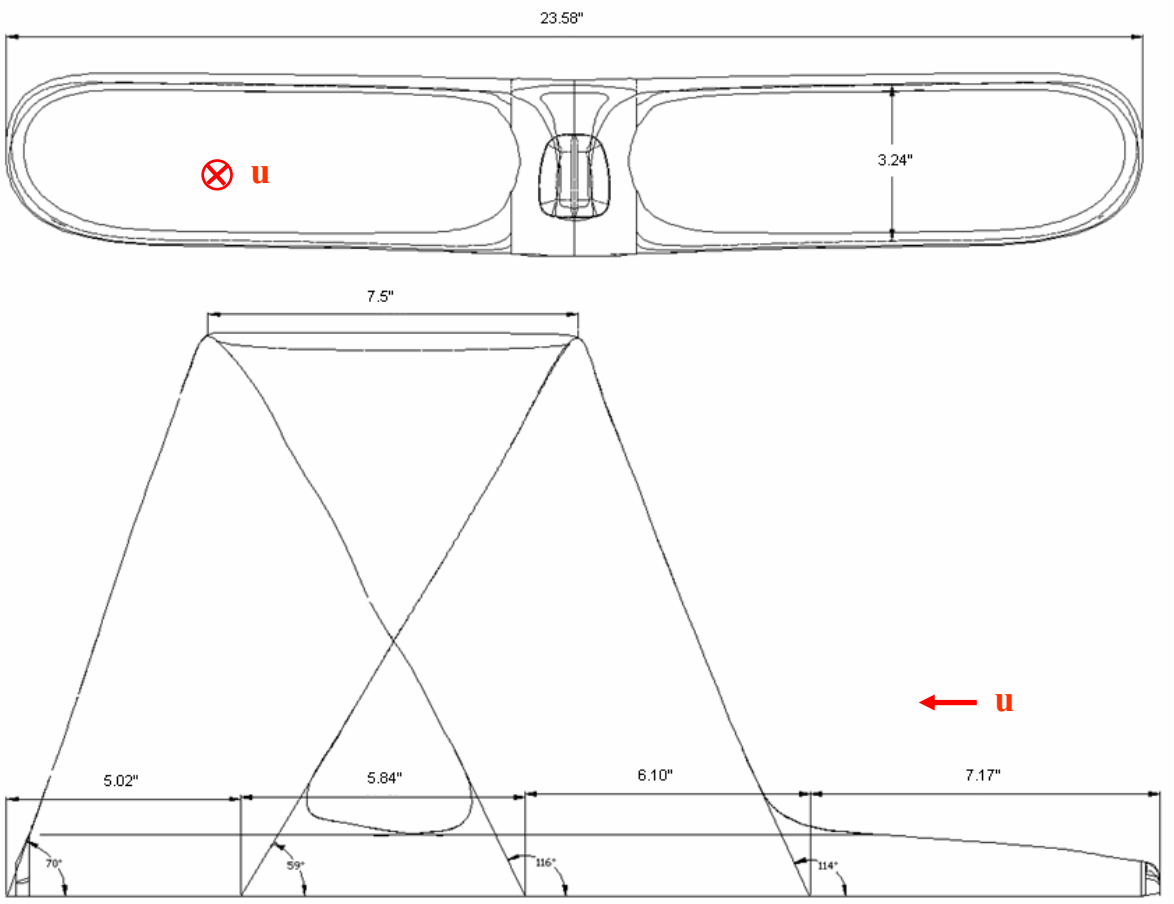

Figure 14: Front and Top View - 24” Houck Configuration with Dimensions

3.2.2 Variations of 24” Houck Configuration

The first stet of variations tested for the 24” Houck Configuration incorporated changes in the aileron deflections. The first variation was the original model with the ailerons deflected 20° down. For the second variation, the ailerons were deflected 20° up. The ailerons are located on the trailing edge of the upper wing and can be seen in the three-view representation of the 24” Houck Configuration in Figure 5. The different aileron variations can be seen in Figure 15.

Figure 15: Different Aileron Variations

Next, different variations in the flow guides were tested. In order to test these variations, the flow guides of the original model needed to be cut using a Dremel tool, equipped with a cutting disc (see Figure 16). The newly formed flow-guide edges were then sanded and taped in order to assure a smooth surface. The creation of the three flow guide variations was performed, chronologically near the end of the investigation.

Figure 16: Tools used to Alter Flow Guides

Three different flow guide variations were created and tested. The first variation was a 1" strip cut out of the center of the flow guide, parallel with the reference angle of attack, $\alpha = 0°$. The 1" cut variation can be seen in Figure 17. The second variation was a 2" strip cut out of the center of the flow guide, parallel with the reference angle of attack. The 2" cut variation can be seen in Figure 18. The third variation with respect to flow guide alterations was a complete removal of the curved flow guides. The variation without flow guides can be seen in Figure 19. This variation was created so that a 24" Houck aircraft without flow guides could be used to compare with the full flow guide configuration (original 24" Houck Configuration). This provides a reference point from which to measure a change in efficiency due to the addition of the patented flow guide design.

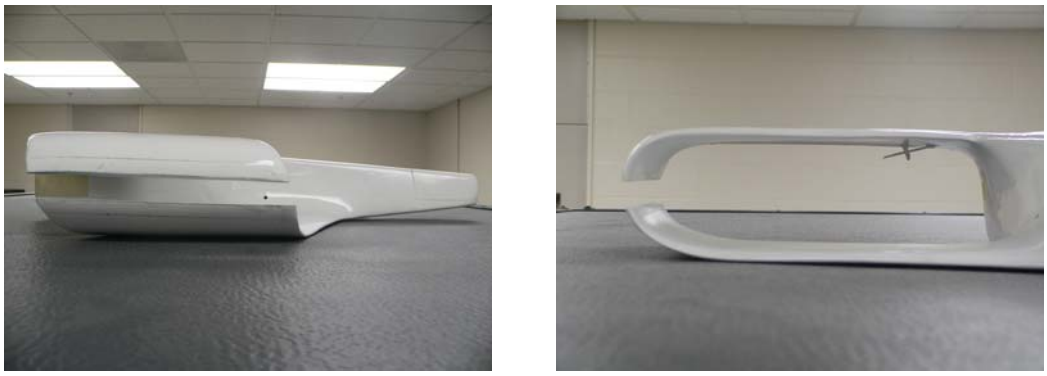

Figure 17: 24” Houck Configuration with 1” Cut in Flow Guide

Figure 18: 24” Houck Configuration with 2” Cut in Flow Guide

Figure 19: 24” Houck Configuration with No Flow Guides

3.2.3 AFIT Low-Speed Wind Tunnel

A low-speed, open-circuit wind tunnel, located at the Air Force Institute of Technology, was utilized for the tests completed in this study. A schematic of the AFIT low-speed wind tunnel can be seen in Figure 20.

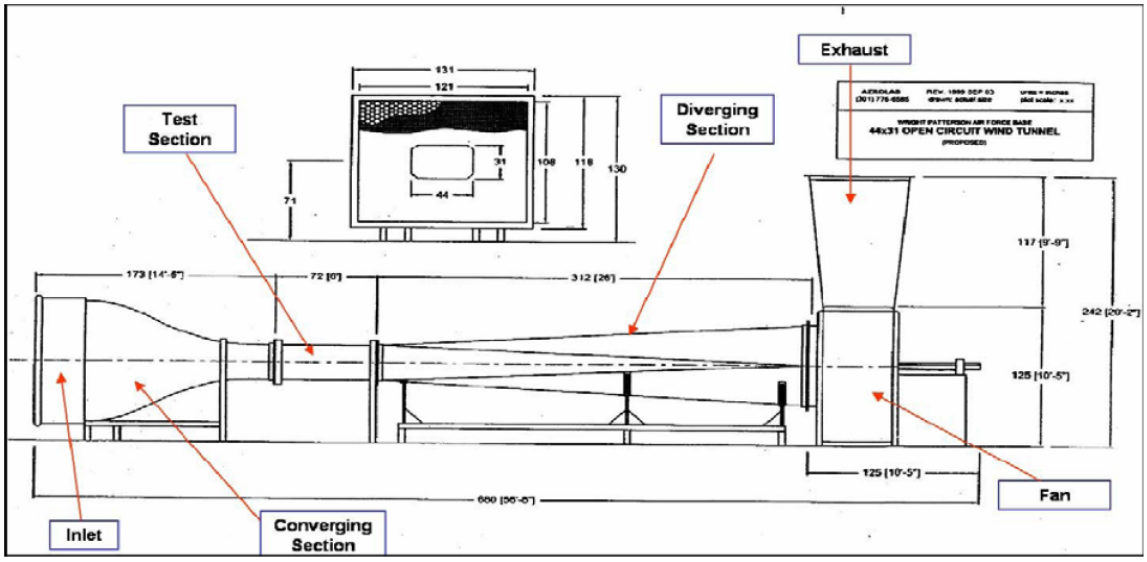

Figure 20: Schematic of Low-Speed Wind Tunnel (reproduced from AFIT LSWT laboratory data)

Initially, the tunnel fan draws ambient air through the intake plenum. Next, the air is guided though an aluminum honeycomb flow-straightener and steel mesh anti-turbulence screens. After the flow passes the last anti-turbulence screen it passes through the convergent portion of the tunnel. The intake and convergent section of the tunnel are shown in Figure 21.

Figure 21: Intake and Convergent Section of Wind Tunnel

The convergent section of the tunnel directs the airflow to the octagon-shaped test section. The test section has a height of 31" and a width of 44". After exiting the test section, the airflow enters a diffuser section and exhausts vertically upward back into the room. The test model is mounted to an internal balance that is attached to a movable sting. The sting is controlled by a movable control table and a pitch control device. Figure 22 shows the wind tunnel test section, sting mechanism, balance, and movable circular table for β measurements.

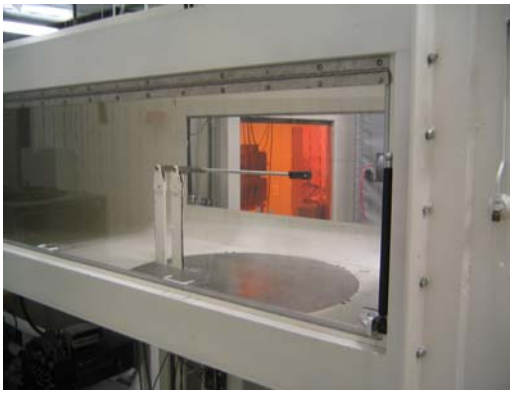

Figure 22: Test Section, Sting Mechanism, and Balance

Once the wind tunnel is set to a desired velocity, measurements can be taken. Angle of attack sweeps can be accomplished by pitching the balance/model using the angle control device (a system of bars and cables) as seen in Figure 23. Sweeps of β, the sideslip angle, can be accomplished by rotating the circular β table (Figure 22).

Figure 23: Angle Control Device

Data acquisition was accomplished using a computerized data acquisition system (see Figure 24) operated by an AFIT lab technician, Dwight Gehring, who has been trained and is proficient in operating the system. All data files for test runs were stored for later data reduction and manipulation. Values collected during each test run were α, β, tunnel speed, unresolved normal force, unresolved axial force, side force, pitch moment, yaw moment, and roll moment. All forces and moments are measured about the balance center.

Figure 24: Data Acquisition Station

Before testing each variation of the 24" Houck Configuration, a tare run was completed for the same alpha sweep that would be tested during the actual test runs. This allows for the weight of the model to be subtracted from the data at all angles of attack. It is also significant to mention that between each change in airspeed, the wind tunnel is brought back to $V = 0$ in order to assure that the balance is still calibrated correctly.

3.2.4 AFIT 10 lb Strain Gage Balance

A 10 lb strain gage balance, manufactured by Modern Machine and Tool Company, was used in the AFIT low-speed wind tunnel to record force measurements on the 24" Houck Configuration. The balance can be seen, set up and ready for use in the wind tunnel, in Figure 25.

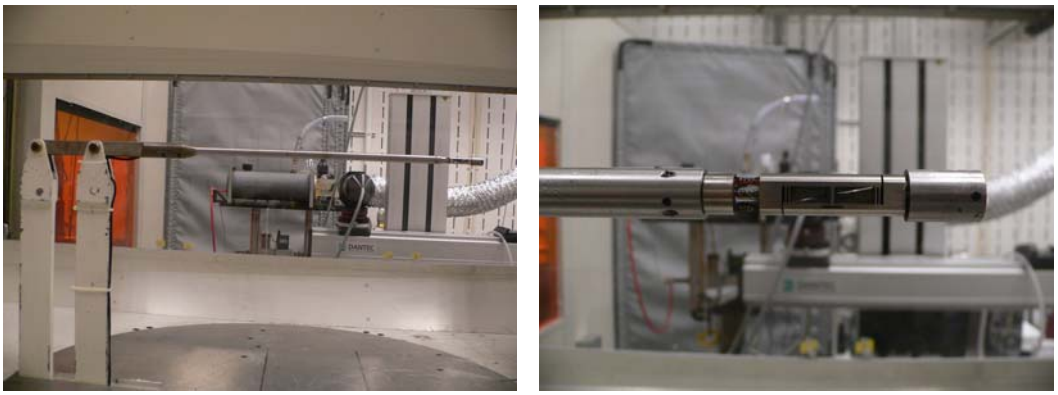

Figure 25: AFIT 10 lb Strain Gage Balance

Initial tests were conducted on the model using a 40 lb balance to test the range of forces acting on the aircraft at different speeds. This was done in order to make sure that the 10 lb balance would not experience forces greater than the allowable range. Forces greater than allowable range of the balance can damage the balance and invalidate calibration. A list of the max allowable forces and moments for the balance can be seen in Table 2.

Table 2: Max Allowable Forces and Moments for 10 lb Balance

Component	Max Load
Normal	10 lbs
Axial	5 lbs
Pitch	10 in-lbs
Roll	4 in-lbs
Yaw	5 in-lbs
Side	5 lbs

The balance's moment center is located 1.3350" aft of the screws where the balance is attached to the model. Other dimensions of the balance can be seen in Appendix A.

3.2.5 Dantec Hot-Wire Anemometer

For the hot-wire analysis in this report, a computer-controlled three-component CTA system was utilized. The specific CTA System used, the Streamline 90N10, is manufactured by Dantec Dynamics. The Dantec hot-wire probe (Figure 26) allows for three-dimensional velocity analysis because of its tri-axis wire configuration. The hot-wire probe is mounted to a computer controlled 3-axis traverse and positioned inside of the wind tunnel. The traverse allows the probe to be accurately positioned and moved along the *x*, *y*, and *z* axes.

Figure 26: Dantec Hot-Wire Anemometer

The Dantec software data acquisition program, when prompted, performs an automatic traverse using a predetermined grid while recording a series of velocity measurements at each step. The area covered by the hot-wire probe (see Figure 28) was a two dimensional grid, in the *y*-*z* plane (150 mm high by 200 mm wide) with x a set distance (0.33”) downstream of the farthest aft point of the aircraft model. The lower right corner of the grid was located 6” from the center line of the model and 1” below the bottom surface of the lower wing. The hot-wire probe starts its path in the lower left corner of the grid and works its way around the grid in the path seen in Figure 27. Measurements were taken at the initial position and then the hot-wire probe moved to its new location. Each movement of the hot-wire probe was at 5 mm increments in the *x* or

y direction (depending on its location within the grid. In all, measurements were taken at 1271 grid points. A total of 1024 velocity measurements per location were recorded by the Dantec software (samples at a rate of 5 KHz) and then transferred to *Microsoft Excel* and *Tecplot* for further manipulation and analysis.

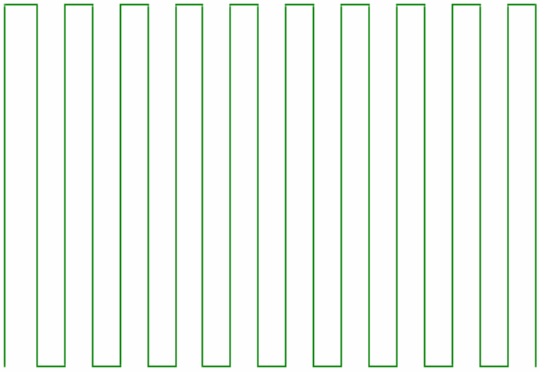

Figure 27: Example Path of Hot-Wire Anemometer

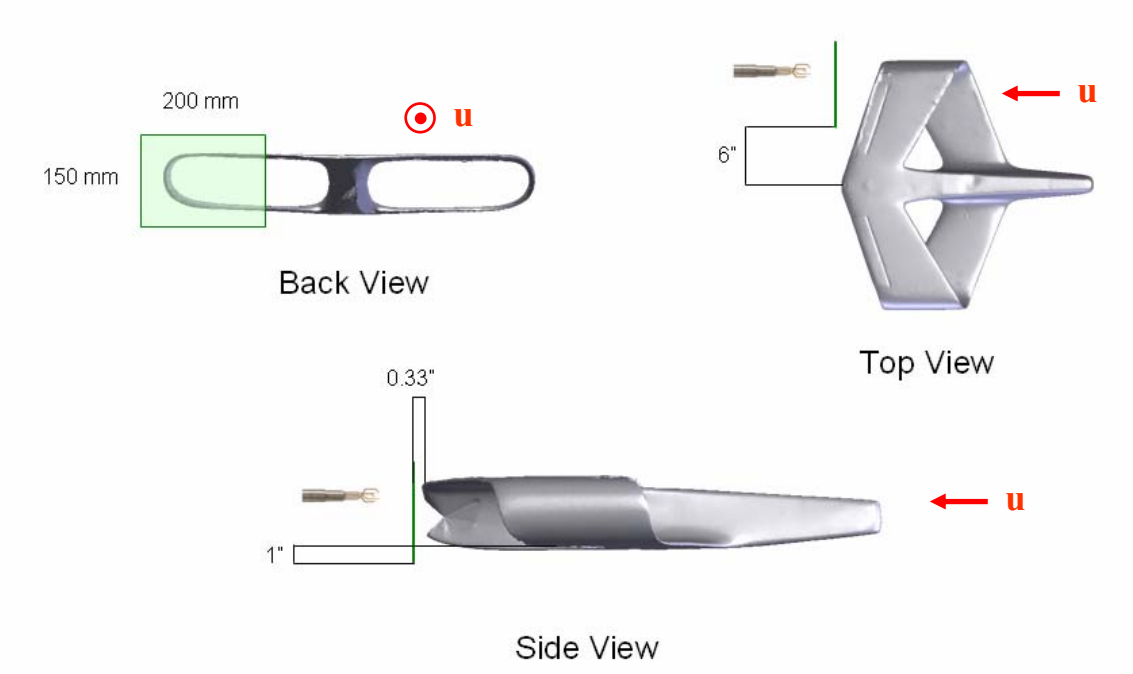

Figure 28: Placement of Hot-Wire Grid with respect to 24" Houck Configuration

3.2.6 Flow Visualization using Tufts

For a portion of testing of the original 24" Houck Configuration, tufts were added to the surface of the wings. The tufts consisted of light weight yarn and were applied to the top and bottom surfaces of the upper and lower wings, including the flow guides. The dark colored (to contrast with the white aircraft body) yarn was cut at a length of 2" and applied to the aircraft using Scotch tape.

Figure 29: Tufts on 24" Houck Configuration for Flow Visualization

The addition of the tufts is used in order to gain a better understanding of the flow around the 24" Houck Configuration. Tufts will often reveal when and where a flow is either steady or unsteady over a wing surface. Regions of separation or buffeting flow can also be determined (3:193-194). Portions of the flow visualization tests were recorded using a digital camera.

3.3 Collecting and Processing the Data

3.3.1 Correction of Balance Data using *MATLAB*

After a wind tunnel test is completed, the data has to be reduced in order to get useable results. This is done using a *MATLAB* m-file to perform a series of operations on the wind tunnel output data. The *MATLAB* code was adapted from previous research accomplished by former AFIT students Rivera Parga and Deluca (26; 8). The *MATLAB* code can be seen in Appendix B. The m-file requires multiple inputs about the model and conditions at the time of testing (e.g., room temperature, barometric pressure) to be modified in the code for accurate results. The weight of the 24" Houck Configuration was measured using a scientific scale and weighed 1.98 lbs (0.898 kg). The temperature and pressure in the room at the time of testing usually varied for each wind tunnel run. These values were recorded at the time of testing and input into the code when needed.

When the aircraft is mounted on the balance, it is not at the reference zero angle of attack. The aircraft angle of attack, AoA, is offset 4.13° from the angle at which the balance is positioned. This means that when the balance is at the 0° position, the aircraft is at 4.13° AoA. For data reduction, calculations were done using the angle of the balance. This is because the force measurements are with respect to the balance position. When discussing the aircraft's position and performance, the offset aircraft reference AoA will be used. The offset angle of attack can be seen in Figure 30. The dashed red line is the aircraft reference line where the AoA is zero. The dashed blue line represents the balance positioned inside of the model. When the balance is level, the aircraft is pitched up at an angle of 4.13°.

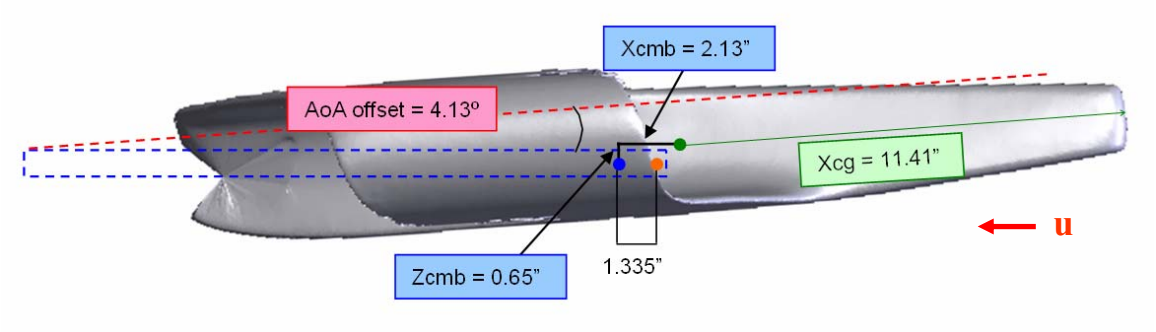

Figure 30: Location of Aircraft Center of Gravity and Balance Moment Center

In order to obtain moment data from the balance, a reference center of gravity for the aircraft must be picked. For the data reduction in this study, the center of gravity was placed at the quarter chord location of the two wings (1/4 of the way back from the leading edge of the front/lower wing to the trailing edge of the rear/upper wing). The resulting center of gravity was 11.41" back from the nose of the aircraft in the x-direction and centered in the y and z directions (in the aircraft body coordinate system) (see Figure 30). The aircraft center of gravity (the green dot) is located 2.13" in front of the balance moment center (the blue dot) and 0.65" above balance moment center (in the wind axis coordinate system). These values were input into the *MATLAB* code for data reduction.

Data reduction via the *MATLAB* code starts by subtracting the tare data from the test data. The resulting voltage measurements are used along with the calibration data to calculate the different forces acting on the balance. A few corrections to the data are performed along the way. The first correction made is to account for blockage of flow in the wind tunnel from the model. This is done by determining a blockage correction factor. This correction accounts for any change in the speed of the flow due to a reduction in the available cross-sectional area near the aircraft model. The delta term

(δ_b), a blockage correction factor, is approximated to be equal for all configurations because their effective spans of 23.58" (for the first three variations) and 20.33" (for the variation without flow guides) make little difference in the estimation of the parameter. The δ term was found to be 0.1177 using the chart found in Barlow, Rae, and Pope (3:387). This was done by first calculating the wind tunnel aspect ratio:

$$\lambda = \frac{height_{tunnel}}{width_{tunnel}} \tag{6}$$

where λ is the wind tunnel aspect ratio, $height_{tunnel}$ (ft) is the height of the wind tunnel cross-section, and $width_{tunnel}$ (ft) is the width of the wind tunnel cross-section. For the AFIT low-speed wind tunnel, $\lambda = 0.705$. The next calculation needed was the ratio of the 24" Houck Configuration wingspan to the width of the wind tunnel:

$$k = \frac{b}{width_{tunnel}} \tag{7}$$

where k (-) is the ratio of span to tunnel height, and b (ft, m) is the wing span of the aircraft model. For these tests, $k = 0.536$. The values of λ and k are then used to find the blockage correction factor, δ_b.

A second correction transfers the normal and axial balance data into the proper frame of reference, with respect to the flow. This is so that the lift and drag data are with respect to the free stream velocity, and not the angle of the balance/aircraft. The calculations of the lift and drag coefficients from the normal and axial force acting on the balance follows:

$$C_L = \frac{N \cdot \cos\alpha - A \cdot \sin\alpha}{\frac{1}{2}\rho \cdot V^2 \cdot S} \tag{8}$$

$$C_D = \frac{N \cdot \sin\alpha + A \cdot \cos\alpha}{\frac{1}{2}\rho \cdot V^2 \cdot S} \tag{9}$$

where C_L (-) is the lift coefficient, C_D (-) is the drag coefficient, N (lbs) is the normal force acting on the balance, A (lbs) is the axial force acting on the balance, α (°) is the angle of attack of the balance, ρ is the air density, V (mph, m/s) is the tunnel velocity, and S (in^2) is the planform area (wing area) of the aircraft model.

3.3.2 Hot-Wire Analysis using Tecplot

The hot-wire probe is placed into the wind tunnel through a slot in the top of the test section. This slot runs in the y-direction, but does not cover the full width of the tunnel. For this reason, the hot-wire probe had to be angled-out 20° in order to cover a grid that reached beyond the wingtip of the 24" Houck Configuration. While this allowed the hot-wire probe to cover a grid behind the wing that was of interest, the data now had to corrected to get it into the wind-axis coordinate system. The equations used for this correction follow:

$$u = x \cdot \cos\theta - y \cdot \sin\theta \tag{10}$$

$$v = x \cdot \sin\theta + y \cdot \cos\theta \tag{11}$$

$$w = z \tag{12}$$

where u (m/s) is the u-component of velocity with respect to the wind axis, v (m/s) is the v-component of velocity with respect to the wind axis, w (m/s) is the w-component of velocity with respect to the wind axis, x (m/s) is the *x*-component of velocity with respect to the hot-wire probe, y (m/s) is the *y*-component of velocity with respect to the hot-wire probe, z (m/s) is the *z*-component of velocity with respect to the hot-wire probe, and θ (°) is the angle rotated about the z axis that the hot-wire probe differs from the *u* direction of flow.

After this correction is made in *Microsoft Excel*, the turbulent kinetic energy normalized by the square of the average freestream velocity is calculated (18):

$$Ke = \frac{1}{2}\frac{{u_{rms}}^2 + {v_{rms}}^2 + {w_{rms}}^2}{V^2} \qquad (13)$$

where *Ke* (-) is the normalized turbulent kinetic energy, u_{rms} (m/s) is the root mean squared of all *u*-component velocity measurements, v_{rms} (m/s) is the root mean squared of all the *v*-component velocity measurements, w_{rms} (m/s) is the root mean squared of all the *w*-component velocity measurements, and *V* (m/s) is the average tunnel velocity. By plotting the results from this calculation, the turbulent areas of flow behind the wing will be visible.

Next, the data was imported into *Tecplot*. A vorticity calculation was done in order to visualize the location and strength of flow circulation within the grid behind the aircrafts wing. Only the x-component of curl was needed because the grid is contained in the *y*-*z* plane. The vorticity (curl) equation follows:

$$\omega_x = curl_x V = \frac{\partial w}{\partial y} - \frac{\partial v}{\partial z} \tag{14}$$

where ω_x (1/s) is the *x*-component of vorticity, *w* (m/s) is the *w*-component of velocity, *v* (m/s) is the *v*-component of velocity, *y* (mm) is the *y*-direction with respect to the hot-wire grid, and *z* (mm) is the *z*-direction with respect to the hot-wire grid. From here, three different contour plots can be created: a *u*-component velocity contour, a non-dimensional turbulence contour, and a vorticity contour.

3.3.3 Uncertainty Analysis

Uncertainty analysis was performed on the lift-to-drag ratio for the 24" Houck Configuration. This was done by taking the equation for lift-to-drag and breaking it down into a form consisting only of measurements from the wind tunnel results:

$$L/D = \frac{C_L}{C_D} = \frac{N \cdot \cos\alpha - A \cdot \sin\alpha}{N \cdot \sin\alpha + A \cdot \cos\alpha} \tag{15}$$

where L/D (-) is the lift-to-drag ratio, C_L (-) is the lift coefficient, C_D (-) is the drag coefficient, *N* (lbs) is the normal force measurement from the balance, *A* (lbs) is the axial force measurement from the balance, and α (°) is the angle of the balance to the free stream velocity.

The partial of this equation is then taken with respect to both *N* and *A*:

$$\frac{\partial(L/D)}{\partial N} = \frac{A}{(N \cdot \sin\alpha + A \cdot \cos\alpha)^2} \tag{16}$$

$$\frac{\partial(L/D)}{\partial A} = \frac{-N}{(N \cdot \sin\alpha + A \cdot \cos\alpha)^2} \qquad (17)$$

where $\frac{\partial(L/D)}{\partial N}$ is the partial of the lift-to-drag ratio with respect to the unresolved normal force, and $\frac{\partial(L/D)}{\partial A}$ is the partial of the lift-to-drag ratio with respect to the unresolved axial force.

Next, a worst case possible error and a realistic case possible error in lift-to-drag can be calculated:

$$\Delta(L/D)_{worst} = \left|\frac{\partial(L/D)}{\partial N} \cdot \Delta N\right| + \left|\frac{\partial(L/D)}{\partial A} \cdot \Delta A\right| \qquad (18)$$

$$\Delta(L/D)_{realistic} = \sqrt{(\frac{\partial(L/D)}{\partial N} \cdot \Delta N)^2 + (\frac{\partial(L/D)}{\partial A} \cdot \Delta A)^2} \qquad (19)$$

where $\Delta(L/D)_{worst}$ is a worst-case error value in lift-to-drag ratio, $\Delta(L/D)_{realistic}$ is a more realistic error value in lift-to-drag ratio, ΔN is the possible error in the normal force measurement, and ΔA is the possible error in the axial force measurement.

For the 10 lb balance, the uncertainty in the normal force measurement, ΔN, is nominally specified by the manufacturer to be no more than 0.025 lbs. The uncertainty in the axial force measurement, ΔA, is by the same measure no more than 0.0125 lbs. The range for the possible lift-to-drag ratio can then be determined:

$$L/D_{range} = L/D \pm \Delta(L/D) \qquad (20)$$

where L/D_{range} is the possible range of the lift-to-drag ratio given uncertainty in the measurements taken, L/D is the measured lift-to-drag ratio, and $\Delta(L/D)$ is the possible error in the *L/D* measurement (in one direction).

3.3.4 USAFA Wind Tunnel Results

In the Fall of 2006, a study on a different Houck Configuration was completed at the United States Air Force Academy by students, C1C Brittany Oligney and C1C Margaret Frash, and professor, Dr. Thomas R. Yechout. The model, tested in the USAFA Subsonic Wind Tunnel, was the USAFA 18" Houck Configuration. This variation of the Houck Lifting Foil is similar to the 24" Houck Configuration, but with a few modifications. The 18" model was designed using Eppler airfoil sections for the wings (high camber). The fuselage was also streamlined in order to reduce the drag for the total aircraft. The USAFA 18" Houck Configuration can be seen in Figure 31. Lateral-directional static stability data from the USAFA study is used for comparison with the 24" Houck Configuration. The reference location for the center of gravity used in data reduction was 8.81" from the back of the model.

Figure 31: USAFA 18" Houck Configuration (reproduced from Reference 24)

3.3.5 AFRL Computational Fluid Dynamics Results

In order to test a computational model of the 24" Houck Configuration, one first had to be created. This was task was completed by Jay R. Anderson of AFIT through the use of the FARO Portable Measurement Arm laser-line scanner. The laser-line scanner is a precision measurement instrument and is able to accurately measure a model in three dimensions and create a computational model from it. The model is first scanned manually using the FARO measurement arm. In *Polyworks*, a polygonal file is created and modified to fill any gaps that are present in the data. The file is then exported into an *.stl file for use in *Solid Works*. Once a file existed in *Solid Works*, AFRL/VAAA adapted the computational model further so that it could be used with CFD analysis software. This modified *.stl file can then be exported into *Materialise* and printed out in a three-dimensional modeler. The laser-line scanner allowed the original 24" Houck Configuration, a hand-crafted model, to be replicated both physically and computationally for further testing.

Computational Fluid Dynamics analysis data on the 24" Houck Configuration is used in this report for comparisons with the experimental wind tunnel data. The CFD analysis has been completed by John Staiger of AFRL/VAAI (Air Vehicles Directorate). CFD analysis was completed on the 24" Houck Configuration using a grid with 1.4 million cells generated by *AVUS* (a CFD program).

3.4 Test Plan

3.4.1 Overview

A summary of the tests performed on the various Houck Configurations can be viewed in Table 3. Experimental information has been collected using three primary methods: balance data, hot wire analysis, and flow visualization. Further detail for each variation of the Houck Configuration will be discussed in detail throughout the remainder of this section.

Table 3: Summary of Tests Performed

			Balance Data		Hot Wire			Flow Viz
Configuration	**Re (-)**	**V**	**α Sweep**	**β Sweep**	**α = -2°**	**α = 4°**	**α = 8°**	**50 mph**
Orig. 24" Houck	80K	20 mph	√	√				√
Orig. 24" Houck	125K	30 mph	√	√	√	√	√	
Orig. 24" Houck	170K	40 mph	√					
δ = 20° down	80K	20 mph	√					
δ = 20° down	125K	30 mph	√		√	√	√	
δ = 20° down	170K	40 mph	√					
δ = 20° up	80K	20 mph	√					
δ = 20° up	125K	30 mph	√		√	√	√	
δ = 20° up	170K	40 mph	√					
1" Cut in FG	80K	20 mph	√					
1" Cut in FG	125K	30 mph	√					
2" Cut in FG	80K	20 mph	√					
2" Cut in FG	125K	30 mph	√					
No Flow Guide	80K	20 mph	√					
No Flow Guide	125K	30 mph	√		√	√	√	
AFRL 24" CFD Houck	170K	40 mph	√					
USAFA 18" Houck	545K	M = 0.25	√	√				

3.4.2 Original 24” Houck Configuration

Testing began with the original 24” Houck Configuration variation. The model was placed in the AFIT low speed wind tunnel on the 10 lb balance and data was taken

for three different α sweeps (20 mph (8.94 m/s, Re ≈ 80K), 30 mph (13.41 m/s, Re ≈ 125K), and 40 mph (17.88 m/s, Re ≈ 170K)) from -5º to 15º in 1º increments. Data was also taken for two different β sweeps (20 mph (8.94 m/s, Re ≈ 80K) and 30 mph (13.41 m/s, Re ≈ 125K)) from -8º to 8º in 1º increments. Hot-wire data was then taken at 30 mph (Re ≈ 125K) for three different angles of attack of interest. An angle of attack of -2º was picked because lift was approximately zero at this location, α = 4º was chosen because L/D was approximately maximized at this location, and α = 8º was used because it provided an angle of attack that was into the range where efficiency (in terms of L/D) started to decrease. Flow visualization analysis was also accomplished at a speed of 50 mph (22.34 m/s, Re ≈ 205K) using tufts and a video recorder.

3.4.3 Original 24" Houck Configuration with Aileron Deflections

Next, testing was done on two variations of the 24" Houck Configuration with respect to aileron deflections. In these variations the ailerons were deflected, δ = 20º down and δ = 20º up (δ = 0º has already been tested, the original 24" Houck Configuration). Each variation was placed in the AFIT low speed wind tunnel on the 10 lb balance and data was taken for three different α sweeps (20 mph (8.94 m/s, Re ≈ 80K), 30 mph (13.41 m/s, Re ≈ 125K), and 40 mph (17.88 m/s, Re ≈ 170K)) from -5º to 15º in 1º increments. Hot-wire data was then taken at 30 mph (Re ≈ 125K) for three different angles of attack (α = -2º, 4º, and 8º). The same angles of attack that were tested for the original 24" Houck Configuration with δ = 0º were used again so that comparisons could be made between the results for different variations of the aircraft.

3.4.4 Original 24" Houck Configuration with Changes to the Flow Guides

Next, testing was done on three variations of the 24" Houck Configuration with respect to changing the flow guides. The three variations tested are a 1" cut in the flow guide, a 2" cut in the flow guide, and the flow guides completely cut off (the complete flow guide variation has already been tested, the original 24" Houck Configuration). Each variation was placed in the AFIT low speed wind tunnel on the 10 lb balance and data was taken for two different α sweeps (20 mph (8.94 m/s, Re ≈ 80K), and 30 mph (13.41 m/s, Re ≈ 125K))from -5º to 15º in 1º increments. Testing was not done at 40 mph for the modified models because the structural integrity of the wings had been reduced by cutting the flow guides. Hot-wire data was only taken on the variation with the flow guides completely cut off. Hot-wire data was taken at 30 mph (Re ≈ 125K) for three different angles of attack (α = -2º, 4º, and 8º). The same angles of attack that were tested for the original 24" Houck Configuration with flow guides were used again so that comparisons could be made between the results for the different variations of the aircraft at similar angles of attack.

IV. Results & Analysis

4.1 Chapter Overview

In this chapter, results will be shown for numerous tests conducted on different variations of the 24" Houck Configuration. Six different variations of the 24" Houck Configuration are tested: the original 24" Houck Configuration with no aileron deflection ($\delta = 0°$), the original 24" Houck Configuration with $\delta = 20°$ down, the original 24" Houck Configuration with $\delta = 20°$ up, the 24" Houck Configuration with a 1" section cut out of each flow guide, the 24" Houck Configuration with a 2" section cut out of each flow guide, and the 24" Houck Configuration with no flow guides.

The results will be divided into three main sections. The first section will show the results of the original 24" Houck Configuration, $\delta = 0°$. This section includes flow visualization using tufts, balance data using α sweeps, balance data using β sweeps, and hot-wire analysis all performed in the AFIT low-speed wind tunnel. The second section will compare the three different aileron variations of the original 24" Houck Configuration: $\delta = 0°$, $\delta = 20°$ down, and $\delta = 20$ up°. Only balance data using α sweeps and hot-wire analysis, both performed in the AFIT low-speed wind tunnel, will be described in this section. The third section will compare 4 variations of cuts to the flow guides for the 24" Houck Configuration, $\delta = 0°$: no cuts to the flow guides (original), a 1" section cut from each flow guide, a 2" section cut from each flow guide, and the flow guides completely cut off. Once again, only balance data using α sweeps and hot-wire analysis, both performed in the AFIT low-speed wind tunnel, will be described in this section.

4.2 Original Houck Configuration

4.2.1 Flow Visualization

Analysis of the flow visualization was completed on the 24" Houck Configuration at a speed of 50 mph (Re ≈ 215K). Flow visualization helps to provide a glimpse of how the air flow moves and reacts near the surface of the aircraft. A view of the tufts on the Houck model reacting to the flow (50 mph at $\alpha = 8.22°$) can be seen in Figure 32. In Figure 32(a), the flow can be seen moving upward and around the flow guide. The strength of the upward flow grows as the flow moves over the flow guide. Figure 32(b) shows the direction of the flow as it moves past the underside of the lower wing. The outward spanwise flow grows in strength the as it approaches the wing tip. These two occurrences are a result of air in the high pressure region below the wing circulating about the flow guide toward the low pressure region above the wing in order to reach equilibrium.

(a) (b)

Figure 32: Flow Visualization of 24" Houck Configuration at 50 mph, 8.22° AoA

(a) Flow over and around the wingtip, (b) Flow past the lower wing

To capture the flow visualization for a range of angles of attack, video footage was taken of the 24" Houck Configuration, $\delta = 0°$, with tufts for an alpha sweep ($\alpha = -4°$ to 12°) at a speed of 50 mph (22.35 m/s). This video is summarized in Figure 33 and provides a glimpse at when and where separation occurs on the wings. From angles of attack of -4° to 4°, there is very little change in the direction of the tufts (from a top view of the aircraft). As α increases from 4° to 5°, two tufts start to flutter (1st row of tufts, 2nd and 3rd from the left). This is the start of separation on the lower wing. By $\alpha = 6°$, the separation bubble has grown over the front section of the lower wing. As α increases from 7° to 9°, the region of separation continues to expand toward the trailing edge of the lower wing. When the angle of attack is between 10° and 12°, separation can be seen on the upper wing. This knowledge will be referenced later in the chapter in order to help explain some of the 24" Houck Configuration's performance.

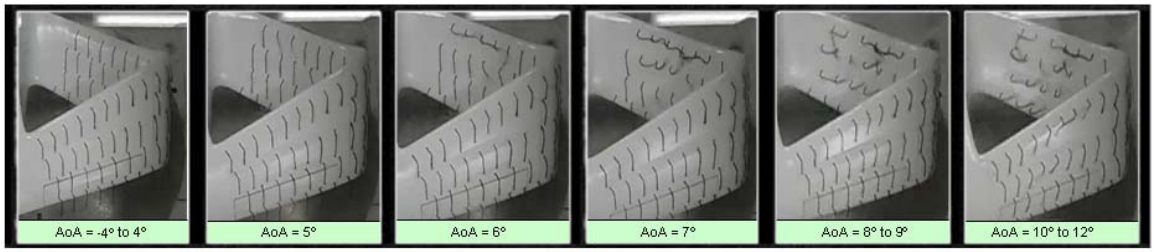

Figure 33: Flow Visualization of 24" Houck Configuration at 50 mph: Progression of Separation

4.2.2 Wind Tunnel Balance Data – Alpha Sweeps

In the AFIT low-speed wind tunnel, an alpha sweep from approximately -5º to 15º by 1º steps was performed on the 24" Houck Configuration at three different speeds: 20 mph (8.94 m/s), 30mph (13.41 m/s), and 40 mph (17.88m/s). A summary of the

resulting aerodynamic performance of the 24" Houck Configuration at Re ≈ 80,000 (20 mph), Re ≈ 125,000 (30 mph), and Re ≈ 170,000 (40 mph) can be seen in Table 4. Each performance parameter will be discussed in this section with its corresponding graph.

Table 4: Aerodynamic Performance of 24" Houck Configuration

		Min Drag		Zero Lift	Slopes	
Configuration	**Re (-)**	**C_{Do} (-)**	**α (°)**	**$\alpha_{0\ Lift}$ (°)**	**$C_{L\alpha}$ (/°)**	**$C_{m\alpha}$ (/°)**
Orig. 24" Houck	80K	0.0281	-0.90	-2.32	0.0488	-0.0061
Orig. 24" Houck	125K	0.0229	-1.01	-2.59	0.0457	-0.0056
Orig. 24" Houck	170K	0.0219	-1.20	-2.62	0.0439	-0.0059

		Max Range				Max Endurance			
Configuration	**Re (-)**	**L/D (-)**	**α (°)**	**C_L (-)**	**C_D (-)**	**$C_L^{(3/2)}/C_D$ (-)**	**α (°)**	**C_L (-)**	**C_D (-)**
Orig. 24" Houck	80K	6.50	4.30	0.286	0.044	3.75	6.70	0.420	0.112
Orig. 24" Houck	125K	7.43	4.20	0.295	0.040	4.20	5.30	0.340	0.081
Orig. 24" Houck	170K	8.02	4.00	0.293	0.037	4.53	5.10	0.340	0.075

The drag coefficient, C_D, for the 24" Houck Configuration is shown in Figure 34 for three different Reynolds numbers based on the average root chord of the upper and lower wings (80K, 125K, and 170K). C_D has been plotted both versus C_L and α. From the drag polar, the minimum drag coefficient, C_{Do}, of the 24" Houck Configuration can be attained. C_{Do} = 0.0281 at α = -0.90° for Re ≈ 80K. C_{Do} = 0.0229 at α = -1.01° for Re ≈ 125K. C_{Do} = 0.0219 at α = -1.20° for Re ≈ 170K. For these Reynolds numbers, the minimum drag coefficient decreases as Reynolds number increases.

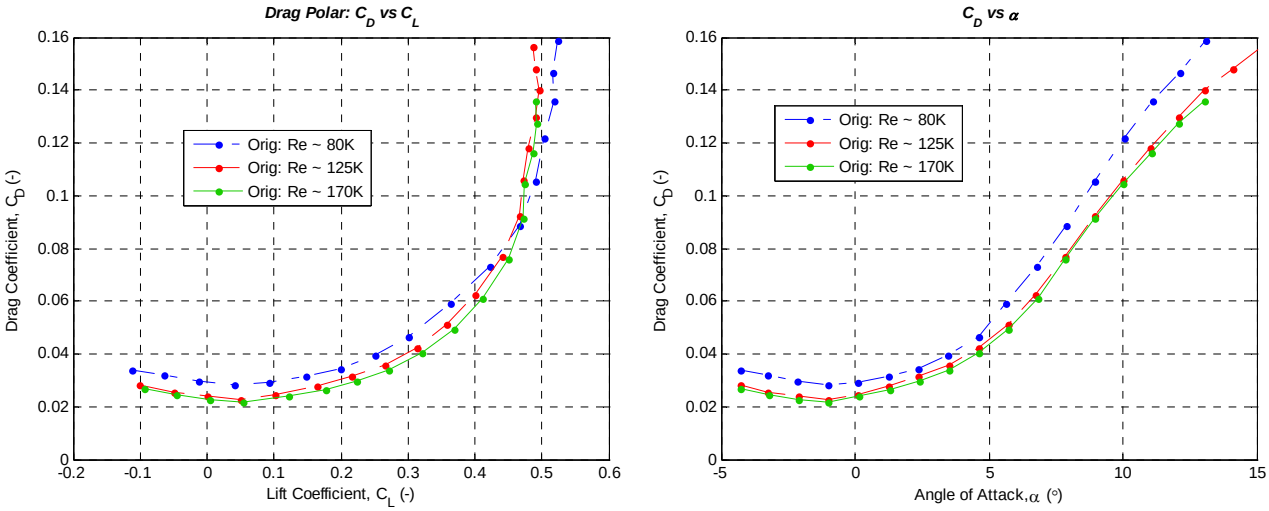

(a) (b)

Figure 34: Drag Coefficient – 24" Houck Configuration

(a) Drag Coefficient vs. Lift Coefficient (Drag Polar), (b) Drag Coefficient vs. Alpha

Figure 35(a) plots the lift coefficient, CL, vs. α for the 24" Houck model at three different Reynolds numbers (80K, 125K, and 170K). From the lift curve, a number of important aerodynamic values can be attained. C_{Lmax} is the maximum lift coefficient of the aircraft. Flying at an angle of attack that yields C_{Lmax} will produce the highest amount of lift for an aircraft at a given speed. C_{Lmax} usually occurs right before the onset of stall. However, in the tests performed, a maximum value of C_L for the aircraft was never achieved for the α range studied due to the gradual stall characteristics of the aircraft. Tests were conducted well past the linear region of $C_{L\alpha}$, but a loss of lift was not detected up to α = 15°. Higher angles of attack may have provided a stall point, but given the reduced strength of the model, higher angles of attack were not attempted in order to reduce the risk of damaging the aircraft or wind tunnel. $C_{L\alpha}$ is the lift curve slope, and gives a ratio of change of C_L with respect to α for the linear region of the lift curve, while

$\alpha_{0\ Lift}$ is the angle of attack where the aircraft produces zero lift. At a Reynolds number of 80K for the 24" Houck Configuration, $\alpha_{0\ Lift} = -2.32°$ and $C_{L\alpha} = 0.0488$ per degree. At a Reynolds number of 125K for the aircraft, $\alpha_{0\ Lift} = -2.59°$ and $C_{L\alpha} = 0.0457$ per degree. At a Reynolds number of 170K for the Houck Configuration, $\alpha_{0\ Lift} = -2.62°$ and $C_{L\alpha} = 0.0439$ per degree.

Figure 35(b) plots the pitching moment coefficient, C_m, vs. the angle of attack, α, for the 24" Houck Configuration at three different Reynolds numbers (80K, 125K, and 170K). The longitudinal static stability derivative, $C_{m\alpha}$, can be attained from this plot. It is desirable to have a negative value for $C_{m\alpha}$. In flight, a negative value of $C_{m\alpha}$ will restore the aircraft to its trim state (where $C_m = 0$) when perturbed. The 24" Houck Configuration is longitudinally stable about the reference CG (11.41" aft of the nose), for all three Reynolds numbers tested. At a Reynolds number of 80K, $C_{m\alpha} = -0.0061$ per degree and $C_m = 0$ at $\alpha \approx -0.9°$. At a Reynolds number of 125K, $C_{m\alpha} = -0.0056$ per degree and $C_m = 0$ at $\alpha \approx -1.3°$. At a Reynolds number of 170K, $C_{m\alpha} = -0.0059$ per degree and $C_m = 0$ at $\alpha \approx -1.4°$.

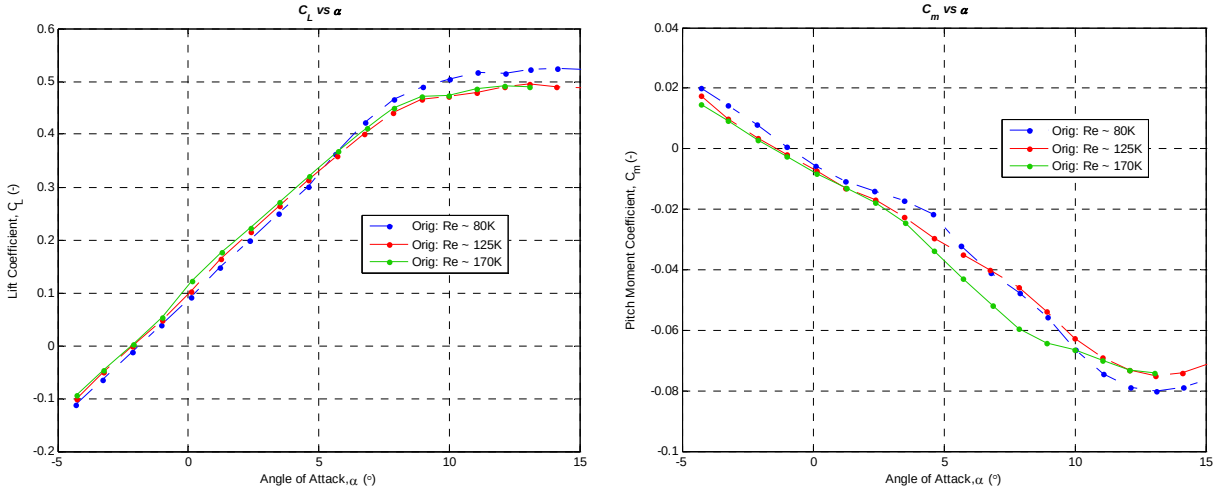

(a) (b)

Figure 35: Lift Coefficient and Pitch Moment Coefficient – 24" Houck Configuration

(a) Lift Coefficient vs. Alpha, (b) Pitch Moment Coefficient vs. Alpha, reference location of CG used

Figure 36 shows the lift-to-drag ratio for the 24" Houck Configuration at three different Reynolds numbers (80K, 125K, and 170K). L/D has been plotted versus α and C_L. Lift-to-drag is one measure of an aircraft's efficiency. When an aircraft is flying at the angle of attack that produces its maximum L/D, the aircraft is maximizing its range (31). At a Reynolds number of 80K for the 24" Houck Configuration, $L/D_{max} = 6.50$ at $\alpha = 4.30°$ and $C_L = 0.286$. At a Reynolds' number of 125K, $L/D_{max} = 7.43$ at $\alpha = 4.20°$ and $C_L = 0.295$. At a Reynolds number of 170K, $L/D_{max} = 8.02$ at $\alpha = 4.00°$ and $C_L = 0.293$. There is a strong correlation between an increase in Reynolds number and an increase in L/D values. The efficiency of the Houck model is increasing as the Reynolds number increases for the Reynolds numbers tested. L/D values for each Reynolds number increase during the range $\alpha \approx -4°$ to 3.9°. Once L/D_{max} at each Reynolds number is reached, the L/D values start to decrease. This occurs beyond $\alpha \approx 4.4°$ and $C_L \approx 0.310$,

and is likely due to the separation that starts to develop on the lower wing around this angle of attack (known from flow visualization).

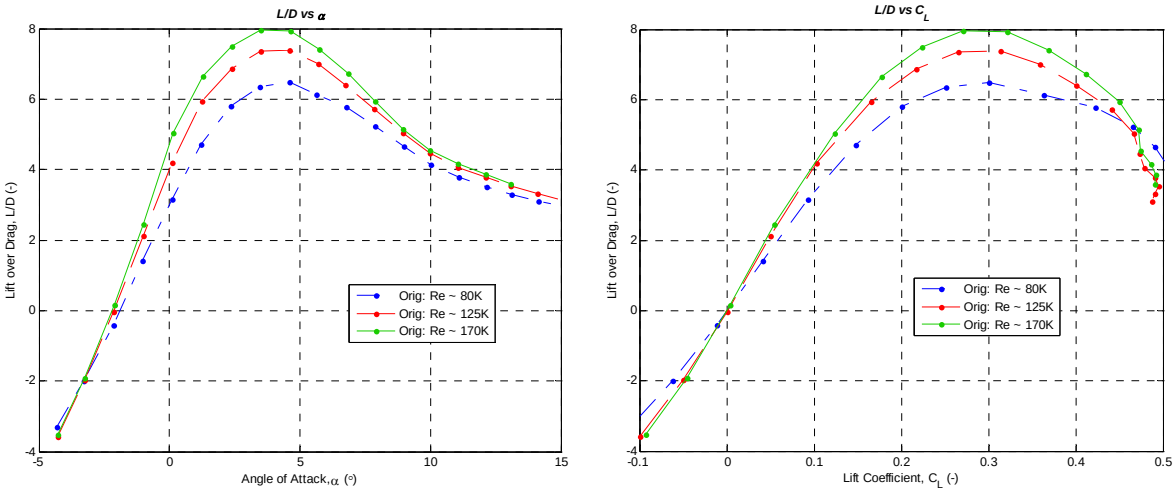

(a) (b)

Figure 36: Lift-to-Drag – Max Range – 24" Houck Configuration

(a) Lift-to-Drag vs. Alpha, (b) Lift-to-Drag vs. Lift Coefficient

Figure 37 shows the lift-to-drag ratio plotted with error bars created through uncertainty analysis using the balance manufacturer's specification for sensitivity. These results can be seen in numerical form in Table 5. A worst case scenario, where each possible source of error occurs at once in the same direction, and a more realistic case have been calculated for each Reynolds number. For a Reynolds number of approximately 80K, the worst case error ranges from 2.09% to 21.07% of the maximum L/D ratio and the more realistic case ranges from 1.69% to 16.07% of L/D_{max}. The possible error at L/D_{max} was 16.20% for the worst case and 12.98% for the realistic case. At Re ≈ 125K, the worst case error ranges from 0.85% to 9.83% of L/D_{max} while the more realistic case ranges from 0.70% to 7.42% of L/D_{max}. The possible worst case error

at L/D_{max} was 6.89% while the more realistic case error was 5.63%. For a Reynolds number of approximately 170K, the worst case error ranges from 0.57% to 5.67% of the maximum L/D ratio and the more realistic case ranges from 0.47% to 4.33% of L/D_{max}. The possible error at L/D_{max} was 4.75% for the worst case and 3.84% for the realistic case. As expected, the error values are decreasing as the Reynolds number is increased since higher velocities correspond to larger balance loading and therefore, increased sensitivity. These uncertainty values are conservative, as the actual uncertainty values for the balance measurements are likely smaller than published in order to help assure the balance meets specifications.

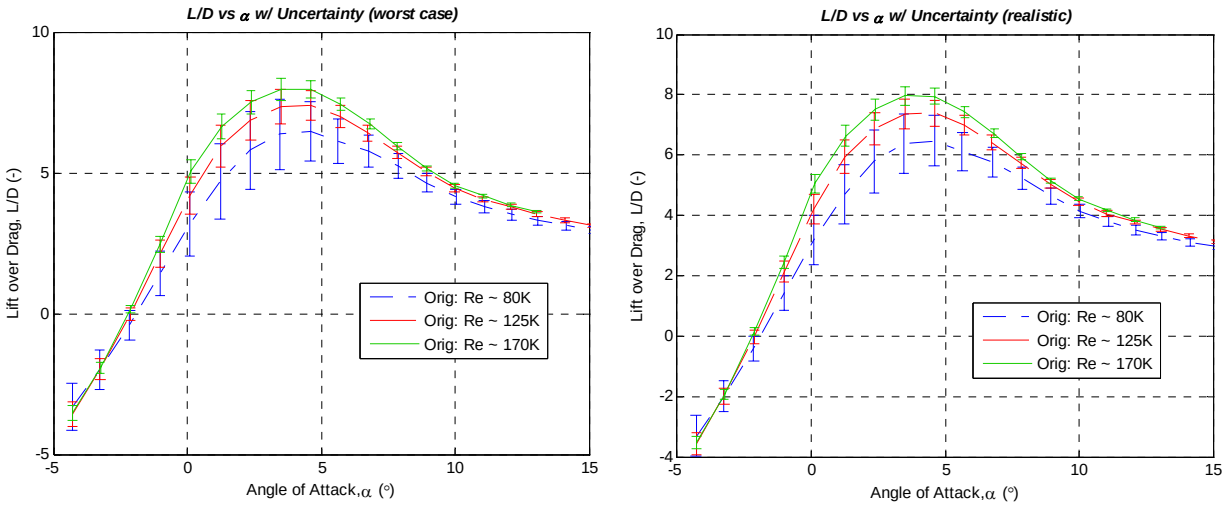

Figure 37: Lift-to-Drag – Uncertainty Analysis – 24" Houck Configuration

(a) Worst Case Uncertainty Analysis, (b) Realistic Uncertainty Analysis

Table 5: Uncertainty Analysis in L/D for 24" Houck Configuration

		Re = 80K (20 mph)			Re = 125K (30 mph)			Re = 170K (40 mph)		
			Error in % of L/D_{max}			% Error of L/D_{max}			% Error of L/D_{max}	
$\alpha_{balance}$ (°)	$\alpha_{aircraft}$ (°)	L/D (-)	Worst	Realistic	L/D (-)	Worst	Realistic	L/D (-)	Worst	Realistic
-8.43	-4.30	-3.31	12.91%	10.48%	-3.58	5.89%	4.89%	-3.53	3.14%	2.60%
-7.40	-3.27	-2.00	11.04%	7.95%	-1.98	4.94%	3.55%	-1.93	2.62%	1.88%
-6.28	-2.15	-0.41	7.95%	6.43%	-0.02	3.08%	2.88%	0.15	1.59%	1.56%
-5.16	-1.03	1.42	12.05%	8.82%	2.13	6.49%	4.61%	2.46	3.73%	2.64%
-4.03	0.10	3.17	17.70%	12.59%	4.20	9.04%	6.54%	5.05	5.25%	3.86%
-2.91	1.22	4.70	20.60%	15.18%	5.94	9.83%	7.42%	6.64	5.67%	4.33%
-1.78	2.35	5.79	21.07%	16.07%	6.86	9.31%	7.25%	7.51	5.38%	4.23%
-0.66	3.47	6.36	19.32%	15.16%	7.36	8.37%	6.70%	7.96	4.75%	3.84%
0.46	4.59	6.48	16.20%	12.98%	7.39	6.89%	5.63%	7.94	3.88%	3.20%
1.51	5.64	6.12	11.97%	9.68%	6.99	5.33%	4.41%	7.42	2.91%	2.43%
2.64	6.77	5.77	9.11%	7.45%	6.41	4.00%	3.33%	6.72	2.13%	1.79%
3.75	7.88	5.24	6.82%	5.59%	5.73	2.96%	2.47%	5.94	1.55%	1.30%
4.83	8.96	4.65	5.14%	4.19%	5.04	2.20%	1.82%	5.16	1.14%	0.95%
5.90	10.03	4.14	4.06%	3.28%	4.45	1.72%	1.42%	4.54	0.90%	0.75%
6.96	11.09	3.80	3.38%	2.73%	4.06	1.43%	1.17%	4.18	0.76%	0.63%
8.00	12.13	3.52	2.91%	2.34%	3.78	1.22%	1.00%	3.86	0.65%	0.53%
8.97	13.10	3.30	2.56%	2.06%	3.54	1.07%	0.87%	3.61	0.57%	0.47%
10.01	14.14	3.12	2.30%	1.85%	3.31	0.95%	0.78%			
11.06	15.19	2.95	2.09%	1.69%	3.11	0.85%	0.70%			

In order to show the conservative nature of the uncertainty analysis, a plot has been prepared to show the repeatability of the wind tunnel tests. Most of the data taken on the original 24" Houck configuration was taken in November of 2006. Prior tests were also completed in the early stages of the study. Figure 38 shows a comparison of lift-to-drag data taken in both September of 2006 and November of 2006 at a Reynolds number of approximately 125K. The data for the September test can be seen in Table 20, Appendix C. The model and 10 lb balance were taken out of the wind tunnel between tests. The balance was then put back into the wind tunnel, the balance was calibrated, and the model was mounted onto the balance. Even after all of these changes, the results

for the two tests are almost indistinguishable from one another. The maximum value for L/D for the September data is 7.313. L/D_{max} for the November data is 7.386. This is a difference of less than 1% between the data points. It is far less than the conservative error of 5.63% determined by the uncertainty analysis.

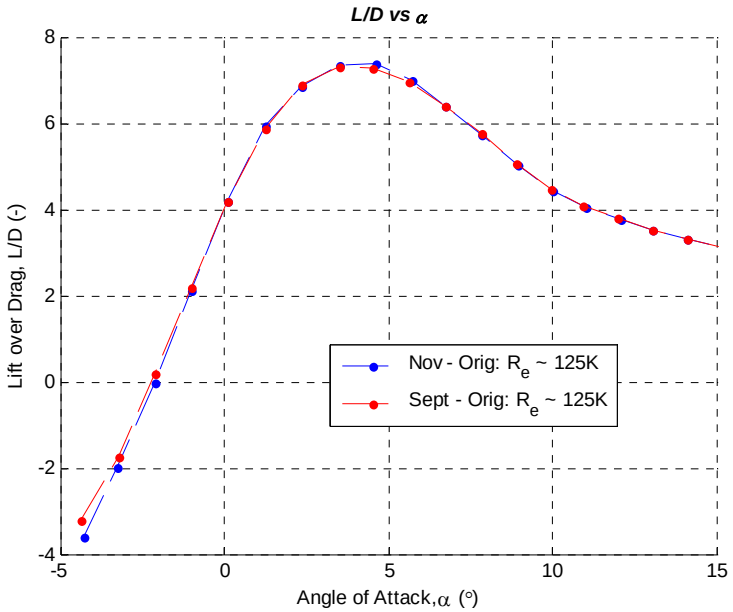

Figure 38: Lift-to-Drag – Repeatability – 24" Houck Configuration

Figure 39 shows the ratio of $C_L^{3/2}/C_D$ for the 24" Houck Configuration at three different Reynolds numbers (80K, 125K, and 170K). $C_L^{3/2}/C_D$ has been plotted both versus α and C_L. $C_L^{3/2}/C_D$ is another measure of an aircraft's efficiency. When an aircraft is flying at the angle of attack that produces its maximum $C_L^{3/2}/C_D$, the aircraft is maximizing its endurance (time in flight with a set amount of fuel). At a Reynolds number of 80K for the 24" Houck Configuration, $C_L^{3/2}/C_{D\ max} = 3.75$ at $\alpha = 6.70°$ and $C_L = 0.420$. At a Reynolds' number of 125K, $C_L^{3/2}/C_{D\ max} = 4.20$ at $\alpha = 5.30°$ and $C_L =$

0.340. At a Reynolds number of 170K, $C_L^{3/2}/C_{D\ max} = 4.53$ at $\alpha = 5.10°$ and $C_L = 0.340$. Similar to L/D, there is a strong correlation between an increase in Reynolds number and an increase in $C_L^{3/2}/C_D$ values. $C_L^{3/2}/C_D$ values for each Reynolds number increase during the range $\alpha \approx -4°$ to 5°. Once $C_L^{3/2}/C_{D\ max}$ at each Reynolds number is reached, the $C_L^{3/2}/C_D$ values start to decrease. This occurs beyond $\alpha \approx 6.8°$ and $C_L \approx 0.43$. The reduction in the endurance efficiency is also likely due to the increasing amount of separation visible on the lower wing around $\alpha = 5°$ and higher.

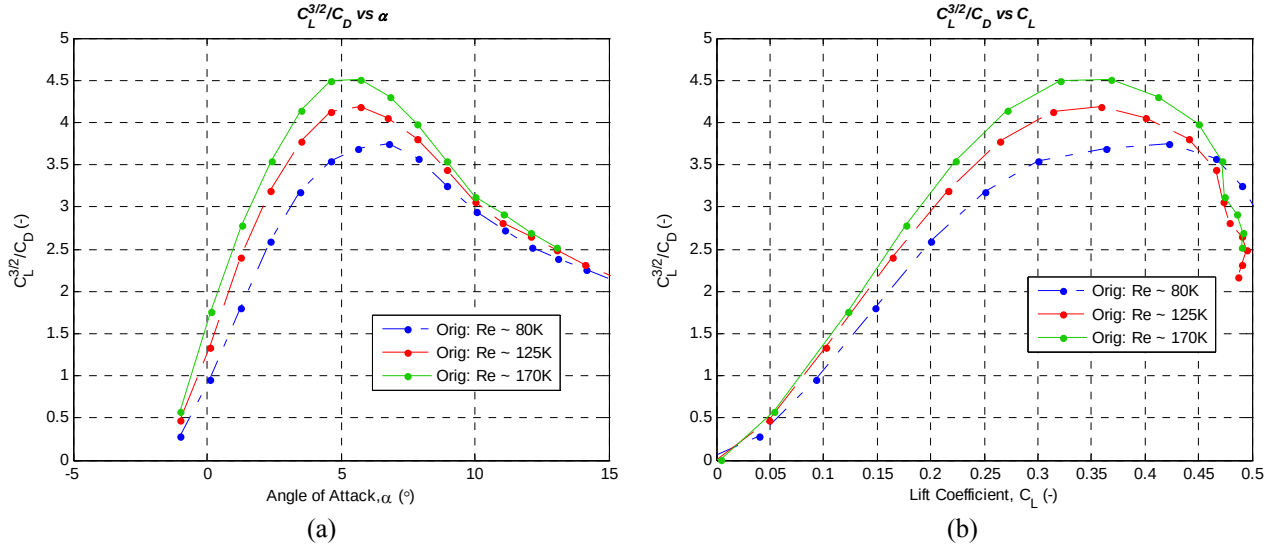

Figure 39: $C_L^{3/2}/C_D$– Max Endurance – 24" Houck Configuration

(a) $C_L^{3/2}/C_D$ vs. Alpha, (b) $C_L^{3/2}/C_D$ vs. Lift Coefficient

The lift-to-drag and $C_L^{3/2}/C_D$ data can also be plotted versus aircraft weight. This is done in order to determine the best speed for maximizing range or endurance for the 24" Houck Configuration flying steady, level unaccelerated flight at sea level. Once a desired aircraft weight is chosen, the velocity (Reynolds number) that provides the best L/D or $C_L^{3/2}/C_D$ can be determined. A trend line has also been added to estimate likely

values between the data points. Since data was only taken at three speeds, interpolation can be done in order to determine intermediate velocity values that were not tested but may be the most efficient at a given aircraft weight.

Figure 40 shows the plot for L/D versus aircraft weight. If the 24" Houck Configuration is flying at an aircraft weight of 1.45 lbs, flying at a velocity of 30 mph would maximize the range of the aircraft. Using interpolation, if the aircraft is flying at a weight of 2 lbs, a velocity of approximately 35 mph would maximize the range.

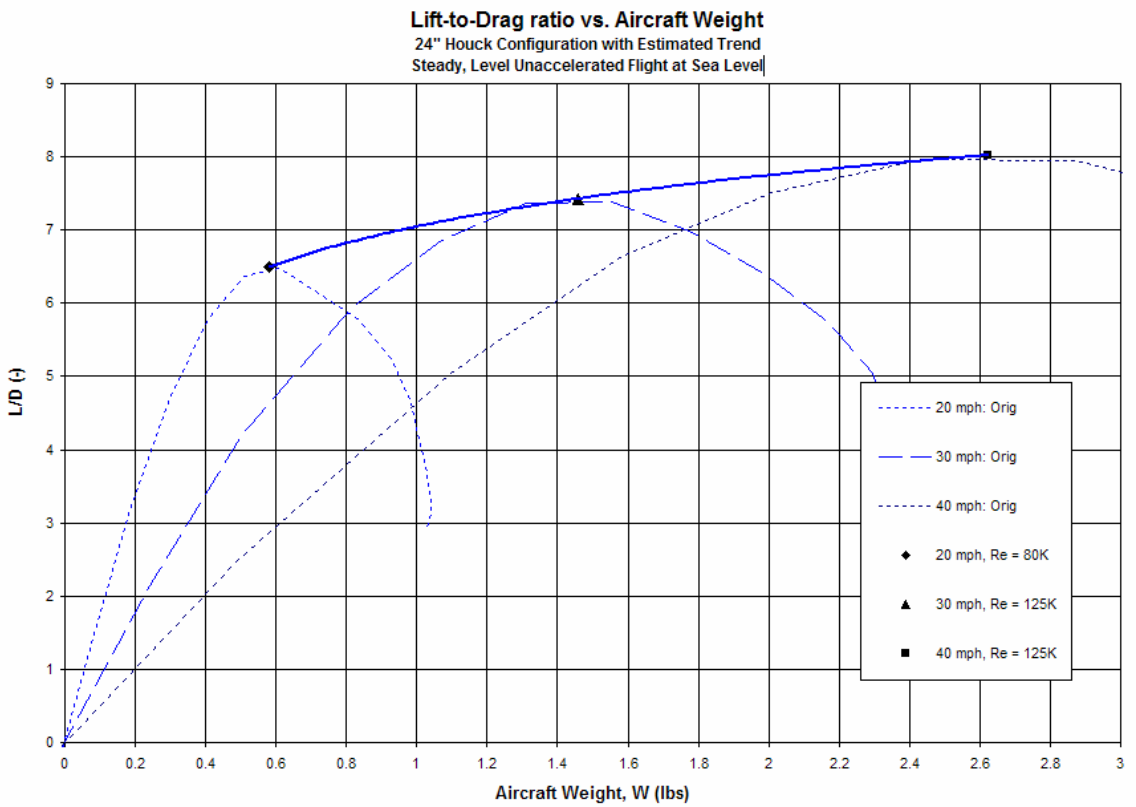

Figure 40: L/D vs. Weight for SLUF at Sea Level – 24" Houck Configuration

Figure 41 shows the plot for $C_L^{3/2}/C_D$ versus aircraft weight. If the 24" Houck Configuration is flying at an aircraft weight of 0.8 lbs, then flying at a velocity of 20 mph

would maximize the endurance of the aircraft. Using interpolation, if the aircraft is flying at a weight of 1.3 lbs, a velocity of approximately 25 mph would maximize the endurance.

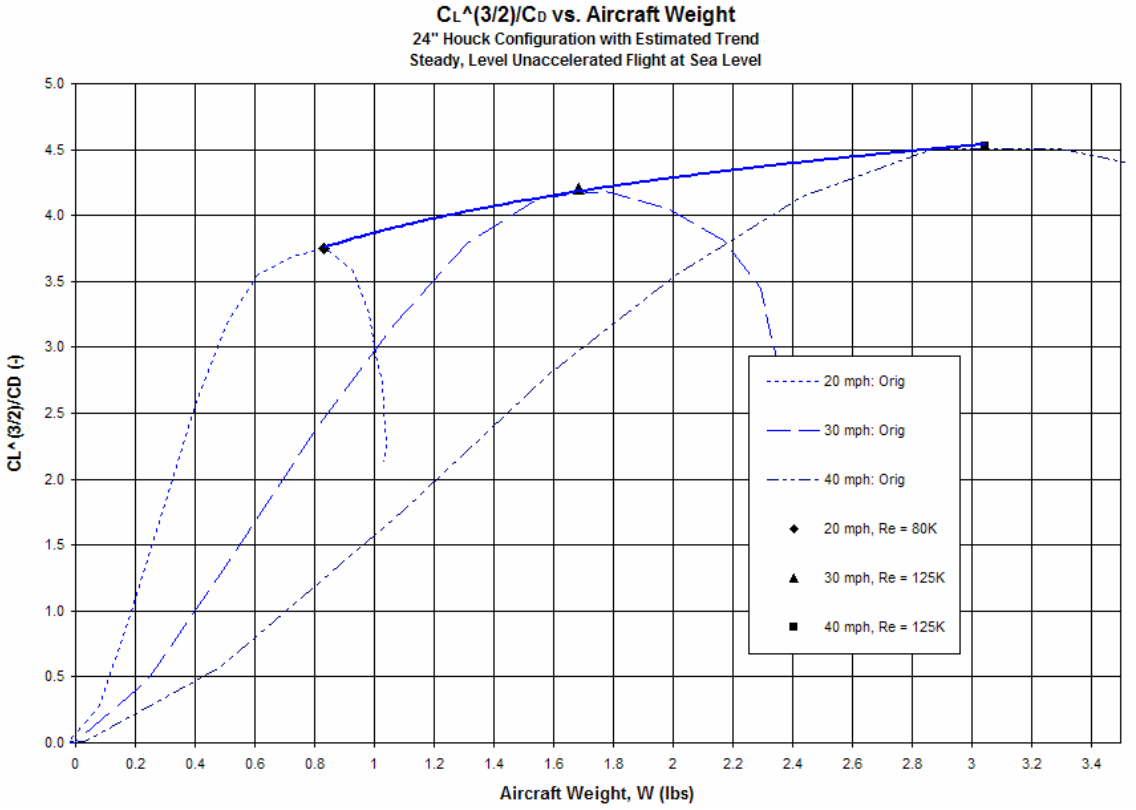

Figure 41: $C_L^{3/2}/C_D$ vs. Weight for SLUF at Sea Level – 24" Houck Configuration

4.2.3 Comparison between Experimental and CFD Results

As a part of the joint study on the performance of the Houck Lifting Foil design, headed by AFRL/VAAA, computational fluid dynamics analysis of the aircraft is done. Initial analysis completed by John Staiger of AFRL/VAAI on the 24" Houck Configuration was done at an aircraft speed of 40 mph (Re ≈ 170K) using AVUS for a 1.4 million cell grid. Further tests and analysis using CFD methods will continue to be

performed by AFRL, but the initial results have been used for comparisons. Plots of the experimental and CFD results can be seen in Figure 42 and Figure 43. The results of the 40 mph CFD test can be seen in Table 21, Appendix C.

Figure 42(a) shows the experimental and CFD drag polar for the 24" Houck model at a Reynolds number of 170K. The experimental and CFD data show similar results. The experimental value of $C_{Do} = 0.0219$, while the CFD value of $C_{Do} = 0.0221$, a difference of only 0.9%.

Figure 42(b) shows the experimental and CFD lift curve for the 24" Houck model. The α values have been shifted from the original CFD data in order to line up the angles of attack where lift was equal to zero. This doesn't change the data, but instead, aligns the reference angle of attack. The experimental lift-curve slope, $C_{L\alpha}$, is equal to 0.0439 per degree. The CFD lift-curve slope is equal to 0.0426 per degree. This difference may be due to a slight flexing of the model in the wind tunnel. The flexing would increase with angle of attack and increase the actual angle of attack of the aircraft while the balance reads a different angle. For example, this could make the data read 5° AoA while the actual AoA would be 5.2° from the flexing. This would account for a difference between the experimental and CFD data value for $C_{L\alpha}$. Testing a model made of stiffer material would possibly mitigate these differences.

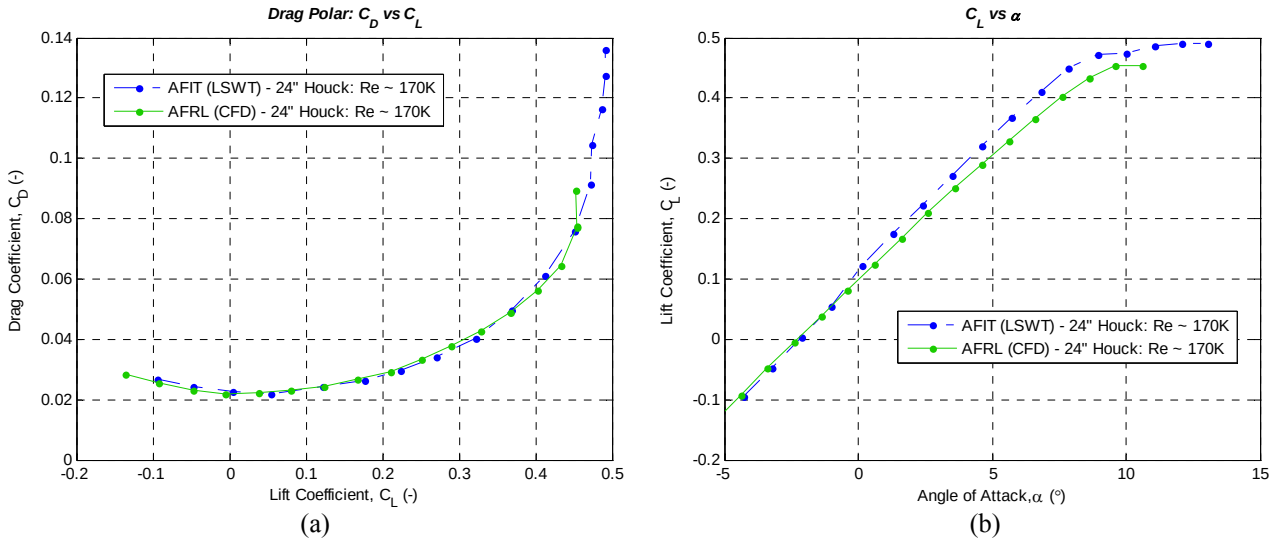

Figure 42: Drag Polar and Lift Curve – Experimental vs. CFD

(a) Drag Coefficient vs. Lift Coefficient, (b) Lift Coefficient vs. Alpha

Comparative plots for max range and max endurance for an aircraft can be seen in Figure 43. Both L/D (Figure 43(a)) and $C_L^{3/2}/C_D$ (Figure 43(b)) are plotted versus C_L. Once again, the plots for the experimental and CFD results are very similar. The experimental value for $L/D_{max} = 8.02$ while the CFD value for $L/D_{max} = 7.73$, a difference of only -3.6%. The experimental value for $C_L^{3/2}/C_{Dmax} = 4.53$ while the CFD value for $C_L^{3/2}/C_{Dmax} = 4.55$, a difference of only 0.5%.

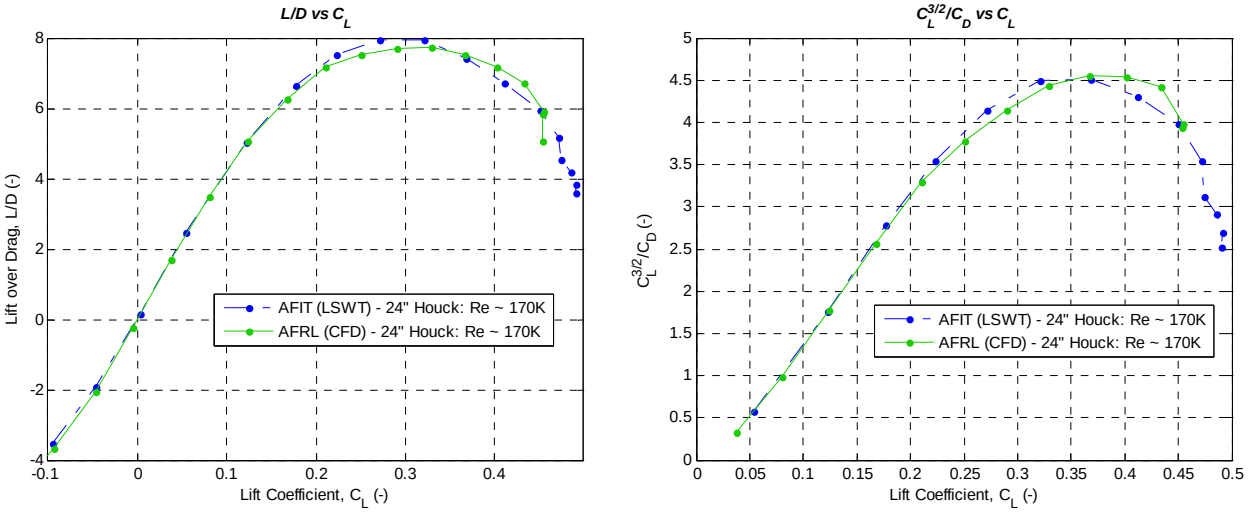

(a) (b)

Figure 43: Max Range and Endurance – Experimental vs. CFD

(a) Lift-to-Drag vs. Lift Coefficient, (b) $C_L^{3/2}/C_D$ vs. Lift Coefficient

These results help to provide confidence in the validity of both the wind tunnel test results and the computational fluid dynamics results. Not only can the CFD analysis be used to support experimental results, but it could possibly be used in instances where wind tunnel testing is not feasible or readily available.

4.2.4 Hot-Wire Analysis

Using the AFIT low-speed wind tunnel, hot-wire analysis at three angles of attack ($\alpha \approx -2°$, 4°, and 8°) was performed on the 24" Houck Configuration, $\delta = 0°$, at a speed of approximately 30 mph (13.41 m/s), resulting in a Reynolds number of around 125K. These tests were performed to document the strength and location of the trailing vortices for the model, since the flow guide patent claims to reduce induced drag. A summary of the angles of attack used for the hot-wire analysis and the resulting lift-to-drag ratios and

aerodynamic coefficients can be seen in Table 6. These angles were chosen because one resulted in close to zero lift ($\alpha \approx -2°$), one resulted in close to L/D_{max} ($\alpha \approx 4°$), and one was far into the range that resulted in separation on the lower wing ($\alpha \approx 8°$). The lift-to-drag ratios and aerodynamic coefficients for the given angles of attack have been taken from the prior tests conducted in this section and can be seen in Table 16, Appendix C.

Table 6: Aerodynamic Data at Angles of Attack used in Hot-Wire Tests for 24" Houck Configuration

Configuration	Re (-)	α (°)	L/D (-)	C_L (-)	C_D (-)
Orig. 24" Houck	125K	-2.04	0.15	0.003	0.024
Orig. 24" Houck	125K	4.13	7.37	0.293	0.040
Orig. 24" Houck	125K	8.22	5.49	0.450	0.082

The hot-wire analysis for the 24" Houck Configuration, $\delta = 0°$, can be seen in Figure 44 ($\alpha = -2.04°$), Figure 45 ($\alpha = 4.13°$), and Figure 46 ($\alpha = 8.22°$). The tests were performed at a speed of approximately 30 mph (13.41 m/s), resulting in a Reynolds number of around 125K. Part (a) plots color contours of the *u* component of velocity with an overlay of *v* and *w* component velocity vectors. The scale for the *u* component of velocity is from 8.1 m/s to 13.1 m/s with 26 steps of resolution. The scale for the *u* component of velocity is held constant for each hot-wire test completed. This allows for easier comparisons between tests. A reference velocity vector (2 m/s) can be seen for comparison with the *v* and *w* component velocity vectors. Part (b) plots color contours of the non-dimensional turbulence (non-dimensional kinetic energy per unit mass) with an overlay of *v* and *w* component velocity vectors. The scale for the non-dimensional turbulence is from 0.001 to 0.041 with 26 steps of resolution. The scale for the non-dimensional turbulence is held constant for each hot-wire test completed. This allows for

easier comparisons between tests. Again, a reference velocity vector (2 m/s) is included. Part (c) plots a color contour of the streamwise component of vorticity with an overlay of the *v* and *w* component velocity vectors. The vorticity values near zero were not plotted so that the position of the wing in front of the hot-wire grid could be seen. The scale for the vorticity is from -1.0 rad/s to 0.8 rad/s with 26 steps of resolution. The scale for the vorticity is held constant for each hot-wire test completed. This allows for easier comparisons between tests. Part (d) shows the actual angle of attack of the 24" Houck Configuration and its position with respect to the hot-wire grid. It is easier to understand what is happening with these references in place.

The hot-wire analysis at $\alpha = -2.04°$ ($Re \approx 125K$) for the 24" Houck Configuration, $\delta = 0°$, can be seen in Figure 44. There is approximately zero lift at this angle of attack. As a result, there is virtually no induced drag and therefore, no vortices forming behind the wing. Since the angle of attack is small, separation has not occurred and there is very little turbulence in the wake of the aircraft. The turbulence that does appear in the turbulence contour plot can be attributed primarily to the blunt trailing edge of the airfoil. Blunt bodies created large pressure differences and leave behind turbulent wakes in their path. This could likely be reduced with a more tapered trailing edge. The normalized turbulent kinetic energy reaches a peak value of approximately 0.012. The *u*-component of the velocity is slower behind the wing because of the turbulence from the blunt trailing edges.

The hot-wire analysis at $\alpha = 4.13°$ for the 24" Houck Configuration, $\delta = 0°$, can be seen in Figure 45. This angle of attack produces an L/D value close to L/D_{max}, the most

efficient angle at maximizing range. The lift coefficient, C_L, at 4.13° AoA is equal to 0.293. As a result of lift being produced, a clockwise (negative vorticity) vortex has formed behind the wing. The shape of the vortex resembles the flow guide with its core strength located just off of the upper wing tip. The strength at the core of the vortex reaches a vorticity of approximately 0.5 rad/s. This vortex creates a downwash that can be seen by the direction of the *v* and *w* vectors behind the wing. 4.13° is close to the angle where separation first occurred on the lower wing in the flow visualization test. This separation results in a turbulent wake and can be seen forming on the lower wing. There is also an increased amount of turbulence at the core of the vortex. The non-dimensional turbulence reaches a peak value of approximately 0.016. The turbulence from the blunt trailing edge of the airfoil is affected by the downwash created from the wing-tip vortex and can also be seen in the turbulence contour. The *u*-component of the velocity is fastest at the core of the vortex and slower in the wake of turbulence created from separation and from the blunt trailing edges of the wings.

The hot-wire analysis at $\alpha = 8.22°$ for the 24" Houck Configuration, $\delta = 0°$, can be seen in Figure 46. At this angle of attack, there is a lot of separation on the lower wing as seen in the flow visualization tests. More lift is created at 8.22° than at 4.13°, but it is not as efficient because of the increased drag. The lift coefficient, C_L, at 8.22° AoA is equal to 0.450. This is the highest value of lift produced for the hot-wire testing of the original 24" Houck Configuration. As a result, the clockwise vortex formed behind the wing is the largest for this value of α. This vortex is circular in shape and has its core strength located just off of the upper wing tip. Similar to the vortex at 4.13°, the maximum

strength of the vortex core at 8.22° reaches a vorticity of approximately 0.5 rad/s (but covers more area). This vortex creates a downwash that can be seen by the direction of the *v* and *w* vectors behind the wing. In the turbulence plot, the growth in turbulence can be seen when compared to an AoA of 4.13°. The increase in turbulence is due to both the increase in separation on the lower wing and the increased induced drag (a larger/stronger vortex). The total turbulence (including turbulence from the blunt trailing edge) inboard of the wing-tip vortex is affected by the downwash created from the vortex. The non-dimensional turbulence reaches a peak value of approximately 0.038 near the vortex core. This is more than two times the maximum turbulence created at 4.13° AoA. The u-component of velocity is no longer fastest at the center of the vortex. The increased turbulence has slowed the velocity down directly behind the entire wing, as the largest values of the *u*-component of velocity are found beyond the reaches of the wings. This set of results is consistent with separated flow.

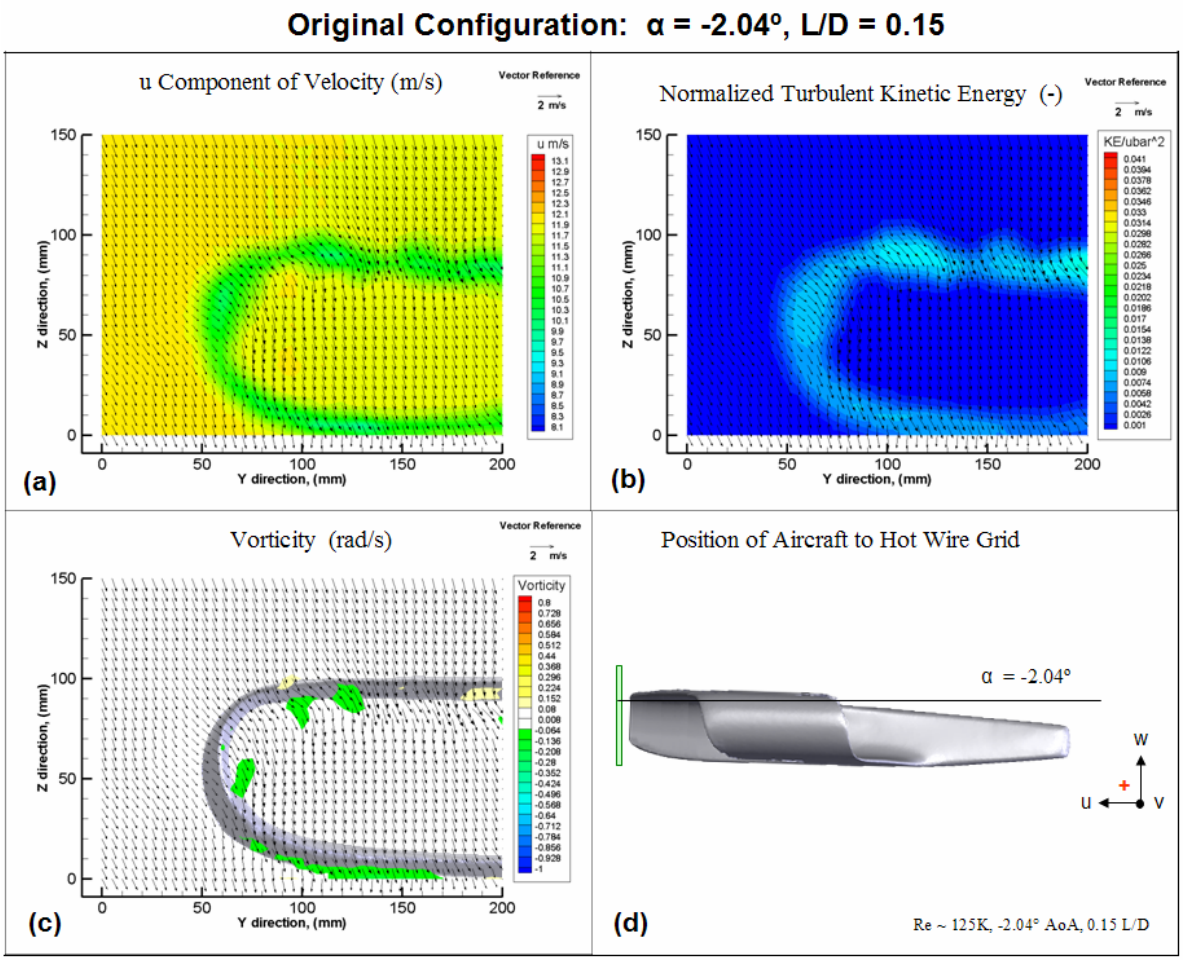

Figure 44: Hot Wire Analysis of 24" Houck Configuration, α = -2.04°, L/D = 0.15

(a) *u*-component contours with *v* & *w* Vectors, (b) Non-dimensional turbulence contours with *v* & *w* vectors,
(c) Vorticity behind wing with *v* & *w* vectors, (d) Position of hot-wire grid with respect to the 24" Houck Configuration

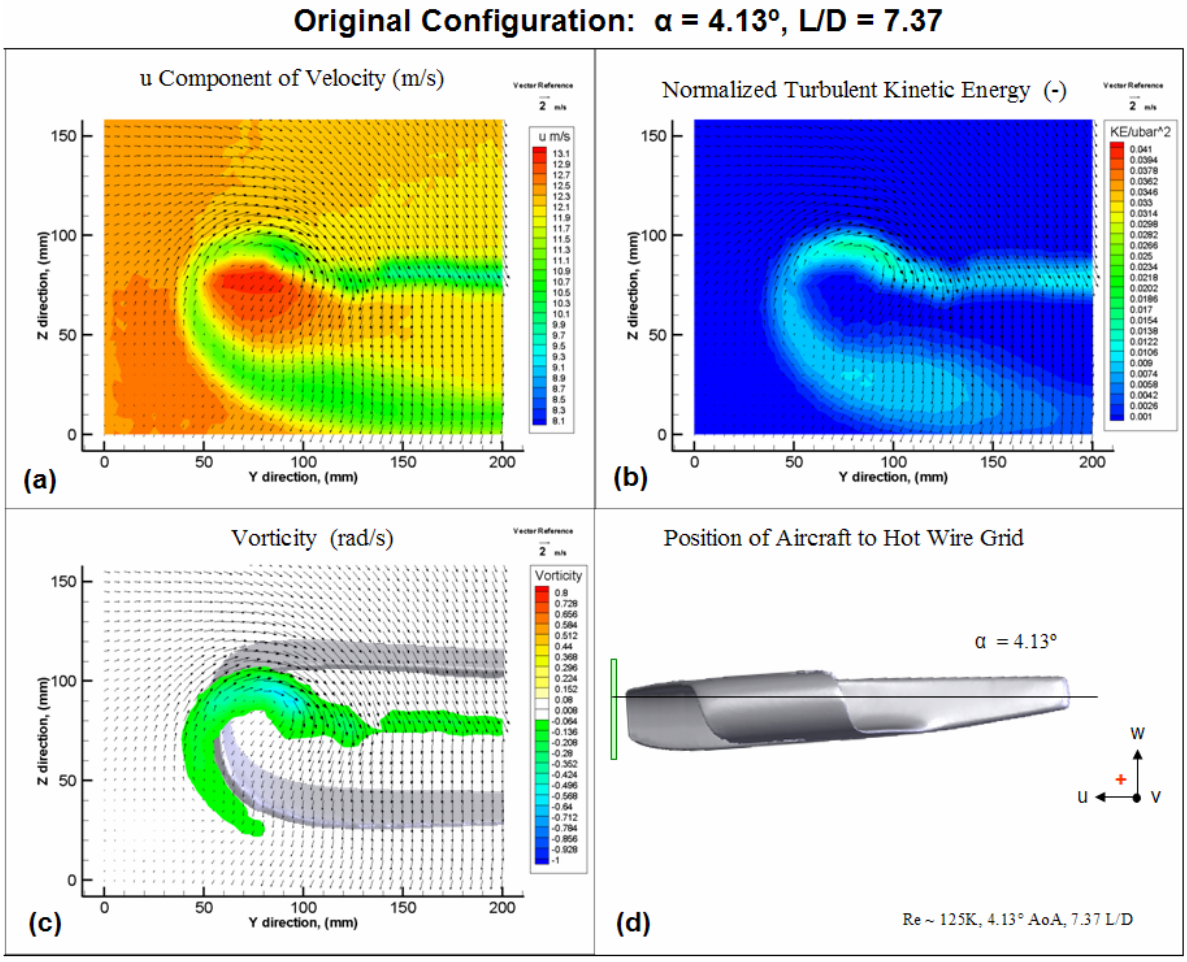

Figure 45: Hot Wire Analysis of 24" Houck Configuration, α = 4.13°, L/D = 7.37

(a) *u*-component contours with *v* & *w* Vectors, (b) Non-dimensional turbulence contours with *v* & *w* vectors,
(c) Vorticity behind wing with *v* & *w* vectors, (d) Position of hot-wire grid with respect to the 24" Houck Configuration

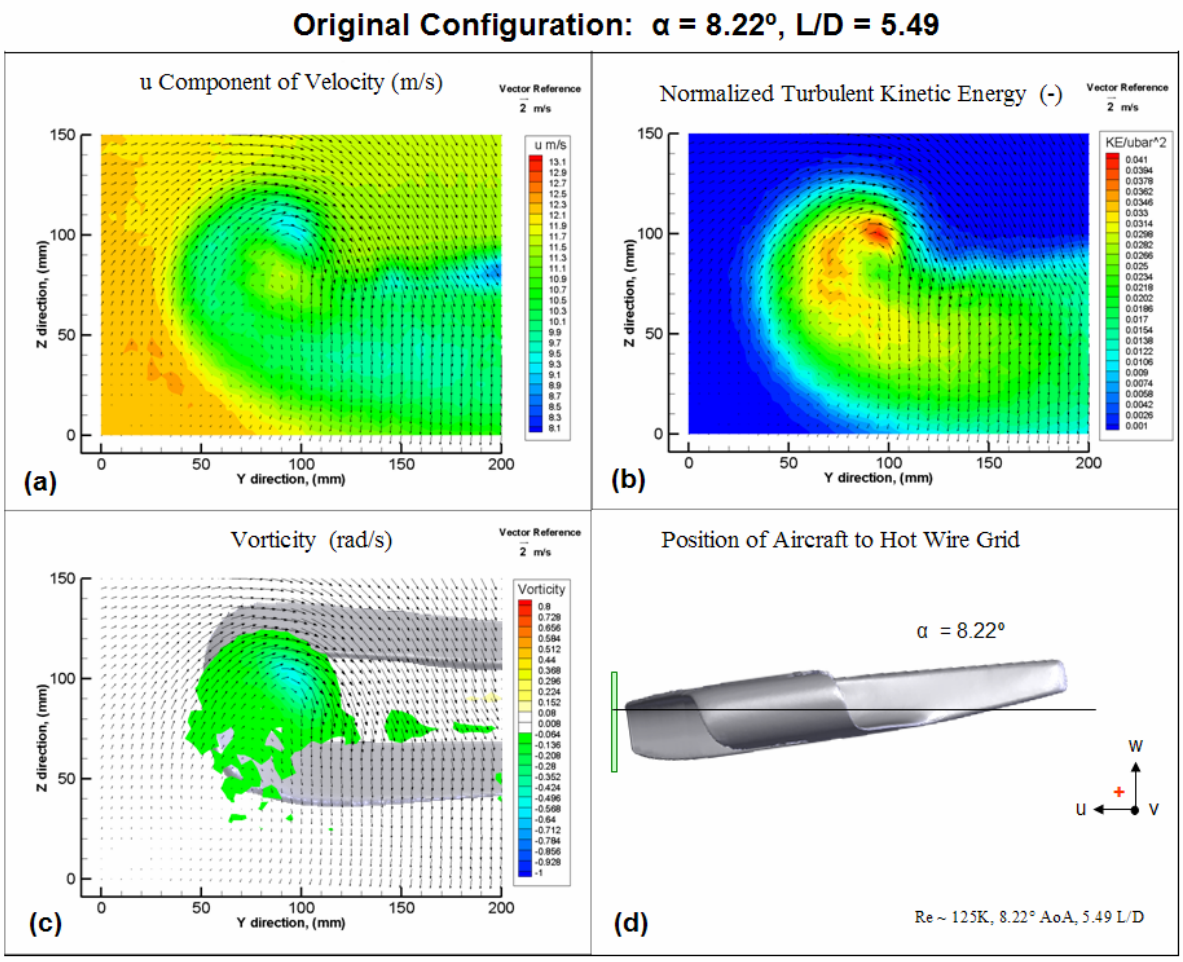

Figure 46: Hot Wire Analysis of 24" Houck Configuration, α = 8.22º, L/D = 5.49

(a) *u*-component contours with *v* & *w* Vectors, (b) Non-dimensional turbulence contours with *v* & *w* vectors,
(c) Vorticity behind wing with *v* & *w* vectors, (d) Position of hot-wire grid with respect to the 24" Houck Configuration

4.2.5 Wind Tunnel Balance Data – Beta Sweeps

In the AFIT low-speed wind tunnel, a beta sweep from approximately -8º to 8º in 1º increments at an AoA of 4.13° was performed on the 24" Houck Configuration at two different speeds: 20 mph (8.94 m/s, Re ≈ 80K) and 30mph (13.41 m/s, Re ≈ 125K). Beta sweeps were also completed on the 18" USAFA Houck Configuration by Air Force Academy students C1C Brittany Oligney and C1C Margaret Frash. Notably, the geometry of the 18" model varied from that of the 24" model in a number of ways (24). They performed beta sweeps on the 18" Configuration at a speed of Mach 0.25 (Re ≈ 545K) at angles of attack of -5°, 0°, 5°, 10°, 15°, and 20°. The results from four of these angles are examined because they were shown to be the most efficient AoA values for maximizing the range of the 18" USAFA model (see Figure 47). The reference locations of the centers of gravity for each aircraft model were used in the data reduction. A summary of the resulting stability derivatives of the 24" Houck Configuration and the 18" USAFA Houck Configuration can be seen in Table 7. A discussion of each stability derivative will be discussed in this section with its corresponding graph. The complete data for each β run can be seen in Table 18, Table 19, and Table 22, Appendix C.

Table 7: Lateral Stability Derivatives for the 24" Houck and the 18" USAFA Houck Configurations

Variation	Re (-)	α (º)	$C_{l\beta}$ (/ º)	$C_{n\beta}$ (/ º)	$C_{l\Psi}$ (/ º)	$C_{n\Psi}$ (/ º)	$C_{Y\beta}$ (/ º)
Orig. 24" Houck	80K	4.13	-0.001293	0.000408	0.001293	-0.000408	-0.007878
Orig. 24" Houck	125K	4.13	-0.001291	0.000303	0.001291	-0.000303	-0.007002
USAFA 18" Houck	545K	0	0.001104	0.000351	-0.001104	-0.000351	no data
USAFA 18" Houck	545K	5	-0.001205	-0.000040	0.001205	0.000040	no data
USAFA 18" Houck	545K	10	-0.002962	-0.000201	0.002962	0.000201	no data
USAFA 18" Houck	545K	15	-0.004719	-0.000432	0.004719	0.000432	no data

The plot of L/D versus α for the 18" USAFA Houck Configuration at a Reynolds number of approximately 545K can be seen in Figure 47. It shows a maximum L/D value of 5.5 at α = 13°, however, the L/D curve is relatively flat from α = 1° to 17°. This trend could possibly be attributed to the heavy camber of the wings on the 18" model. Since the L/D values were highest from 1° to 17°, the β sweeps at α values of 0°, 5°, 10°, and 15° are examined and compared to the 24" Houck β sweep at α = 4.13° (close to L/D_{max}).

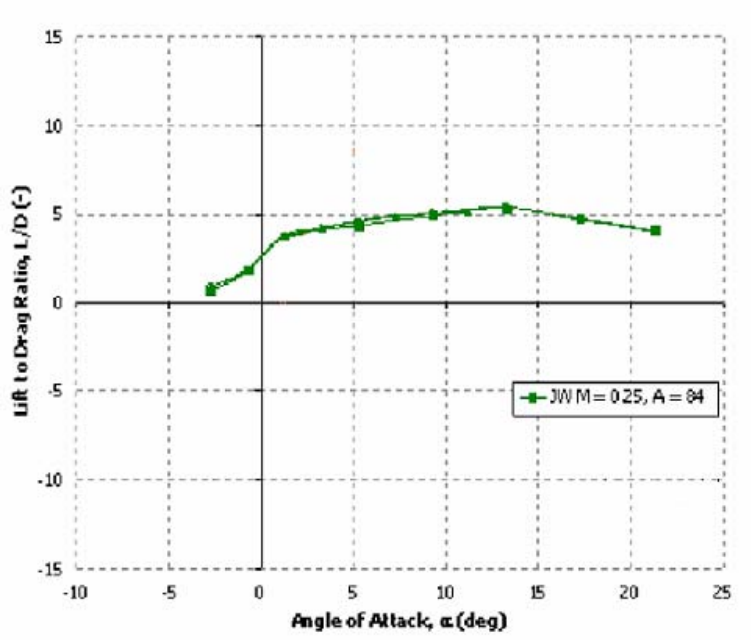

Figure 47: L/D vs. Alpha – USAFA 18" Houck Configuration 'JW' (reproduced from Reference 24)

Figure 48 shows a plot of the roll moment coefficient versus the sideslip angle, β. From this plot, the average slope, $C_{l\beta}$, can be attained. $C_{l\beta}$ is the lateral static stability derivative and is sometimes called the 'dihedral effect' (31:243). A negative value for $C_{l\beta}$ is statically stable and means that an aircraft will generate a rolling moment that rolls

the aircraft away from the direction of sideslip, returning it back toward $\beta = 0°$. A change in angle of attack usually has a significant effect on $C_{l\beta}$ (31). The data for the 18" model backs up this claim. As the angle of attack changes, the value for $C_{l\beta}$ changes from positive (0.00110 at $\alpha = 0°$) to negative (-0.00120 at $\alpha = 5°$) to highly negative (-0.00472 at $\alpha = 15°$). For the 24" Houck Configuration ($\alpha = 4.13°$), $C_{l\beta} = -0.00129$ at both Reynolds numbers. This value is closest to the $C_{l\beta}$ value for the 18" aircraft when flying at $\alpha = 5°$.

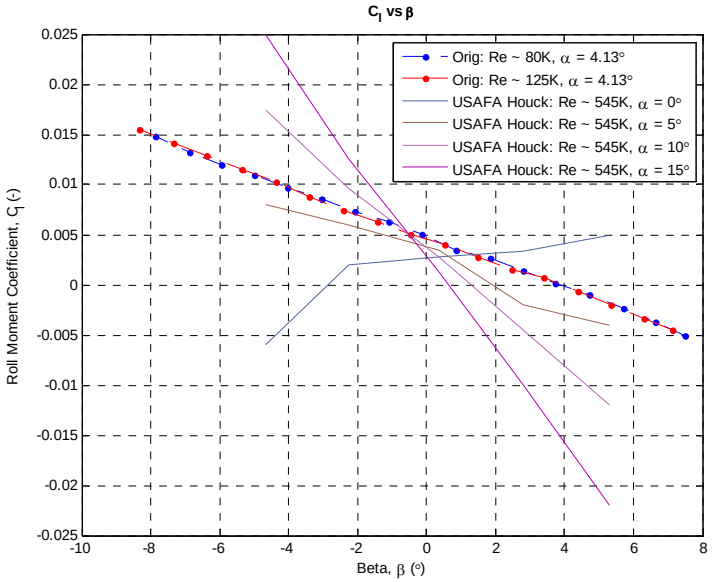

Figure 48: Roll Moment Coefficient vs. Beta – 24" Houck & USAFA 18" Houck Configurations

Figure 49 shows a plot of the yaw moment coefficient, C_n, versus β. From this plot, the average slope, $C_{n\beta}$, can be calculated. $C_{n\beta}$ is the directional static stability derivative and is also referred to as the 'weathercock stability derivative' (31:248). A positive value for $C_{n\beta}$ is considered statically stable. A positive value of $C_{n\beta}$ means that when the sideslip angle is perturbed (in the positive direction) from its trim condition, the

aircraft will create a positive yawing moment which reduces the sideslip angle back toward its trim state (usually $\beta = 0°$). The directional static stability of an aircraft is easily altered by changing the location of the center of gravity. If a higher value of $C_{n\beta}$ is desired, then moving the center of gravity forward will accomplish this goal. For the 24" Houck Configuration ($\alpha = 4.13°$), $C_{n\beta} = 0.00041$ at Re ≈ 80K and $C_{n\beta} = 0.00030$ at Re ≈ 125K. These values are closest to the $\alpha = 0°$ case for the 18" USAFA model ($C_{n\beta} = 0.00035$ at Re ≈ 545K).

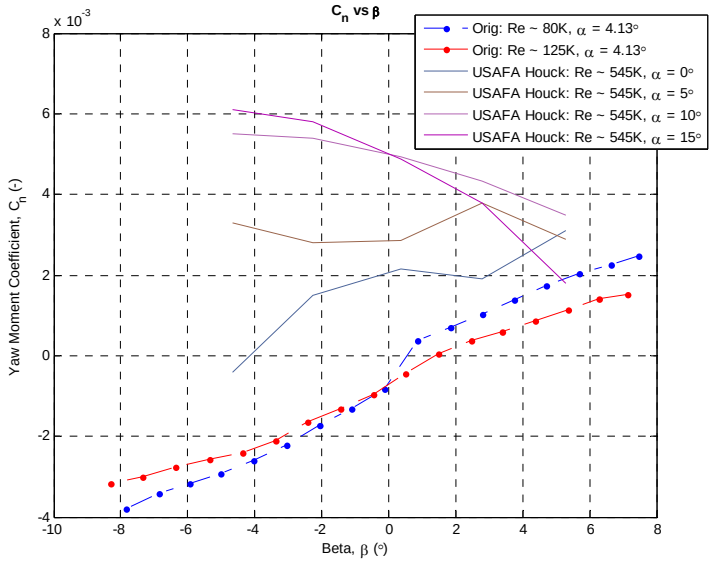

Figure 49: Yaw Moment Coefficient vs. Beta – 24" Houck & USAFA 18" Houck Configurations

By plotting the directional stability, $C_{n\psi}$, vs. the effective dihedral, $C_{l\psi}$, an estimate of the flyability of the models (at their different angles of attack) can be determined. Figure 50 shows flyability plot for the 24" Houck ($\alpha = 4.13°$ while Re ≈ 80K and 125K) and 18" USAFA Houck ($\alpha = 0°$, 5°, 10°, and 15° while Re ≈ 545K) Configurations. $C_{n\psi}$ and $C_{l\psi}$ are simply $-C_{n\beta}$ and $-C_{l\beta}$, respectively, because $\beta = -\psi$. For all of the points plotted, the $C_{n\psi}$ values are not negative enough and point toward a

problem with directional divergence. However, this is not a major issue because simply moving the center of gravity forward in each case will move the data points higher towards a more desired location. The centers of gravity were places at the quarter chord location for each model, but moving the CG location forward will likely resolve this issue. Once the center of gravity is adjusted, three data points will be in the satisfactory flyability region (24" model: $\alpha = 4.13°$, Re ≈ 80K, 125K and the 18" model: $\alpha = 5°$, Re ≈ 545K). The data points for the 18" model at $\alpha = 0°$, 10°, and 15° would lie in the unsatisfactory region.

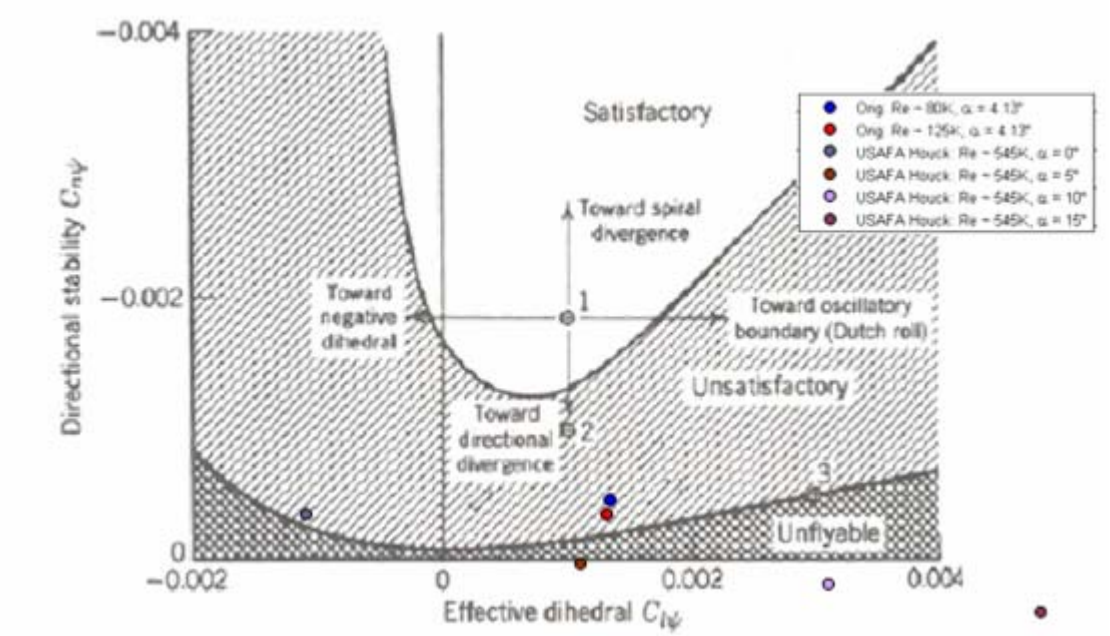

Figure 50: Directional Stability vs. Effective Dihedral (reproduced from reference 3)

A plot of the sideslip coefficient, C_Y, versus β can be seen in Figure 51 for the 24" Houck Configuration. From this plot, the average slope, $C_{Y\beta}$, can be attained. $C_{Y\beta}$ is normally negative for most aircraft and has an important influence on dutch roll dynamics (31:235). At $\alpha = 4.13°$ and a Reynolds number of approximately 80K, $C_{Y\beta}$ is

equal to -0.007878. At a Reynolds number of approximately 125K, $C_{Y\beta}$ = -0.007002. Data for the 18" USAFA Houck Configuration was not examined.

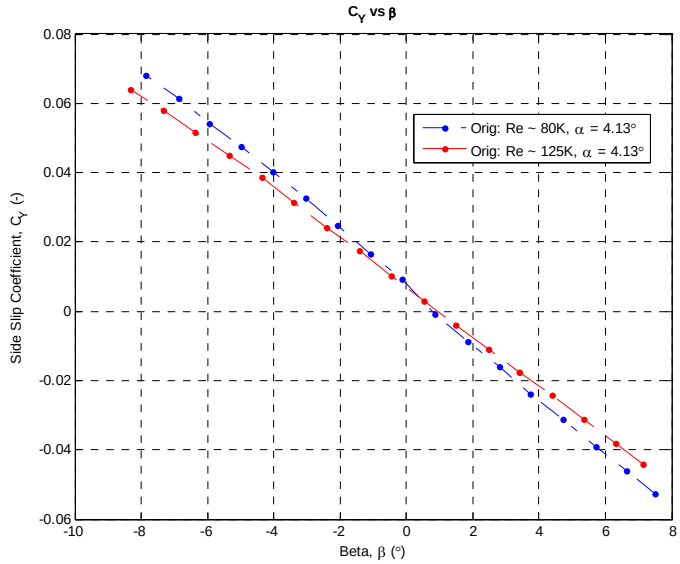

Figure 51: Sideslip Coefficient vs. Beta – 24" Houck Configuration

4.3 Original Configuration with Aileron Deflections

4.3.1 Wind Tunnel Balance Data – Alpha Sweeps

Tests were also performed on two different aileron deflection variations of the original 24" Houck Configuration in the low-speed wind tunnel. The first variation was a downward deflection of the ailerons, δ = 20º down. The second variation was an upward deflection of the ailerons, δ = 20º up. An alpha sweep on each model, from approximately -15º to 5º in 1º increments, was performed at three different speeds: 20 mph (8.94 m/s), 30mph (13.41 m/s), and 40 mph (17.88m/s). These results are then compared to the data from the original 24" Houck Configuration tests, δ = 0º. A summary of the resulting aerodynamic performance of the 24" Houck Configuration with

aileron deflection variations at Re ≈ 80,000 (20 mph), Re ≈ 125,000 (30 mph), and Re ≈ 170,000 (40 mph) can be seen in Table 8. A discussion of each performance parameter will be discussed in this section with its corresponding graph.

Table 8: Aerodynamic Performance of 24" Houck Configuration with Aileron Deflections

		Min Drag		Zero Lift	Slopes	
Configuration	**Re (-)**	**C_{Do} (-)**	**α (°)**	**$\alpha_{0\ Lift}$ (°)**	**$C_{L\alpha}$ (/°)**	**$C_{m\alpha}$ (/°)**
δ = 0°	80K	0.0281	-0.90	-2.32	0.0488	-0.0061
δ = 0°	125K	0.0229	-1.01	-2.59	0.0457	-0.0056
δ = 0°	170K	0.0219	-1.20	-2.62	0.0439	-0.0059
δ = 20° down	80K	0.035	-1.93	< -4	0.0474	-0.0052
δ = 20° down	125K	0.029	-4.08	< -4	0.0437	-0.0041
δ = 20° down	170K	0.027	-3.08	< -4	0.0431	-0.0041
δ = 20° up	80K	0.043	-0.12	0.82	0.0483	-0.0048
δ = 20° up	125K	0.037	-0.08	0.34	0.0489	-0.0095
δ = 20° up	170K	0.033	-0.02	-0.33	0.0478	-0.0087

		Max Range				Max Endurance			
Configuration	**Re (-)**	**L/D (-)**	**α (°)**	**C_L (-)**	**C_D (-)**	**$C_L^{(3/2)}/C_D$ (-)**	**α (°)**	**C_L (-)**	**C_D (-)**
δ = 0°	80K	6.50	4.30	0.286	0.044	3.75	6.70	0.420	0.112
δ = 0°	125K	7.43	4.20	0.295	0.040	4.20	5.30	0.340	0.081
δ = 0°	170K	8.02	4.00	0.293	0.037	4.53	5.10	0.340	0.075
δ = 20° down	80K	6.54	3.67	0.386	0.059	4.26	4.79	0.437	0.103
δ = 20° down	125K	7.28	2.53	0.320	0.044	4.43	4.76	0.414	0.093
δ = 20° down	170K	7.65	2.52	0.314	0.041	4.66	4.75	0.407	0.087
δ = 20° up	80K	4.03	7.65	0.314	0.078	2.33	8.76	0.356	0.152
δ = 20° up	125K	4.91	6.59	0.300	0.061	2.85	7.71	0.352	0.123
δ = 20° up	170K	5.58	5.51	0.281	0.050	3.18	7.74	0.375	0.118

Figure 52(a) plots the drag polar, C_D vs. C_L, for the 24" Houck Configuration with varying aileron deflections at three different Reynolds numbers (80K, 125K, and 170K). As expected, the minimum drag coefficient, C_{Do}, increases when the ailerons are deflected and decreases as the Reynolds number is increased. Figure 52(b) plots the lift coefficient, C_L, vs. α for three different Reynolds numbers (80K, 125K, and 170K). The

variation with ailerons deflected 20° down has higher C_L values across the entire range of tested angles of attack, as expected. It does this because the 20° downward deflection increases camber, producing more lift at a given reference angle of attack. For this same reason, the angle of attack that produces zero lift ($\alpha_{0\ Lift} = -5°$) is noticeably lower than the original Houck ($\alpha_{0\ Lift} = -2.59°$). The variation with a 20° upward deflection in the ailerons does the opposite. It produces less lift than the original Houck, $\delta = 0°$, at a given angle of attack because the wings act like a wing with negative camber. Likewise, it has a higher zero lift angle of attack ($\alpha_{0\ Lift} = 0.34°$) than the original Houck Configuration. Similar to the original Houck Configuration, stall is never fully seen for either variation with aileron deflections. The lift-curve slope, $C_{L\alpha}$ is not greatly affected by the variation in aileron deflection. $C_{L\alpha}$ for each variation hovers around 0.045 per degree.

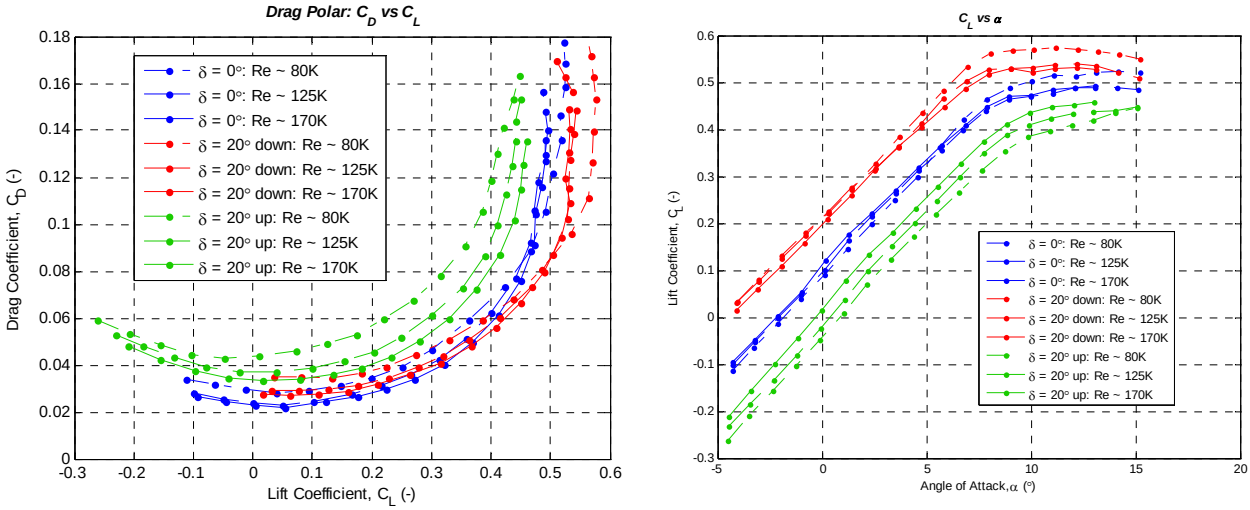

(a) (b)

Figure 52: Drag Polar and Lift Curve – 24" Houck Configuration with Aileron Deflections

(a) Drag Coefficient vs. Lift Coefficient, (b) Lift Coefficient vs. Alpha

The plots for L/D_{max} (max range) and $C_L^{3/2}/C_{D\ max}$ (max endurance) for the 24" Houck Configuration with aileron deflections can be seen in Figure 53. As would be expected, the aircraft variation with $\delta = 20°$ up (the variation that creates more drag and less lift than the original model) has the worst range and endurance of the three variations. The comparisons between the original Houck and the variation with ailerons deflected 20° down (the variation that produces more drag and more lift than the original model) are much more interesting. In comparison to the original configuration, the variation with ailerons deflected 20° down produces a max L/D value 4.6% lower and a max $C_L^{3/2}/C_D$ value 2.9% higher at a Reynolds number of 170K. There may be an aileron deflection angle between 0°and 20° that would prove to be more efficient in both range and endurance. However, this was not within the scope of the research.

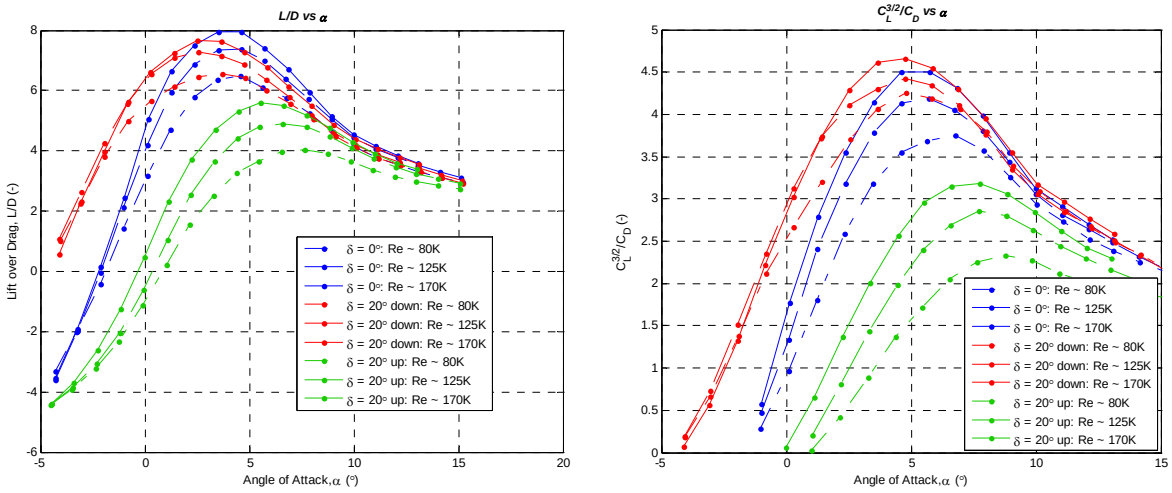

(a) (b)

Figure 53: Max Range and Endurance – 24" Houck Configuration with Aileron Deflections

(a) Lift-to-Drag vs. Alpha, (b) $C_L^{3/2}/C_D$ vs. Alpha

4.3.2 Hot-Wire Analysis

Using the AFIT low-speed wind tunnel, hot-wire analysis at three angles of attack ($\alpha \approx -2°$, 4°, and 8°) was performed on the 24" Houck Configuration, $\delta = 20°$ down and $\delta = 20°$ up, at Re ≈ 125K (30 mph, 13.41 m/s). A summary of the lift-to-drag ratios and aerodynamic coefficients at the tested values for α can be seen in Table 9. These angles were chosen so that comparisons to the 24" Houck Configuration with $\delta = 0°$ could be made. The lift-to-drag ratios and aerodynamic coefficients at the given angles of attack have been taken from the prior tests conducted in this section and can be seen in Table 24 and Table 27, Appendix C. The hot-wire analysis for the 24" Houck Configuration, $\delta = 0°$, has already been presented and can be seen in Figure 44, Figure 45, and Figure 46.

Table 9: Aerodynamic Data at Angles of Attack used in Hot-Wire Tests for 24" Houck Configuration with Aileron Deflections

Configuration	Re (-)	α (°)	L/D (-)	C_L (-)	C_D (-)
δ = 0°	80K	-2.04	0.15	0.003	0.024
δ = 0°	80K	4.13	7.37	0.293	0.040
δ = 0°	80K	8.22	5.49	0.450	0.082
δ = 20° down	80K	-2.04	4.10	0.122	0.030
δ = 20° down	80K	4.13	7.03	0.385	0.055
δ = 20° down	80K	8.22	5.04	0.529	0.105
δ = 20° up	80K	-2.04	-2.80	-0.119	0.042
δ = 20° up	80K	4.13	4.22	0.189	0.045
δ = 20° up	80K	8.22	4.66	0.370	0.079

The hot-wire analysis for the 24" Houck Configuration, $\delta = 20°$ down at $\alpha = 4.13°$ can be seen in Figure 54. The other two angles of attack are not discussed in the text, but are located in Figure 66 ($\alpha = -2.04°$) and Figure 67 ($\alpha = 8.22°$), Appendix D. The hot-wire analysis for the 24" Houck Configuration, $\delta = 20°$ up at $\alpha = 4.13°$ can be

seen in Figure 55. The other two angles of attack are not discussed in this section, but are located in Figure 68 ($\alpha = -2.04°$) and Figure 69 ($\alpha = 8.22°$), Appendix D.

The hot-wire analysis for aileron deflection variations are plotted using the same scales as the hot-wire analysis for the original 24" Houck Configuration. By keeping the scales constant within each type of plot, it is easier to compare and contrast using the colors of the contours without referring back to a different legend for every vorticity or turbulence plot. The only scale that may change is the length of the 2 m/s reference vector. The length of this vector is dependent on the magnitude of the v & w vectors shown in each plot.

The hot-wire analysis at $\alpha = 4.13°$ for the 24" Houck Configuration, $\delta = 20°$ down, can be seen in Figure 54. The flow behind the wing is similar to that of the $\alpha = 4.13°$ for the $\delta = 0°$ case. There is a slightly stronger wing-tip vortex (clockwise) for the variation with the ailerons deflected 20° down. This is because it produces more lift due to the "cambered" effect on the wings. There is also a second vortex that forms off of the outer edge of the deflected aileron. This vortex is the stronger of the two existing vortices and approaches a rotation of -0.9 rad/s (clockwise). The addition of this vortex and the increased strength of the original vortex result in a slight increase in turbulence from the original test for $\delta = 0°$. The deflection of the aileron directs the flow directly behind the aileron downward and contains more turbulence that slows the flow down. This is a primary reason for the increase in drag in this variation from the original configuration. This area directly behind the deflected aileron is the slowest region with respect to the *u*-component of velocity aft of the wing.

The hot-wire analysis at $\alpha = 4.13°$ for the 24" Houck Configuration, $\delta = 20°$ up, can be seen in Figure 55. The flow behind the wing is slightly similar to that of the $\alpha = 4.13°$ for the $\delta = 0°$ case. The wing-tip vortex strongly resembles the wing-tip vortex of the original configuration in both strength and size. However, there is a second vortex that forms off of the outer edge of the deflected aileron. This vortex rotates in the opposite direction and approaches a rotation of 0.5 rad/s (counter-clockwise) at its core. The vortex is rotating counter-clockwise because it has formed at the outer edge of the aileron/wing section that is producing negative lift due to the upward deflection. The addition of this vortex and the increased strength of the original vortex result in a slight increase in turbulence from the original test for $\delta = 0°$. The deflection of the aileron directs the flow directly behind the aileron upward and causes more turbulence to form in that region. The u-component of velocity is the smallest at the core of the counter-clockwise vortex.

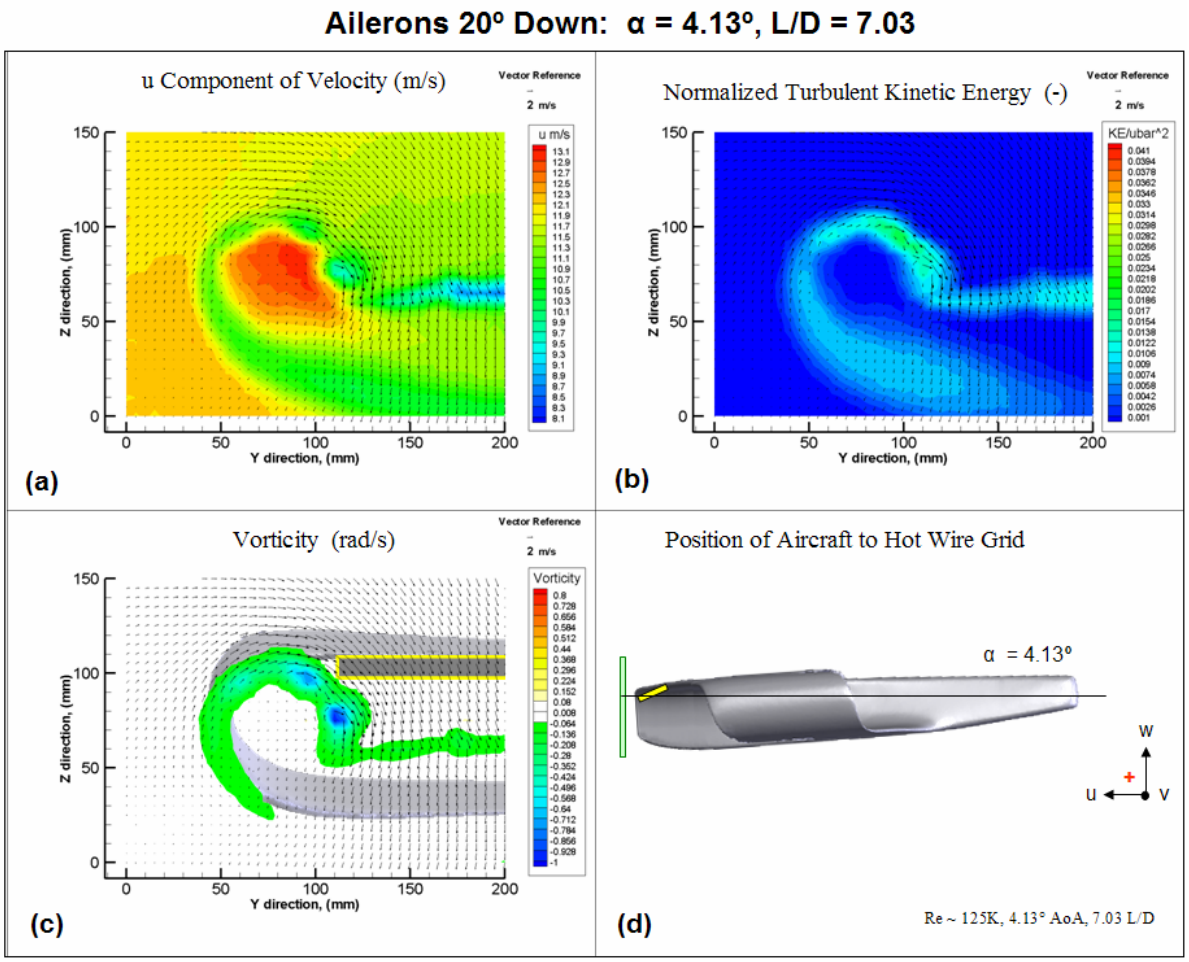

Figure 54: Hot-Wire Analysis of 24" Houck Configuration, δ = 20º down, α = 4.13º, L/D = 7.03

(a) *u*-component contours with *v* & *w* Vectors, (b) Non-dimensional turbulence contours with *v* & *w* vectors,
(c) Vorticity behind wing with *v* & *w* vectors, (d) Position of hot-wire grid with respect to the 24" Houck Configuration

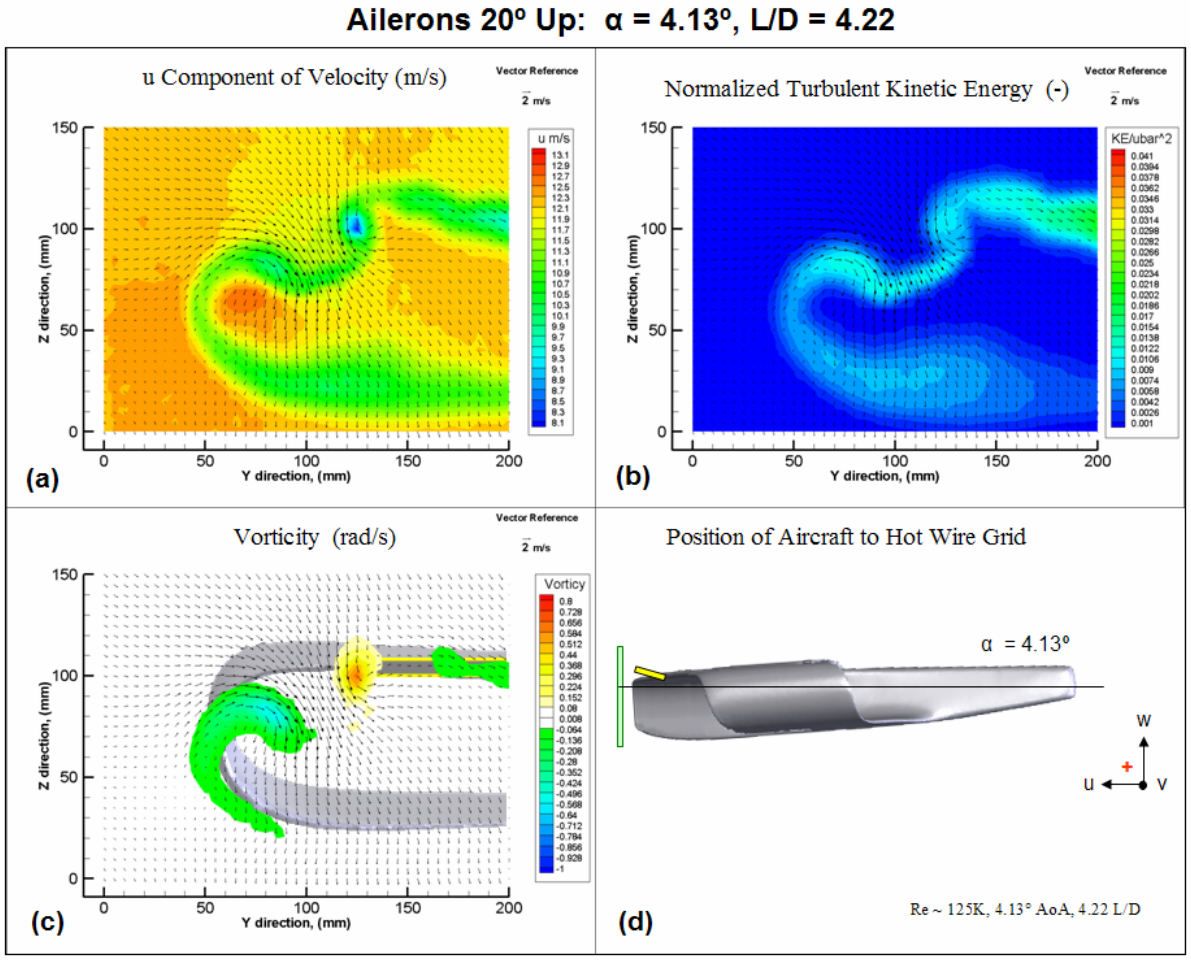

Figure 55: Hot-Wire Analysis of 24" Houck Configuration, δ = 20º up, α = 4.13º, L/D = 4.22

(a) *u*-component contours with *v* & *w* Vectors, (b) Non-dimensional turbulence contours with *v* & *w* vectors,
(c) Vorticity behind wing with *v* & *w* vectors, (d) Position of hot-wire grid with respect to the 24" Houck Configuration

4.4 Original Configuration with Changes to Flow Guides

4.4.1 Wind Tunnel Balance Data – Alpha Sweeps

The third set of tests performed was on variations of the original 24" Houck Configuration with respect to the flow guides. A 1" cut in the flow guide was made for the first variation. For the second variation, the 1" gap was expanded to 2". The final variation of the 24" Houck model had the flow guides completely removed. The variation without flow guides was to provide a reference model from which to gage changes in performance. An alpha sweep from approximately -15º to 5º in 1º increments, was performed at three different Reynolds numbers: Re ≈ 80K (20 mph, 8.94 m/s), Re ≈ 125K (30mph, 13.41 m/s), and Re ≈ 170K (40 mph, 17.88m/s). These results are then compared to the data from the original 24" Houck Configuration data. The reference area used to calculate the aerodynamic coefficients for the original 24" Houck Configuration, the 1" flow guide cut variation, and the 2" cut flow guide variation was 307 in^2 with a wingspan of 23.58". The reference area used for the variation without flow guides was 254 in^2 with a wingspan equal to 20.33". The large fluctuation in reference area is due to the inverse taper ratio of the Houck model (the root chord is shorter than the tip chord). A summary of the results can be seen in Table 10. A discussion of each performance parameter will be discussed in this section with its corresponding figure.

Table 10: Aerodynamic Performance of 24" Houck Configuration with Flow Guide Cuts

			Min Drag			Zero Lift	Slopes	
Configuration	**Re (-)**	**S (in^2)**	**C_{Do} (-)**	**α (°)**	**D (lbs)**	**$\alpha_{0\ Lift}$ (°)**	**$C_{L\alpha}$ (/°)**	**$C_{m\alpha}$ (/°)**
Orig. 24" Houck	80K	307	0.0281	-0.90	0.0563	-2.32	0.0488	-0.0061
Orig. 24" Houck	125K	307	0.0229	-1.01	0.1123	-2.59	0.0457	-0.0056
1" Cut in FG	80K	307	0.0264	-1.30	0.0550	-2.68	0.0525	-0.0064
1" Cut in FG	125K	307	0.0230	-1.90	0.1167	-2.80	0.0407	-0.0054
2" Cut in FG	80K	307	0.0267	-0.10	0.0530	-2.68	0.0496	-0.0069
2" Cut in FG	125K	307	0.0224	-1.10	0.1112	-2.90	0.0462	-0.0058
No Flow Guide	80K	254	0.0296	-1.20	0.0473	-2.72	0.0576	-0.0078
No Flow Guide	125K	254	0.0239	-1.85	0.0990	-3.02	0.0469	-0.0069

			Max Range					
Configuration	**Re (-)**	**S (in^2)**	**L/D (-)**	**α (°)**	**CL (-)**	**CD (-)**	**L (lbs)**	**D (lbs)**
Orig. 24" Houck	80K	307	6.50	4.30	0.286	0.044	0.6090	0.0940
Orig. 24" Houck	125K	307	7.43	4.20	0.293	0.039	1.5523	0.2102
1" Cut in FG	80K	307	6.80	3.80	0.295	0.043	0.5493	0.0811
1" Cut in FG	125K	307	7.50	3.70	0.263	0.035	1.3378	0.1794
2" Cut in FG	80K	307	6.93	3.70	0.295	0.043	0.5590	0.0809
2" Cut in FG	125K	307	7.68	3.50	0.270	0.035	1.3597	0.1772
No Flow Guide	80K	254	6.67	4.50	0.386	0.058	0.5865	0.0881
No Flow Guide	125K	254	7.45	3.60	0.303	0.041	1.1852	0.1595

			Max Endurance					
Configuration	**Re (-)**	**S (in^2)**	**$C_L^{(3/2)}/C_D$ (-)**	**α (°)**	**C_L (-)**	**C_D (-)**	**L (lbs)**	**D (lbs)**
Orig. 24" Houck	80K	307	3.75	6.70	0.420	0.112	0.8374	0.1452
Orig. 24" Houck	125K	307	4.20	5.30	0.340	0.081	1.7754	0.2539
1" Cut in FG	80K	307	4.16	6.30	0.432	0.104	0.7577	0.1170
1" Cut in FG	125K	307	4.09	5.80	0.345	0.084	1.7927	0.2546
2" Cut in FG	80K	307	4.05	5.50	0.375	0.093	0.7657	0.1168
2" Cut in FG	125K	307	4.38	5.00	0.344	0.079	1.8161	0.2542
No Flow Guide	80K	254	4.30	5.90	0.450	0.105	0.6823	0.1053
No Flow Guide	125K	254	4.35	5.40	0.375	0.086	1.5948	0.2270

Figure 56 plots the drag polar, C_D vs. C_L, for the 24" Houck Configuration and variations with alterations to the flow guides for two different Reynolds numbers (80K and 125K). The variation without flow guides had the highest value for C_{Do} at both

Reynolds numbers, but this is deceiving because of the reference area used for calculating the coefficients differed from the other variations. Even though it has the highest value of CD_o, it produces the least amount of parasite drag of the four variations. In fact, as the surface area of the flow guides decreases, the parasite drag decreases as well.

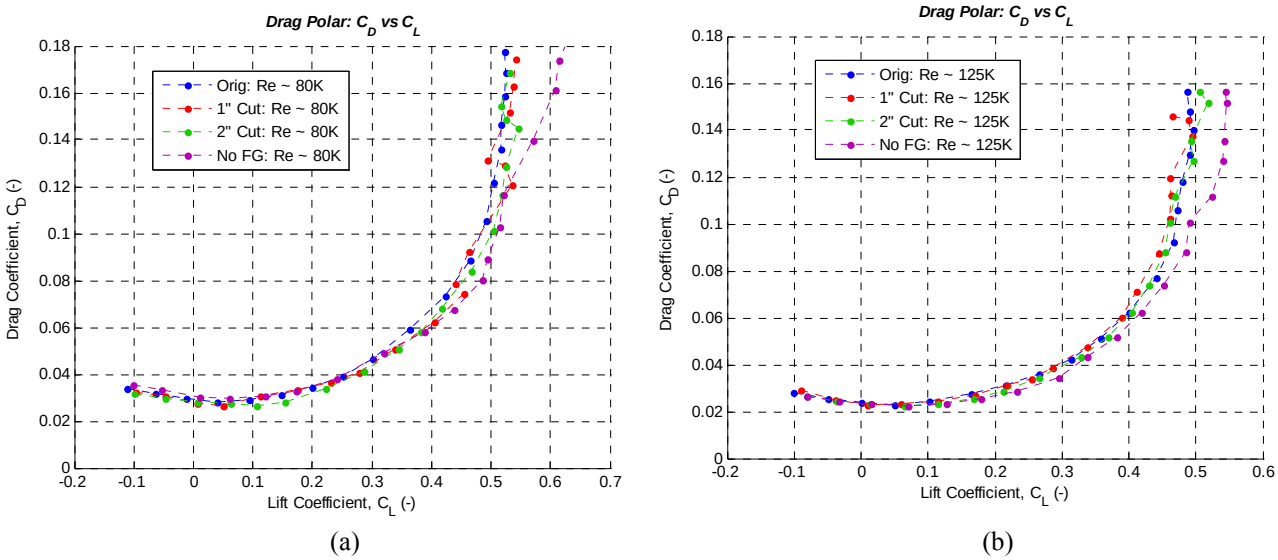

(a) (b)

Figure 56: Drag Polar – 24" Houck Configuration with Flow Guide Variations

(a) Re ≈ 80K, (b) Re ≈ 125K

Figure 57 plots the C_m vs. α for the flow guide variations at two different Reynolds numbers (80K and 125K). All four variations show longitudinal static stability at the Reynolds numbers tested. As more material is cut away from the flow guides, the angle of attack where $C_m = 0$ decreases while the longitudinal static stability of the model increases, although only slightly.

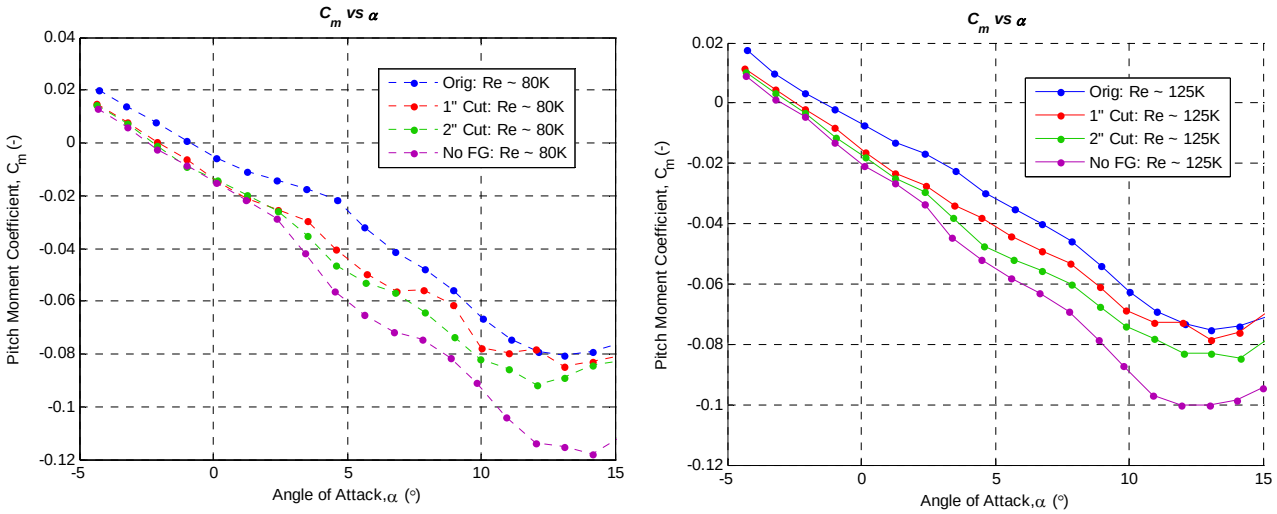

Figure 57: Pitch Moment Coefficient vs. α – 24" Houck Configuration with Flow Guide Variations

(a) Re ≈ 80K, reference location of CG used, (b) Re ≈ 125K, reference location of CG used

The lift coefficient, C_L, is plotted versus α for two different Reynolds numbers (80K and 125K) in Figure 58. The angle of attack that produces zero lift decreases as pieces of the flow guide are cut away, although the change is not drastic. At Re ≈ 80K, the value for $\alpha_{0\ Lift}$ ranges from -2.32° for the original 24" Houck variation to -2.72 for the variation with no flow guides. Just as in earlier tests, the onset of stall is never fully achieved for the angle of attack range tested. The lift curve slopes are also slightly affected by the alteration of the flow guides, but most of the variation can be attributed to the increased flexing of the wings at higher angles of attack. This is because in the original configuration, the flow guides supported the wings at the tips and gave them strength. Once the flow guides were cut, the wings were more likely to flex with higher speeds and angles of attack. The lift curve slopes are almost identical at lower angles of attack until they start to diverge around α = 3°.

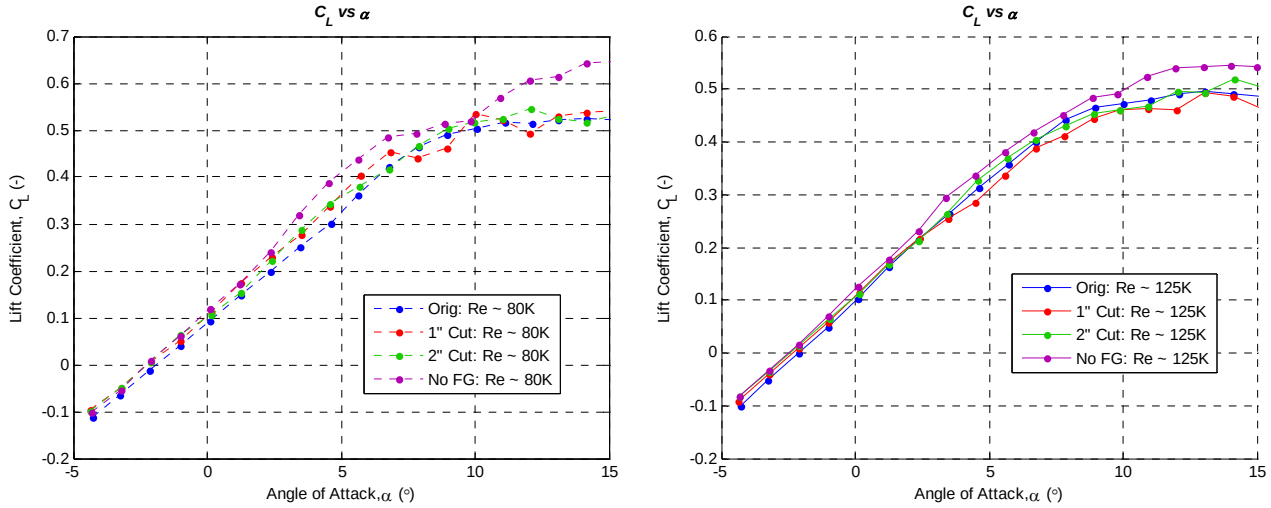

(a) (b)

Figure 58: Lift Coefficient vs. α – 24" Houck Configuration with Flow Guide Variations

(a) Re ≈ 80K, (b) Re ≈ 125K

A plot of the lift-to-drag versus angle of attack for the flow guide variations can be seen in Figure 59. A summary of the results were shown in Table 10 and the percent of change from the model without flow guides can be seen in Table 11. The variation without flow guides is used as a reference point in order to see how the addition of flow guides affects the performance of the aircraft. At a Reynolds number of approximately 80K, the original Houck Configuration produces an L/D_{max} value 2.5% less than the model without flow guides. At Re ≈ 125K, the original Houck Configuration produces an L/D_{max} value 0.3% less than the model without flow guides. While at first glance this doesn't look promising, the gap in performance is closing as Reynolds number increases. If this trend continues, the performance of the original Houck Configuration could possibly surpass (or level out asymptotically) the performance of the variation without flow guides at a higher Reynolds number. Interestingly, the two variations with strips cut

out of the flow guides (1” cut and 2” cut) out perform the model without flow guides at both tested Reynolds numbers. This is likely due to a reduction in the parasite drag from cutting away wing material, while still retaining the overall flow guide design. The gaps created by cutting the flow guides may be small enough so that the airflow around the wings is not greatly affected. However, as the Reynolds number increases between the two tests, the percent improvement over the model without flow guides decreases for both variations. Higher testing speeds (higher Reynolds numbers) could not be achieved in this study because of the loss of structural integrity of the models due to the flow guide alterations. However, it would be of high interest to test a form of this model at higher Reynolds numbers to further analyze this trend.

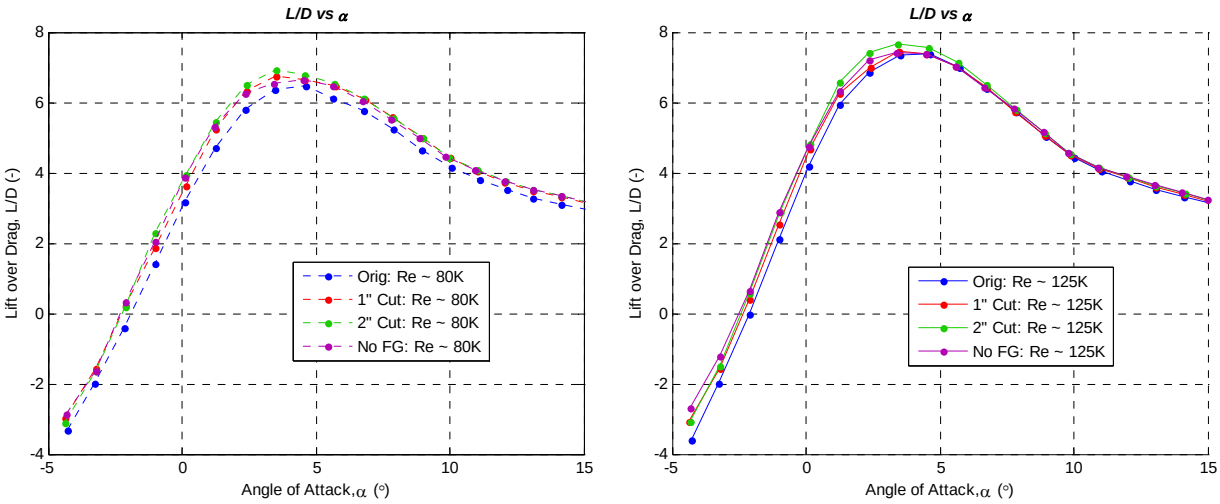

(a) (b)

Figure 59: Lift-to-Drag vs. α – 24” Houck Configuration with Flow Guide Variations

(a) Re ≈ 80K, (b) Re ≈ 125K

Table 11: Percent Change in Performance of Variations of 24" Houck due to Flow Guide Alterations as Compared to Variation without Flow Guides

		% Change	
Configuration	**Re (-)**	**L/D_{max}**	**$C_L^{(3/2)}/C_{Dmax}$**
Orig. 24" Houck	80K	-2.5%	-12.8%
1" Cut in FG	80K	1.9%	-3.3%
2" Cut in FG	80K	3.9%	-5.8%
No Flow Guide	80K	-	-
Orig. 24" Houck	125K	-0.3%	-3.4%
1" Cut in FG	125K	0.7%	-6.0%
2" Cut in FG	125K	3.1%	0.7%
No Flow Guide	125K	-	-

In Figure 60, the lift-to-drag data has been plotted versus aircraft weight. For any of the four models with flow guide variations, the best speed for maximizing range while flying SLUF at sea level can be determined. Once a desired aircraft weight is chosen, the velocity that provides the best L/D can be determined. Trend lines have been added so that interpolation between the data at different speeds can be done. This graph allows a comparison to be made between different model variations. Some of the Reynolds number trends that were discussed earlier can be seen. The decreasing performance gap between the model without flow guides and the two variations with strips cut from the flow guides can be seen from Re ≈ 80K to Re ≈ 125K. The decreasing performance gap between the original Houck configuration and the model without flow guides is not visible in this plot of the two data points. The decrease in lift seen at Re ≈ 125K (30 mph) for the model without flow guides has shifted the data point to the left and kept the performance gap between the two variations at a relatively constant value between the two tested Reynolds numbers. This shows that the gap may not be decreasing as

previously thought, but the fact remains that more tests at higher Reynolds numbers must be performed in order to gain a better understanding of the relationship between the two model variations.

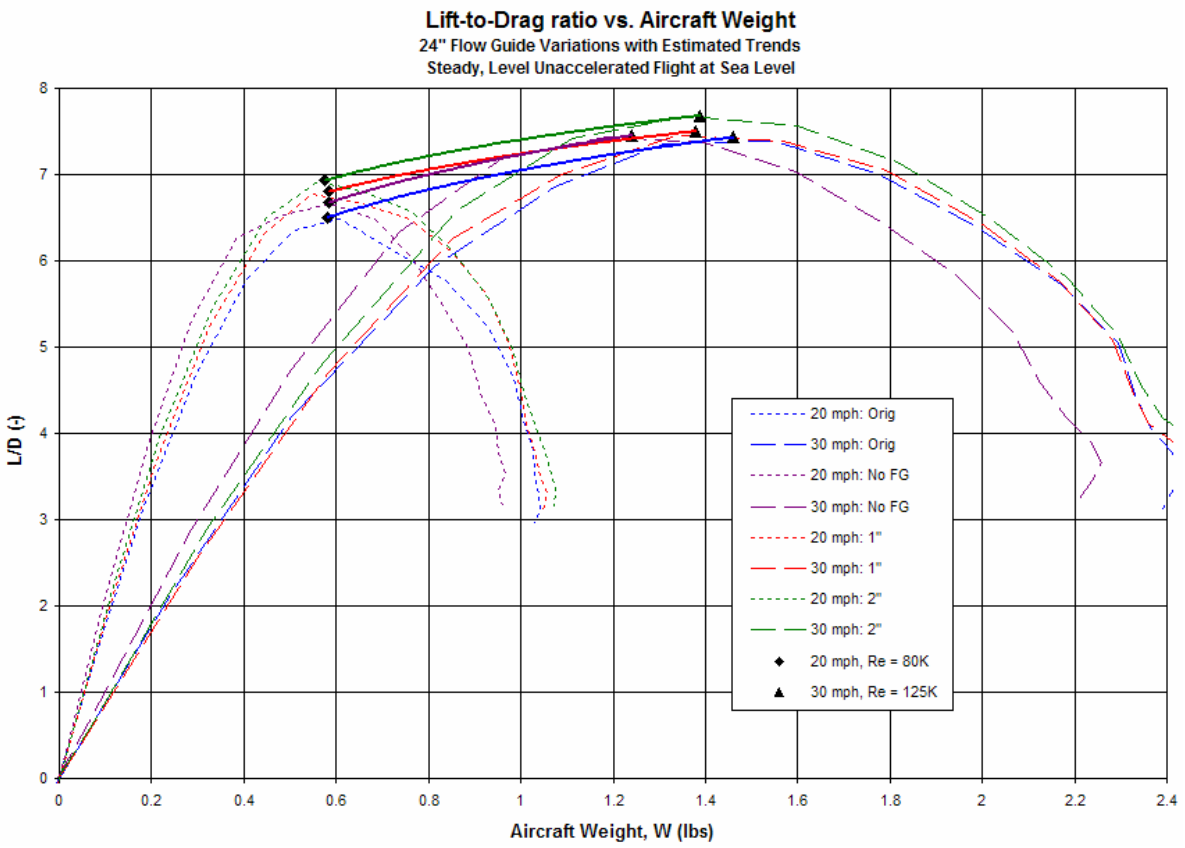

Figure 60: L/D vs. Weight for SLUF at Sea Level – 24" Houck with Flow Guide Variations

A comparison of the induced drag for the 24" Houck Configuration with and without flow guides can be seen in Table 12. For a Reynolds number of 80K, the original model produces less induced drag (0.034 lbs) than the model with out flow guides (0.043 lbs) at the maximum L/D value. For a Reynolds number of 125K, the original model produces more induced drag (0.088 lbs) than the model without flow guides (0.066 lbs).

It is tough to make a direct comparison between these two models, because they are producing different amounts of lift. When looking at a ratio of lift-to-induced drag, the original model produces less induced drag per unit of lift for the lower Reynolds number, and roughly the same amount of induced drag per unit lift at the higher Reynolds number. It would seem advantageous to produce less induced drag per unit lift, but the trend here is opposite to the closing performance gap seen in the maximum lift-to-drag comparisons. More tests are needed at higher Reynolds numbers in order to gain some perspective into this relationship. Ultimately, improving the L/D ratio is desirable.

Table 12: Comparison of Induced and Parasite Drag – 24" Houck with and without Flow Guides

Configuration	Re (-)	L/D	C_{Do}	C_{Di}	C_{Di}/C_D	L (lbs)	D (lbs)	D_{min}	D_i	L/D_i
Orig. 24" Houck	80K	6.50	0.0281	0.0159	36.1%	0.609	0.094	0.060	0.034	17.93
Orig. 24" Houck	125K	7.43	0.0229	0.0165	41.9%	1.552	0.210	0.122	0.088	17.63
No Flow Guide	80K	6.67	0.0296	0.0283	48.9%	0.586	0.088	0.045	0.043	13.63
No Flow Guide	125K	7.45	0.0239	0.0168	41.2%	1.185	0.160	0.094	0.066	17.96

A plot of the $C_L^{3/2}/C_D$ versus angle of attack for the flow guide variations can be seen in Figure 61. These results can be used to determine which flow guide variation is best for optimizing endurance at a given Reynolds number. A summary of the results were shown in Table 10 and the percent of change from the model without flow guides can be seen in Table 11. At a Reynolds number of approximately 80K, the original Houck Configuration produces a $C_L^{3/2}/C_{Dmax}$ value 12.8% less than the model without flow guides. At Re ≈ 125K, the original Houck Configuration produces a $C_L^{3/2}/C_{Dmax}$ value 3.4% less than the model without flow guides. Once again, the performance gap between the two model variations is decreasing as the Reynolds number increases. More

testing at higher Reynolds numbers is recommended. The original Houck configuration is outperformed by the other three flow guide variations at Re ≈ 80K, but closes the gap and surpasses the 1" cut variation at Re ≈ 125K.

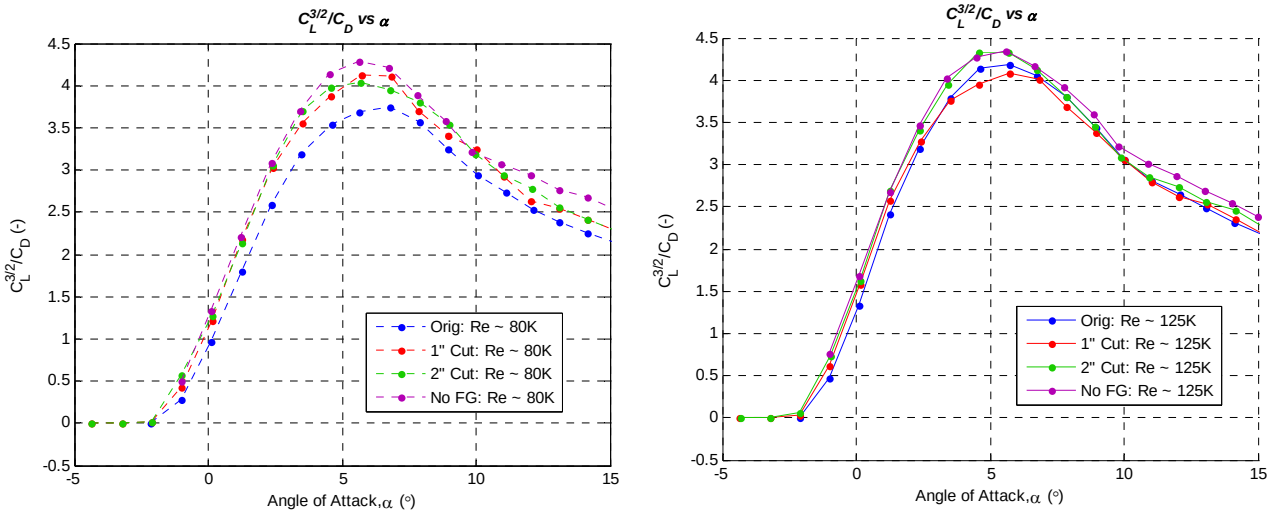

(a) (b)

Figure 61: $C_L^{3/2}/C_D$ vs. α – 24" Houck Configuration with Flow Guide Variations

(a) Re ≈ 80K, (b) Re ≈ 125K

In Figure 62, the $C_L^{3/2}/C_D$ data has been plotted versus aircraft weight. For any of the four models with flow guide variations, the best speed for maximizing endurance while flying SLUF at sea level can be determined. In this plot, the performance gap in endurance decreases greatly from 30 mph (Re ≈ 80K) to 40mph (Re ≈ 125K). The performance of the 24" Houck Configuration increases the most out of the variations over this Reynolds number range. It is easy to see how the 24" Houck Configuration could surpass the other variations at a higher testing speed if this trend were to continue. However, this could only be determined with further testing.

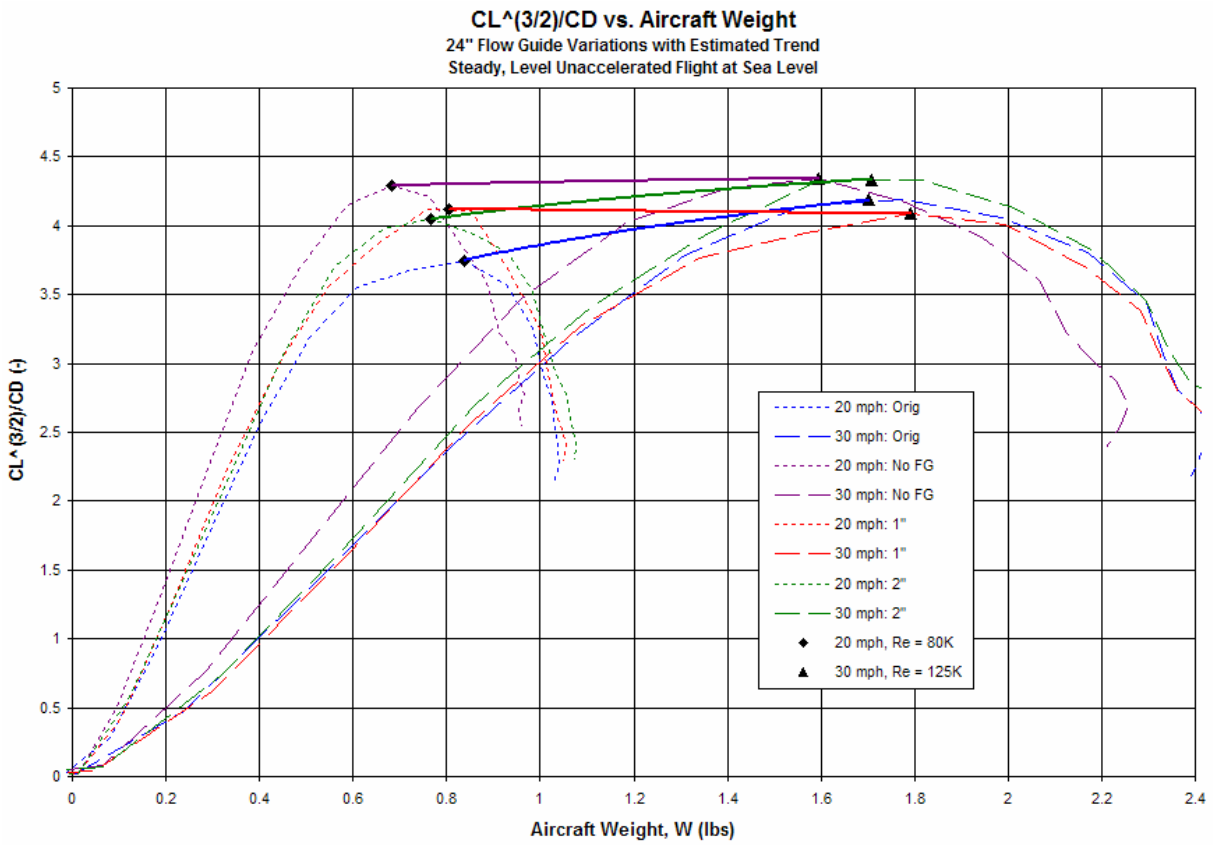

Figure 62: $C_L^{3/2}/C_D$ vs. Weight for SLUF at SL – 24" Houck with Flow Guide Variations

The effective aspect ratio, *e AR*, has been calculated for the four flow guide variations at Re ≈ 80K and 125K. This data can be seen in Table 13. The induced drag coefficient and lift coefficient data for each calculation was taken at L/D_{max} for all four variations. The effective aspect ratio for the original 24" Houck Configuration is 1.638 at Re ≈ 80K and 1.653 at Re ≈ 125K. For this range of Reynolds number, the effective aspect ratio is increasing as the Reynolds number increases. The 1" cut variation has a better effective aspect ratio than the original model at Re ≈ 125K, while the 2" cut variation has a better effective aspect ratio at both Reynolds numbers tested. A direct comparison of the aerodynamic coefficients for the original model and the model without

flow guides is difficult to make because of the differences in wingspan and reference area between the two variations. The lift-to-drag ratio is one way to compare the models, because the reference area is cancels out, however, the two models still have different aspect ratios. The first three variations have a wingspan of 23.58" and a reference area of 307 in^2, while the variation without flow guides has a wingspan of 20.33" and a reference area of 254 in^2. The aspect ratio of each model was not calculated due to the numerous definitions available for different wing configurations (e.g., monoplane, biplane, and joined-wing).

Table 13: Effective Aspect Ratio of 24" Houck Configuration with Flow Guide Cuts

Configuration	Re (-)	eAR (-)
Orig. 24" Houck	80K	1.638
1" Cut in FG	80K	1.631
2" Cut in FG	80K	1.746
No Flow Guide	80K	1.678
Orig. 24" Houck	125K	1.653
1" Cut in FG	125K	1.825
2" Cut in FG	125K	1.819
No Flow Guide	125K	1.742

4.4.2 Hot-Wire Analysis

Using the AFIT low-speed wind tunnel, hot-wire analysis at three angles of attack ($\alpha \approx -2°$, 4°, and 8°) was performed on the 24" Houck Configuration without flow guides. The tests were performed at a speed of approximately 30 mph (13.41 m/s), resulting in a Reynolds number of around 125K. A summary of the lift-to-drag ratios and aerodynamic coefficients at the tested values of α can be seen in Table 14. These angles were chosen

so that comparisons to the 24" Houck Configuration with full flow guides could be made. The lift-to-drag ratios and aerodynamic coefficients at the given angles of attack have been taken from the prior tests conducted in this section and can be seen in Table 34, Appendix C. The hot-wire analysis for the 24" Houck Configuration with flow guides has already been presented and can be seen in Figure 44, Figure 45, and Figure 46.

Table 14: Aerodynamic Data at Angles of Attack used in Hot-Wire Tests for 24" Houck Configuration with No Flow Guide

Configuration	Re (-)	α (°)	L/D (-)	C_L (-)	C_D (-)
Orig. 24" Houck	80K	-2.04	0.15	0.003	0.024
Orig. 24" Houck	80K	4.13	7.37	0.293	0.040
Orig. 24" Houck	80K	8.22	5.49	0.450	0.082
No Flow Guide	80K	-2.13	0.78	0.019	0.024
No Flow Guide	80K	4.13	7.39	0.324	0.044
No Flow Guide	80K	8.22	5.53	0.466	0.085

The hot-wire analysis for the variation without flow guides are plotted using the same scales as the hot-wire analysis for the original 24" Houck Configuration. The hot-wire analysis at $\alpha = -2.13°$ for the 24" Houck Configuration with no flow guides can be seen in Figure 63. The hot-wire results are similar to the results from the original 24" Houck Configuration with the exception of the area around the absence of the flow guides. This is the only area that will be discussed. The biggest difference between the results of the two model variations is the additional vortex that forms at the wingtips, one on the upper wing and one on the lower wing. In the results for the original Houck Configuration, only one vortex ever formed and it took the shape of the flow guide. At this angle of attack, very little lift is being created. As a result, the vortices that are

formed on the tips of the upper and lower wing are small still (max vorticity ≈ -0.4 rad/s (clockwise)). Notice that the stronger vortex forms on the lower wing. The lower wing showed signs of separation/stall in the flow visualization before the upper wing did for the swept alpha range. This suggests that the lower wing is producing a majority of the lift at angles of attack less than 5°, before separation occurs, and is confirmed here by the resulting strengths of the wingtip vortices. The vortices create turbulence which results in slower streamwise (u-component) velocities in that region.

The hot-wire analysis at $\alpha = 4.13°$ for the 24" Houck Configuration with no flow guides can be seen in Figure 64. 4.13° is close to being the most efficient angle of attack for maximizing range. With the increase in lift, when compared to $\alpha = -2.13°$, the vortices grow both in strength (max vorticity ≈ -0.9 rad/s) and size. Once again, the stronger vortex forms behind the lower wing. This angle of attack is close to where separation starts to form on the lower wing, but it hasn't yet started to decrease the lift created by the lower wing, resulting in a stronger wingtip vortex when compared to the upper wing. The onset of separation on the lower wing can be seen in the turbulence plot. There is also turbulence created in the regions of the wingtip vortices. At the core of the lower vortex, the fastest streamwise velocity can be seen, 12.8 m/s, but the speed quickly decreases away from the center of the vortex core.

The hot-wire analysis at $\alpha = 8.22°$ for the 24" Houck Configuration with no flow guides can be seen in Figure 65. The upper and lower wingtip vortices still appear behind the wing. The lower vortex has decreased in strength (from -0.9 rad/s to -0.65 rad/s), while the upper vortex has increased in strength (-0.75 rad/s to -0.9 rad/s). This is

a signal that the majority of the lift is now being produced by the upper wing. At this angle of attack, separation has fully developed over the lower wing (as seen in the flow visualization). This can be seen in both the turbulence plots (high turbulence above the lower wing) and in the *u*-component of velocity plot (lower speeds above the lower wing). The turbulence plot shows a large circular region of heavy turbulence (Ke ≈ 0.41) near the location of the lower wing vortex. The high turbulence results in a very slow region of streamwise flow (only 9.3 m/s).

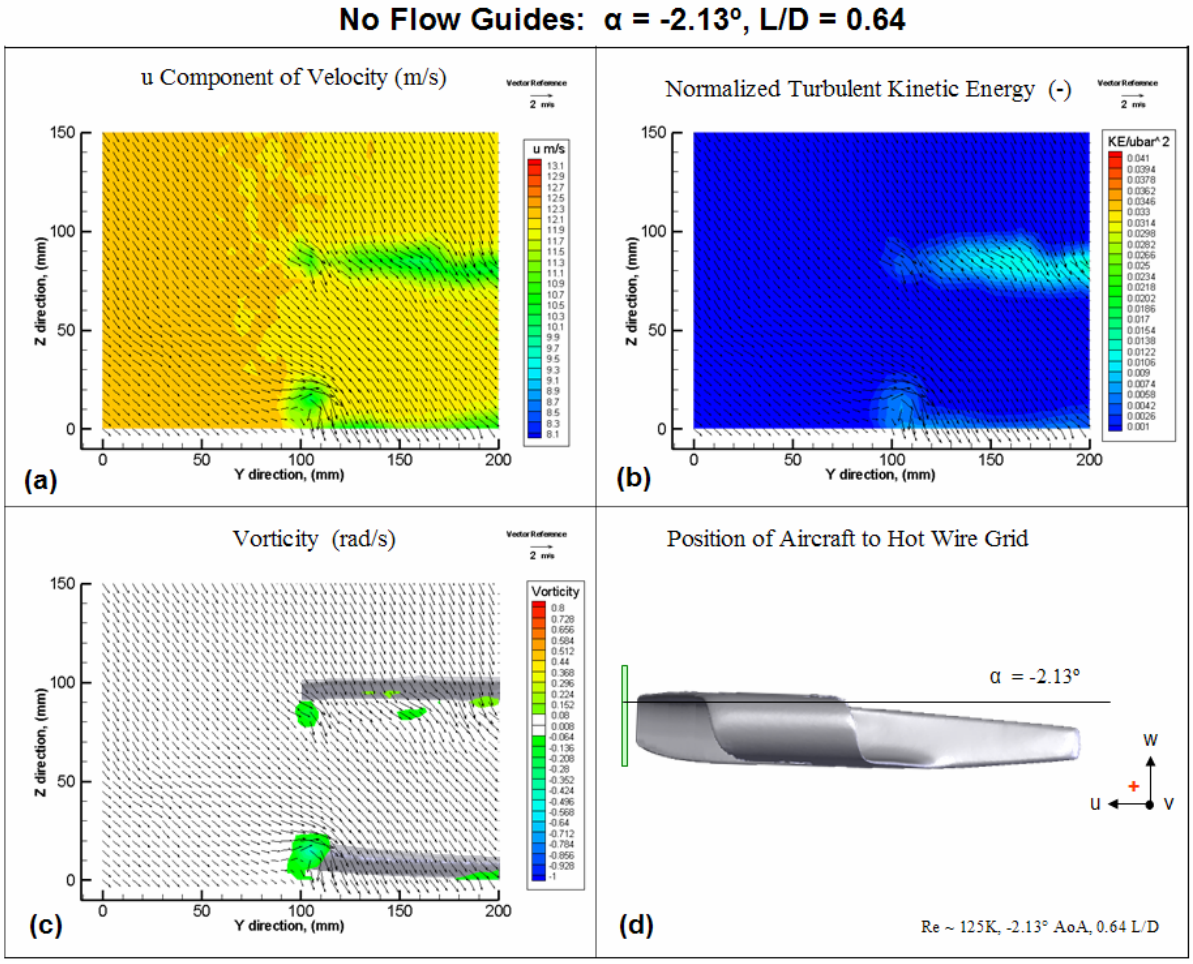

Figure 63: Hot-Wire Analysis of 24" Houck Configuration, No Flow Guides, α = -2.13°, L/D = 0.64

(a) *u*-component contours with *v* & *w* Vectors, (b) Non-dimensional turbulence contours with *v* & *w* vectors,
(c) Vorticity behind wing with *v* & *w* vectors, (d) Position of hot-wire grid with respect to the 24" Houck Configuration

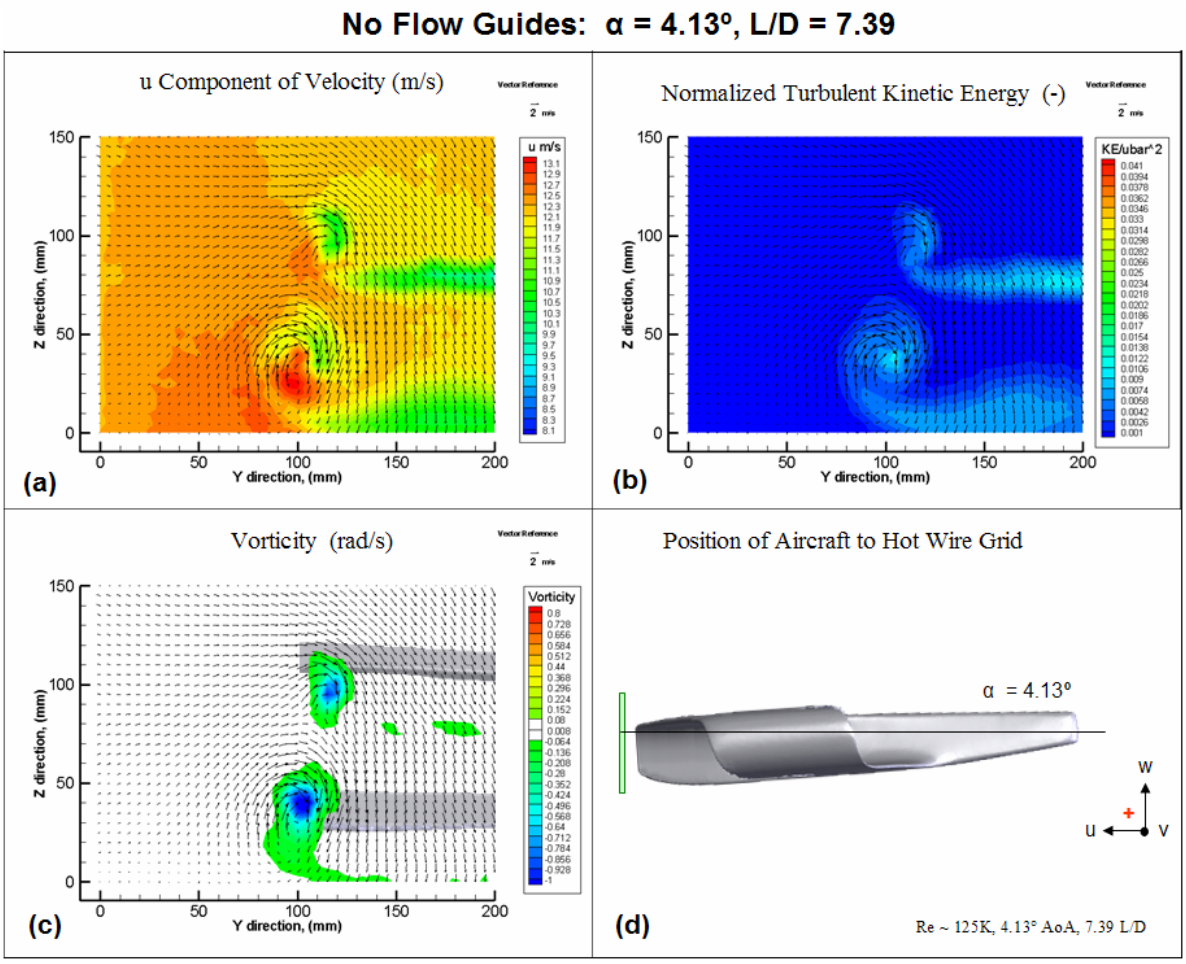

Figure 64: Hot-Wire Analysis of 24" Houck Configuration, No Flow Guides, α = 4.13º, L/D = 7.39

(a) *u*-component contours with *v* & *w* Vectors, (b) Non-dimensional turbulence contours with *v* & *w* vectors,
(c) Vorticity behind wing with *v* & *w* vectors, (d) Position of hot-wire grid with respect to the 24" Houck Configuration

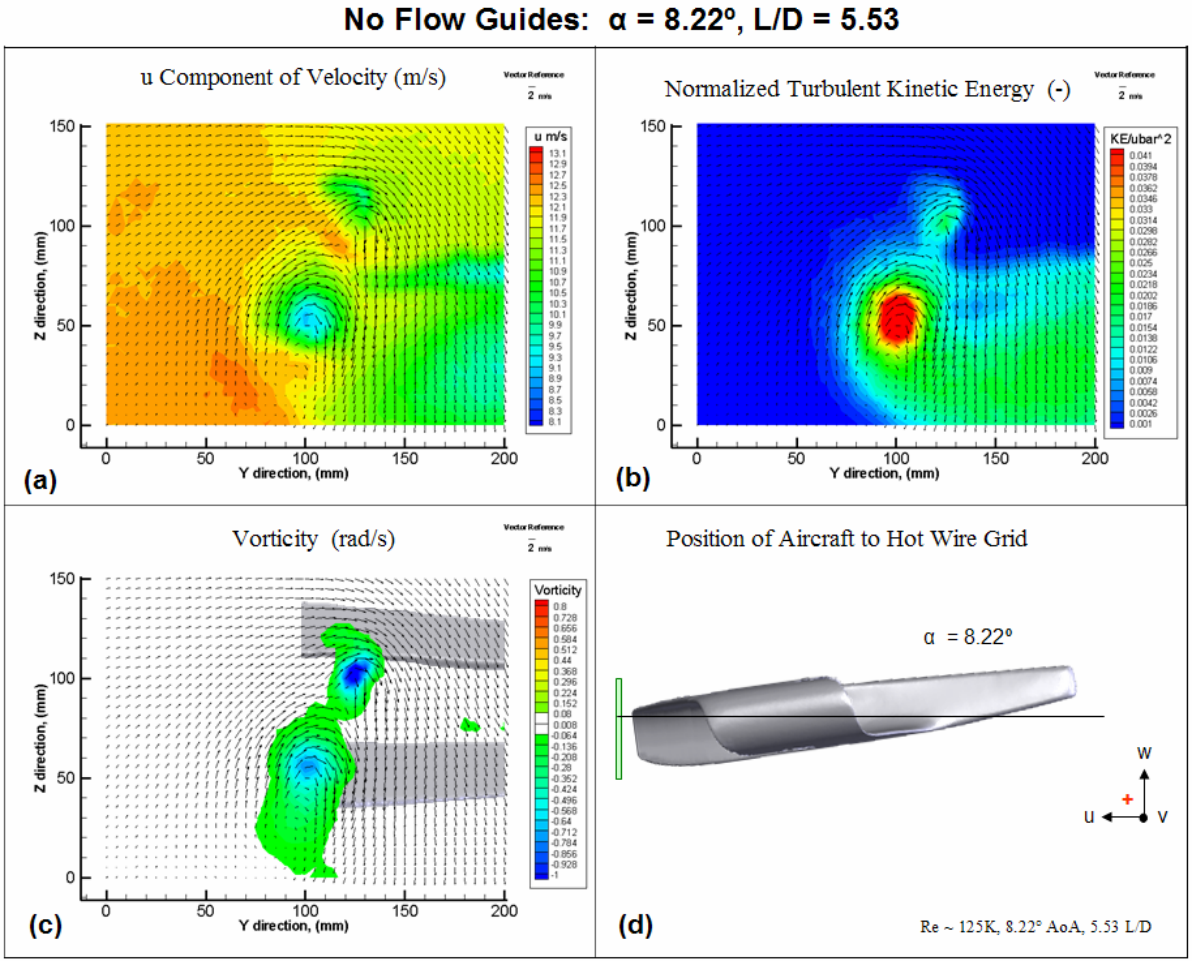

Figure 65: Hot-Wire Analysis of 24" Houck Configuration, No Flow Guides, α = 8.22, L/D = 5.53

(a) *u*-component contours with *v* & *w* Vectors, (b) Non-dimensional turbulence contours with *v* & *w* vectors,
(c) Vorticity behind wing with *v* & *w* vectors, (d) Position of hot-wire grid with respect to the 24" Houck Configuration

V. Conclusions and Recommendations

5.1 Conclusions of Research

The purpose of this study was to analyze the aerodynamic performance of the 24" Houck Configuration and the Houck Lifting Foil concept. It has been shown that the 24" Houck Configuration is capable of values for L/D_{max} equal to 6.50 at Re ≈ 80K, 7.43 at Re ≈ 125K, and 8.02 at Re ≈ 170K. These are comparable to historical L/D values as shown previously in Figure 13 and have the potential to increase with optimization of the aircraft fuselage, wing configuration, and testing at higher Reynolds numbers. Maximum values of $C_L^{3/2}/C_D$ were shown to be equal to 3.75 at Re ≈ 80K, 4.20 at Re ≈ 125K, and 4.53 at Re ≈ 170K. It has also been shown that at Reynolds numbers of approximately 80K and 125K, the 24" Houck Configuration shows longitudinal, directional, and lateral static stability.

When compared to the variation without flow guides, the 24" Houck Configuration was shown to have a 2.5% decrease in L/D_{max} at Re ≈ 80K and a 0.3% decrease at Re ≈ 125K. It was also shown to have 12.8% decrease in $C_L^{(3/2)}/C_{Dmax}$ at Re ≈ 80K and a 3.4% decrease at Re ≈ 125K. For both cases, maximizing range and endurance, the gap in performance between the 24" Houck Configuration and the model without flow guides decreases as the Reynolds number increases. Further testing is needed to determine what would happen at higher Reynolds numbers.

The effective aspect ratio, *e AR*, was calculated to be 1.6375 at Re ≈ 80K and 1.653 at Re ≈ 125K. The designed flow guides proved to be successful in combining the upper and lower wing-tip vortices into a single vortex. The flow guides alter what would

be two smaller compact vortices and instead produce a slightly larger, spread out vortex which follows the curve of the flow guide. Ultimately, evidence of improvements in aerodynamic efficiency will need to be shown before other claims of the design are demonstrated to be fully successful.

5.2 Recommendations for Future Research

It is recommended to continue testing the Houck Lifting Foil concept in order to better understand the design and how it works. Both experimental wind tunnel testing as well as CFD analysis is suggested. Experimentally, a more generic and geometrically specified baseline model with interchangeable flow guides should be tested in order to determine the validity of the patent claims. The model should be constructed with wind tunnel testing in mind and built to withstand higher speeds and angles of attack. This will allow further analysis into the performance of a Houck aircraft at higher Reynolds numbers. If possible, use the same wingspan and planform area for each flow guide variation tested. Flow guides with varying camber should also be tested to determine if there are any optimal layouts. CFD analysis should also be continued in order to compare to experimental results and explore areas that are not as easily tested in an experimental setting.

Appendix A: 10 lb Balance Dimensions

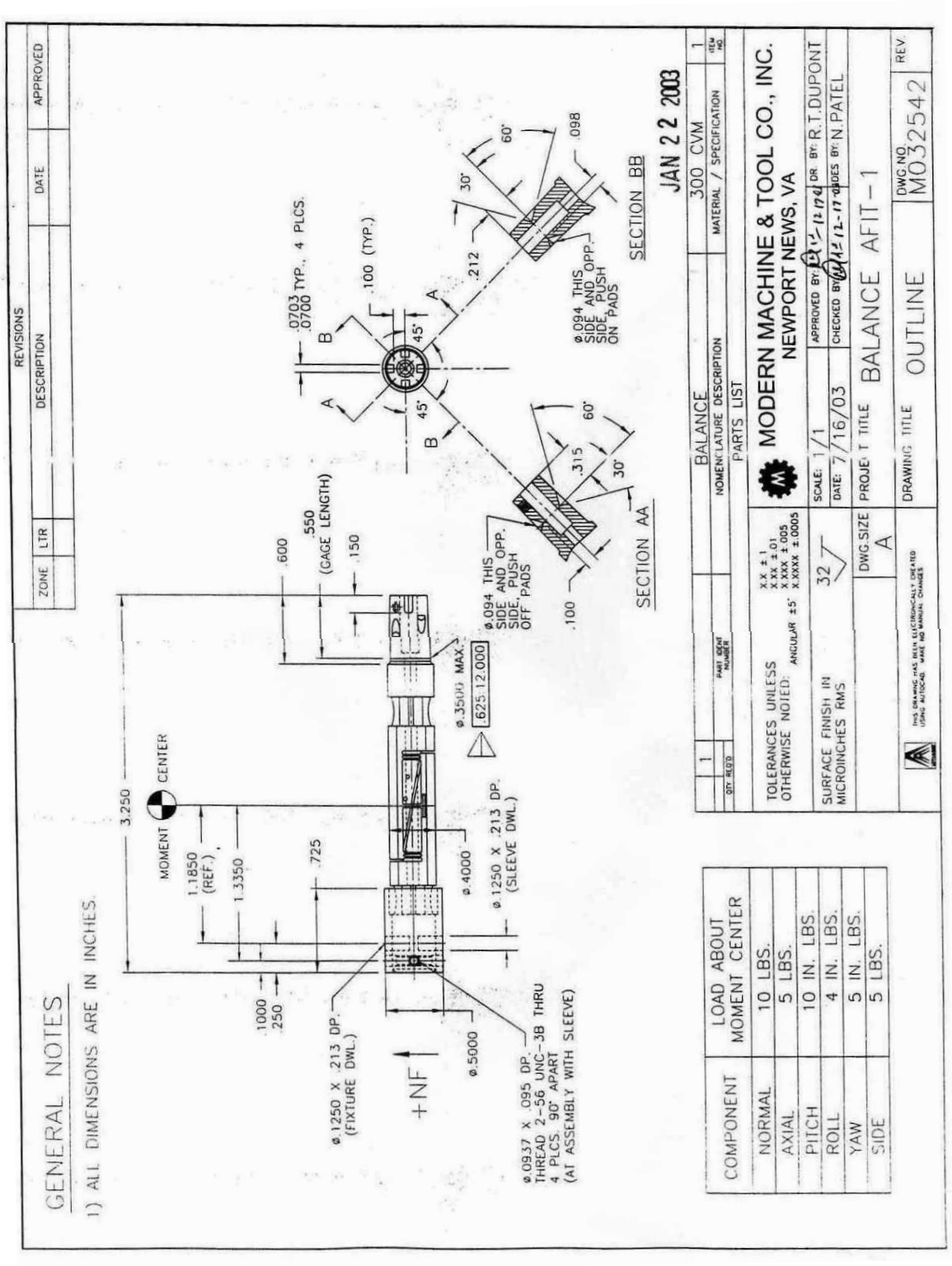

Appendix B: *MATLAB* 10 lb Balance Code

```
%************************************************************************
%************************************************************************
%**********        Lt. Gebbie & Capt Anthony DeLuca    ******************
%******   Adapted for the Balance AFIT 1 by Lt. Rivera Parga **************
%*********     re-adapted by Troy Leveron, ENS, USNR    ******************
%**********     Calculation of Lift, Drag, Moments      ******************
%**********     FLEX WING, Prop OFF, ALPHA SWEEPS       ******************
%************************************************************************
%***********  re-adapted by 1Lt Michael Walker, ENY, USAF  ***************
%************************************************************************
%This Code will transfer measured Forces and Moments on the AFIT 1 balance to Wind
%(earth) centered frame of reference by correctiing for tare effects, balance
%interactions, and wind tunnel irregularities, then gives a file with all the
%corrected data

clear; clc; close all;
format long
%#########################################################################
%                          INPUT DECK
%FIRST FILL THE FOLLOWING INFORMATION (modified by M. Walker on 11 Sept, 2006)

Masskg=0.89825;                 % kgs - Mass of Houck configuration - (2 lbs)
T_room = mean([74.6]) + 459.67;           %deg R  ****Room Temperature on 14 Nov 2006****
P_barro = mean([28.8058]) * 0.4911541;     %Psi   ****Pressure on 14 Nov 2006****

load Houck_Nov_10lb_TARE_alpha_n8to10_B0.txt;              %tarefile tare.txt - CHANGE FOR EACH
TEST RUN
TareFile = Houck_Nov_10lb_TARE_alpha_n8to10_B0(:,1:9);

load Houck_Orig_10lb_30mph_alpha_n8to10_B0.txt;              %datafile .txt - CHANGE FOR EACH
TEST RUN
DataFile = Houck_Orig_10lb_30mph_alpha_n8to10_B0(:,1:9);

%Offset distances from the Mounting Block to the Model C.G.,%(inches)
Y_cmb =  0;
X_cmb = 2.13;                       %inches  (from origin @ balance center w/ + forward)
Z_cmb = 0.65;                       %inches  (from origin @ balance center w/ + down)

    % Requeried for the Solid body blockage corrections due to wing and fuselage

Body_Volume = 248.37/(12^3) ;      %(ft^3): FROM DR. TIM FRY'S CFD MODEL
Wing_Area = 307/(12^2);        %(ft^2): FROM DR. TIM FRY'S CFD MODEL
c_bar = 12.27/12;            % (ft): FROM DR. TIM FRY'S CFD MODEL
span = 23.58/12;             % (ft): FROM DR. TIM FRY'S CFD MODEL
root_chord = 5.56/12;        % (ft): FROM DR. TIM FRY'S CFD MODEL
%************************************************************************
% Requeried for the Pitching Moment Correction (NOT USED FOR HOUCK MODEL)

% l_t =  9/12;                        % ft = length from tail MAC to aircraft CG
% Span_t =(4+(6/16)) / 12;                % ft = horizontal span
% Tail_Area = (9.42962435) / 144;           % ft^2 =  horizontal tail area
```

```
%**********************************************************************
 %######################################################################
%II.-   Room Conditions and Model Specifics :
%       UNITS are in Ft, Sec, lbm, Psf, Rankine, fps
%######################################################################

Mass = (Masskg * 1000) * 0.0022046;                    %lbm (24 in Houck Model)
Gas_Const = 1716;                                  %ft-lbf/Slug-R
Density = (P_barro * 144)/(1716 * T_room);              %lbm/ft^3 or lbf-s^2/ft^4
Root_Chord = root_chord;                             %ft
Span = span;                                   %ft
Aspect_Ratio = Span^2 / Wing_Area;
Kinematic_Viscosity = .372e-6;                         %slug/ft-s
Speed_of_Sound = sqrt(1.4 * T_room * Gas_Const);          %fps

%######################################################################
%III.-     Solid body blockage corrections due to wing and fuselage
%######################################################################

K_1 = 0.9;
K_3 = 0.93;
delta = 0.1177;
Tau_1 = 0.83125;                % from page XXX in text - Figure XX
X_Section = (31/12)*(44/12);                         %ft^2
Wing_Volume = Body_Volume;                           %ft^3

Epsilon_sb_w = (K_1*Tau_1*Wing_Volume) / X_Section^(3/2);
Epsilon_sb_b = (K_3*Tau_1*Body_Volume) / X_Section^(3/2);
Epsilon_tot = Epsilon_sb_w + Epsilon_sb_b;
%Epsilon_tot = Epsilon_sb_w ;

%######################################################################
% III.-  Load the static tare data for the alpha sweep w/o the wind ,
%       separate each force from the file, and fit a 4th order poly
%       as an x-y plot (AoA vs.Force) for each of the 6 force sensors.
%######################################################################

FILE=TareFile(:,:);                % Pulls in tare data file

j=1;
k=1;
L=length(FILE);

for i=1:L                        %Run for all data points # of rows
   if i~=L                       %if current row is not last row, go to next
      NEXT=i+1;                     %set next equal to the value of the next row
      VALUE2=FILE(NEXT,1);          %set value2 as next row column 1
   else if i==L                  %unless the it is the last value
      VALUE2=50;                    %value2 set to 50 to end the sequence
   end
   end
   A(j,:)=FILE(i,:);              %set row j of A equal to row i of FILE
   VALUE1=FILE(i,1);                %set value1 equal to row i column 1 of FILE
   if VALUE1==VALUE2                %if value1 equals value2, go to next row
```

```
      j=j+1;
   else if VALUE1~=VALUE2            %if value1 and value2 are different check
      if length(A(:,1))<5            %if less than 5 values, ignored due to angle change
         j=1;
         clear A;
      else if length(A(:,1))>5       %if more than 5 values
            C=length(A(:,1));        %find length of A
            for m=1:9                %Average all rows of the like values in A
               B(k,m)=mean(A(4:C,m));    %disregarding first 3 for vibrations
            end
            j=1;
            k=k+1;
            clear A
      end
      end

   end
   end
end

if B(k-1,1)<B((k-2),1)
   B=B(1:(k-2),:)
end

tare=[B];

%_____________________________________End of inserted code
[row,col] = size(tare);

for k = 1:row;

theta_tare(k,:,:)   = tare(k,1).* (pi/180);
NF_tare(k,:,:)      = tare(k,4);
PM_tare(k,:,:)      = tare(k,5);
AF_tare(k,:,:)      = tare(k,6);
SF_tare(k,:,:)      = tare(k,7);
YM_tare(k,:,:)      = tare(k,8);
RM_tare(k,:,:)      = tare(k,9);

end

NF_poly = polyfit(theta_tare,NF_tare,4);
PM_poly = polyfit(theta_tare,PM_tare,4);
AF_poly  = polyfit(theta_tare,AF_tare,4);
SF_poly = polyfit(theta_tare,SF_tare,4);
YM_poly = polyfit(theta_tare,YM_tare,4);
RM_poly  = polyfit(theta_tare,RM_tare,4);
```

```
%#########################################################################
%IV.- Load the specific test run files,
%#########################################################################

clear ('AA','B','C','L')
%_____________________________________________

FILE=DataFile(:,:);                % Pulls in test data file

j=1;
k=1;
L=length(FILE);

for i=1:L                          %Run for all data points # of rows
   if i~=L                         %if current row is not last row, go to next
      NEXT=i+1;                    %set next equal to the value of the next row
      VALUE2=FILE(NEXT,1);         %set value2 as next row column 1
   else if i==L                    %unless the it is the last value
      VALUE2=50;                   %value2 set to 50 to end the sequence
   end
   end
   A(j,:)=FILE(i,:);               %set row j of A equal to row i of FILE
   VALUE1=FILE(i,1);               %set value1 equal to row i column 1 of FILE
   if VALUE1==VALUE2               %if value1 equals value2, go to next row
      j=j+1;
   else if VALUE1~=VALUE2          %if value1 and value2 are different check
      if length(A(:,1))<5          %if less than 5 values, ignored due to angle change
         j=1;
         clear A;
      else if length(A(:,1))>5     %if more than 5 values
            C=length(A(:,1));      %find length of A
            for m=1:9              %Average all rows of the like values in A
               B(k,m)=mean(A(4:C,m));    %disregarding first 3 for vibrations
            end
            j=1;
            k=k+1;
            clear A
      end
      end
   end
   end
end

%  if B(k-1,1)<B((k-2),1)
%     B=B(1:(k-2),:)
%  end

sample_data=[B];

%_____________________________________End of inserted code

[row2,col2] = size(sample_data);
 for i = 1:row2;
```

```
%Angles of the model during test runs (Roll, Pitch {AoA}, Yaw {Beta}):

phi               = 0;
theta(i,:)        = sample_data(i,1) .* (pi/180)-(0*pi/180);          %radians
si(i,:)           = sample_data(i,2) .* (pi/180);                     %radians
Wind_Speed(i,:)   = sample_data(i,3) .* (5280/3600);                  %fps

%Flight Parameters (Re#, Ma#, Dynamic Pressure):

q = (.5 * Density) .* Wind_Speed.^2;                                  %lbf/ft^2
q_Corrected = q .* (1 + Epsilon_tot)^2;                               %lbf/ft^2
Wind_Speed_Corrected = Wind_Speed .* (1 + Epsilon_tot);                       %fps
Mach_Number = Wind_Speed_Corrected ./ Speed_of_Sound;                         %NonDimensional
Reynolds_Number = ((Density * Root_Chord) .* Wind_Speed_Corrected) ./ Kinematic_Viscosity;
%NonDimensional
Flight_Parameters = [Mach_Number Reynolds_Number q_Corrected]

%individual forces and moments for each sensor:

%NEW NOTATION
NF_test(i,:,:)      = sample_data(i,4);
PM_test(i,:,:)      = sample_data(i,5);
AF_test(i,:,:)      = sample_data(i,6);
SF_test(i,:,:)      = sample_data(i,7);
YM_test(i,:,:)      = sample_data(i,8);
RM_test(i,:,:)      = sample_data(i,9);

%##########################################################################
%V.-   Subtract the effect of the static
%     weight with the tare polynominals above
%##########################################################################

%Evaluating the actual test theta angle (AoA) in the tare polynominal to
%determine the tare values for the angles tested in each run.

NF_eval = polyval(NF_poly,theta);
PM_eval = polyval(PM_poly,theta);
AF_eval  = polyval(AF_poly,theta);
SF_eval = polyval(SF_poly,theta);
YM_eval = polyval(YM_poly,theta);
RM_eval  = polyval(RM_poly,theta);

%The Time-Averaged (raw) forces and momentums NF,AF,SF,PM,YM AND RM measurd in the wind
%tunnel (body axis) with the tare effect of the weight subtracted off.

NF_resolved = NF_test - (NF_eval);
PM_resolved = PM_test - (PM_eval);
AF_resolved  = AF_test -  (AF_eval); % check this 8-17-04
SF_resolved = SF_test - (SF_eval);
YM_resolved = YM_test - (YM_eval);
RM_resolved  = RM_test -  (RM_eval);
```

```
Forces_minus_tare = [NF_resolved, AF_resolved, PM_resolved, RM_resolved, YM_resolved,
SF_resolved]';
 %#########################################################################
%VI.- CORRECT FORCES AND MOMENTS FOR BALANCE INTERATIONS (body axis)
%#########################################################################

%USING THE REDUCTION EQUATIONS
%LET US SET A MAXIMUN NUMBER OF INTERATIONS (FOR AVOIDING AN INFINIT LOOP)
MAXIT=100;
%SET THE LIMIT FOR THE DIFFERENCE BETWEEN INTERATIONS(CRITERIA FOR FINISH
THE INTERATIONS)
LIMIT=  10E-14;

%MATCHING EACH NAME WITH  THE DATA
% Prof. Reeder added :i
MNF=NF_resolved(i);
MAF=AF_resolved(i);
MPM=PM_resolved(i);
MRM=RM_resolved(i);
MYM=YM_resolved(i);
MSF=SF_resolved(i);

%INPUT OF THE CONSTANTS VALUES FROM THE MATRIX FOR SENSITIVITIES AND
INTERATIONS
K=[0  -1.3567E-03  -3.8021E-03  -4.2814E-03  -1.6966E-03   1.7567E-03  ...
   5.3167E-05  -1.3867E-04  -5.5629E-05  3.5181E-05  1.0601E-05  -2.5271E-04...
   5.6693E-05  -1.9537E-04   1.7908E-05  -3.6606E-05  -4.9934E-05  4.1205E-05...
   2.5648E-05  -1.9289E-05  8.9661E-05  -1.9594E-05  -4.9859E-04  -1.1599E-03...
   5.7163E-05  8.9798E-05  -7.8591E-05  9.3187E-03  0  -3.8421E-03  3.5740E-03...
   9.7714E-05  -2.7776E-03  -1.3552E-04  5.1538E-04  2.2082E-04  -1.2706E-05...
  -2.3637E-05  1.3686E-05  1.1085E-04  -3.6557E-06  4.9876E-06  8.1085E-06...
   3.7381E-05  1.2791E-04  -9.4527E-06  -2.3083E-06  -1.2046E-06  7.8161E-04...
   -1.1997E-03  -3.0560E-05  -6.6202E-05  3.7227E-04  -2.1469E-04  4.8386E-03...
   -3.7387E-03  0  -1.8479E-02  3.9077E-03  9.9165E-04  -1.4825E-05  -1.4830E-06...
   6.0845E-05  8.0667E-05  1.8547E-05  -5.0212E-05  1.0539E-04  -2.2676E-04...
   4.3793E-05  -1.0456E-05  -8.1186E-06  -2.1653E-05  -3.3070E-05  1.7280E-05...
   -7.4509E-05  -3.4399E-05  -8.2999E-04  -6.7962E-04  4.0521E-05  -5.1604E-05...
   9.1132E-06  -5.7360E-03  -2.2213E-04  9.9131E-04  0  -9.5790E-03  6.7114E-03...
   3.6824E-05  1.0056E-04  -3.7105E-05  -9.0295E-05  -7.4580E-05  1.4814E-04...
   7.2634E-05  -8.4778E-06  6.3486E-05  5.6328E-05  -1.3617E-04  2.2196E-05...
   1.3606E-05  -3.6689E-05  8.3283E-05  1.1865E-04  1.8544E-05  -1.9831E-05...
   1.7894E-05  -6.8164E-05  -7.0892E-05  1.2378E-03  1.6961E-03  -6.5102E-03...
   -9.3202E-03  0  5.1349E-03  1.3612E-05  -1.3175E-04  7.2442E-06  5.6705E-04...
   -1.4723E-05  -4.8656E-05  -1.4282E-04  5.9711E-05  5.9046E-05  -3.6490E-04...
   7.4881E-05  5.4601E-06  1.0129E-03  -1.3867E-04  8.1617E-05  6.6053E-05...
   -1.3417E-05  9.0025E-05  -4.5362E-05  -4.4672E-06  9.5087E-05  -3.4077E-02...
   7.9142E-04  1.6667E-03  -6.6512E-03  8.1538E-03 0  -1.4185E-05  7.3209E-05...
   -2.5849E-05  1.2325E-03  -4.1696E-05  4.6266E-05  8.6146E-05  2.1436E-05...
   5.0874E-05  -3.2738E-04  2.2218E-04  8.6478E-06  7.3395E-04  -4.1453E-05...
   3.5719E-05  2.5313E-05  1.5182E-04  3.6007E-05  -2.8844E-05  8.9741E-05...
  -7.3257E-05];
```

```
%COMPUTE THE UNCORRECTED FORCES AND MOMENTS BY
%CONSIDERING THAT THE PRIME SENSITIVITY CONSTANTS ARE ALREADY APLIED:

NF1=MNF;
AF1=MAF;
PM1=MPM;
RM1=MRM;
YM1=MYM;
SF1=MSF;

%FOR THE FIRST INTERACTION LET US INITIALIZE THE VALUES OF FORCES AND
%MOMENTS WITH THE VALUES OF THE UNCORRECTED FORCES AND MOMENTS

NF(1)=NF1;
AF(1)=AF1;
PM(1)=PM1;
RM(1)=RM1;
YM(1)=YM1;
SF(1)=SF1;

%DOING THE INTERACTION EQUATIONS:

for n=2:MAXIT;

NF(n)=NF1-((K(2)*AF(n-1))+(K(3)*PM(n-1))+(K(4)*RM(n-1))+(K(5)*YM(n-1))+(K(6)*SF(n-
1))+(K(7)*NF(n-1)^2)+...
      (K(8)*(NF(n-1)*AF(n-1)))+(K(9)*(NF(n-1)*PM(n-1)))+(K(10)*(NF(n-1)*RM(n-
1)))+(K(11)*(NF(n-1)*YM(n-1)))+...
      (K(12)*(NF(n-1)*SF(n-1)))+(K(13)*(AF(n-1)^2))+(K(14)*(AF(n-1)*PM(n-1)))+(K(15)*(AF(n-
1)*RM(n-1)))+...
      (K(16)*(AF(n-1)*YM(n-1)))+(K(17)*(AF(n-1)*SF(n-1)))+(K(18)*(PM(n-1)^2))+(K(19)*(PM(n-
1)*RM(n-1)))+...
      (K(20)*(PM(n-1)*YM(n-1)))+(K(21)*(PM(n-1)*SF(n-1)))+(K(22)*(RM(n-1)^2))+(K(23)*(RM(n-
1)*YM(n-1)))+...
      (K(24)*(RM(n-1)*SF(n-1)))+(K(25)*(YM(n-1)^2))+(K(26)*(YM(n-1)*SF(n-1)))+(K(27)*(SF(n-
1)^2)));

AF(n)=AF1-((K(28)*NF(n-1))+(K(30)*PM(n-1))+(K(31)*RM(n-1))+(K(32)*YM(n-1))+(K(33)*SF(n-
1))+(K(34)*NF(n-1)^2)+...
      (K(35)*(NF(n-1)*AF(n-1)))+(K(36)*(NF(n-1)*PM(n-1)))+(K(37)*(NF(n-1)*RM(n-
1)))+(K(38)*(NF(n-1)*YM(n-1)))+...
      (K(39)*(NF(n-1)*SF(n-1)))+(K(40)*(AF(n-1)^2))+(K(41)*(AF(n-1)*PM(n-1)))+(K(42)*(AF(n-
1)*RM(n-1)))+...
      (K(43)*(AF(n-1)*YM(n-1)))+(K(44)*(AF(n-1)*SF(n-1)))+(K(45)*(PM(n-1)^2))+(K(46)*(PM(n-
1)*RM(n-1)))+...
      (K(47)*(PM(n-1)*YM(n-1)))+(K(48)*(PM(n-1)*SF(n-1)))+(K(49)*(RM(n-1)^2))+(K(50)*(RM(n-
1)*YM(n-1)))+...
      (K(51)*(RM(n-1)*SF(n-1)))+(K(52)*(YM(n-1)^2))+(K(53)*(YM(n-1)*SF(n-1)))+(K(54)*(SF(n-
1)^2)));

PM(n)=PM1-((K(55)*NF(n-1))+(K(56)*AF(n-1))+(K(58)*RM(n-1))+(K(59)*YM(n-1))+(K(60)*SF(n-
1))+(K(61)*NF(n-1)^2)+...
```

```
      (K(62)*(NF(n-1)*AF(n-1)))+(K(63)*(NF(n-1)*PM(n-1)))+(K(64)*(NF(n-1)*RM(n-
1)))+(K(65)*(NF(n-1)*YM(n-1)))+...
      (K(66)*(NF(n-1)*SF(n-1)))+(K(67)*(AF(n-1)^2))+(K(68)*(AF(n-1)*PM(n-1)))+(K(69)*(AF(n-
1)*RM(n-1)))+...
      (K(70)*(AF(n-1)*YM(n-1)))+(K(71)*(AF(n-1)*SF(n-1)))+(K(72)*(PM(n-1)^2))+(K(73)*(PM(n-
1)*RM(n-1)))+...
      (K(74)*(PM(n-1)*YM(n-1)))+(K(75)*(PM(n-1)*SF(n-1)))+(K(76)*(RM(n-1)^2))+(K(77)*(RM(n-
1)*YM(n-1)))+...
      (K(78)*(RM(n-1)*SF(n-1)))+(K(79)*(YM(n-1)^2))+(K(80)*(YM(n-1)*SF(n-1)))+(K(81)*(SF(n-
1)^2)));

RM(n)=RM1-((K(82)*NF(n-1))+(K(83)*AF(n-1))+(K(84)*PM(n-1))+(K(86)*YM(n-1))+(K(87)*SF(n-
1))+(K(88)*NF(n-1)^2)+...
      (K(89)*(NF(n-1)*AF(n-1)))+(K(90)*(NF(n-1)*PM(n-1)))+(K(91)*(NF(n-1)*RM(n-
1)))+(K(92)*(NF(n-1)*YM(n-1)))+...
      (K(93)*(NF(n-1)*SF(n-1)))+(K(94)*(AF(n-1)^2))+(K(95)*(AF(n-1)*PM(n-1)))+(K(96)*(AF(n-
1)*RM(n-1)))+...
      (K(97)*(AF(n-1)*YM(n-1)))+(K(98)*(AF(n-1)*SF(n-1)))+(K(99)*(PM(n-1)^2))+(K(100)*(PM(n-
1)*RM(n-1)))+...
      (K(101)*(PM(n-1)*YM(n-1)))+(K(102)*(PM(n-1)*SF(n-1)))+(K(103)*(RM(n-
1)^2))+(K(104)*(RM(n-1)*YM(n-1)))+...
      (K(105)*(RM(n-1)*SF(n-1)))+(K(106)*(YM(n-1)^2))+(K(107)*(YM(n-1)*SF(n-
1)))+(K(108)*(SF(n-1)^2)));

YM(n)=YM1-((K(109)*NF(n-1))+(K(110)*AF(n-1))+(K(111)*PM(n-1))+(K(112)*RM(n-
1))+(K(114)*SF(n-1))+(K(115)*NF(n-1)^2)+...
      (K(116)*(NF(n-1)*AF(n-1)))+(K(117)*(NF(n-1)*PM(n-1)))+(K(118)*(NF(n-1)*RM(n-
1)))+(K(119)*(NF(n-1)*YM(n-1)))+...
      (K(120)*(NF(n-1)*SF(n-1)))+(K(121)*(AF(n-1)^2))+(K(122)*(AF(n-1)*PM(n-1)))+(K(123)*(AF(n-
1)*RM(n-1)))+...
      (K(124)*(AF(n-1)*YM(n-1)))+(K(125)*(AF(n-1)*SF(n-1)))+(K(126)*(PM(n-
1)^2))+(K(127)*(PM(n-1)*RM(n-1)))+...
      (K(128)*(PM(n-1)*YM(n-1)))+(K(129)*(PM(n-1)*SF(n-1)))+(K(130)*(RM(n-
1)^2))+(K(131)*(RM(n-1)*YM(n-1)))+...
      (K(132)*(RM(n-1)*SF(n-1)))+(K(133)*(YM(n-1)^2))+(K(134)*(YM(n-1)*SF(n-
1)))+(K(135)*(SF(n-1)^2)));

SF(n)=SF1-((K(136)*NF(n-1))+(K(137)*AF(n-1))+(K(138)*PM(n-1))+(K(139)*RM(n-
1))+(K(140)*YM(n-1))+(K(142)*NF(n-1)^2)+...
      (K(143)*(NF(n-1)*AF(n-1)))+(K(144)*(NF(n-1)*PM(n-1)))+(K(145)*(NF(n-1)*RM(n-
1)))+(K(146)*(NF(n-1)*YM(n-1)))+...
      (K(147)*(NF(n-1)*SF(n-1)))+(K(148)*(AF(n-1)^2))+(K(149)*(AF(n-1)*PM(n-1)))+(K(150)*(AF(n-
1)*RM(n-1)))+...
      (K(151)*(AF(n-1)*YM(n-1)))+(K(152)*(AF(n-1)*SF(n-1)))+(K(153)*(PM(n-
1)^2))+(K(154)*(PM(n-1)*RM(n-1)))+...
      (K(155)*(PM(n-1)*YM(n-1)))+(K(156)*(PM(n-1)*SF(n-1)))+(K(157)*(RM(n-
1)^2))+(K(158)*(RM(n-1)*YM(n-1)))+...
      (K(159)*(RM(n-1)*SF(n-1)))+(K(160)*(YM(n-1)^2))+(K(161)*(YM(n-1)*SF(n-
1)))+(K(162)*(SF(n-1)^2)));
```

```
% SET THE LIMIT FOR THE DIFFERENCE BETWEEN INTERATIONS(CRITERIA FOR FINISH
THE INTERATIONS)

DIFFNF(n)=abs(NF(n)-NF(n-1));
DIFFAF(n)=abs(AF(n)-AF(n-1));
DIFFPM(n)=abs(PM(n)-PM(n-1));
DIFFRM(n)=abs(RM(n)-RM(n-1));
DIFFYM(n)=abs(YM(n)-YM(n-1));
DIFFSF(n)=abs(SF(n)-SF(n-1));

if DIFFNF(n)&DIFFAF(n)&DIFFPM(n)&DIFFRM(n)&DIFFYM(n)&DIFFSF(n) < LIMIT
 break

end

end

%disp('THE FINAL VALUES ARE (NF,AF,PM,RM,YM,SF):')
Corrected_Data(:,i)= [NF(n);AF(n);PM(n);RM(n);YM(n);SF(n)];

%disp('THE FINAL DIFFERENCE BETWEEN INTERATIONS ARE(FOR NF,AF,PM,RM,YM,SF) :')
%FINAL_DIFFERENCE=[DIFFNF(n),DIFFAF(n),DIFFPM(n),DIFFRM(n),DIFFYM(n),DIFFSF(n)]

%disp('THE NUMBER OF INTERATIONS USED WAS:')
%n

%#########################################################################
%VII.- Calculation of the Axial, Side, & Normal Forces from the corrected balance
%      forces in the Body Axis reference frame
%#########################################################################

Forces_b(:,i) = [Corrected_Data(2,i); Corrected_Data(6,i); Corrected_Data(1,i)];


%Calculation of the Drag, Side, & Lift Forces in the Wind Axis reference
%frame

Forces_w = [Forces_b(1,:).*cos(theta').*cos(si')+Forces_b(2,:).*sin(si')+Forces_b(3,:).*sin(theta').*cos(si');
%in radians
        -Forces_b(1,:).*sin(si').*cos(theta')+Forces_b(2,:).*cos(si')-Forces_b(3,:).*sin(theta').*sin(si');
        -Forces_b(1,:).*sin(theta')+Forces_b(3,:).*cos(theta')];

%First entry is the moments calculated by the balance or direct calculation
%in the Body Reference Frame.  Balance measures Roll (l), Yaw is about the
%z-axis (n), and Pitch is about the y-axis (m).  Distances from strain
%gages to C.G. are in INCHES.  Moments are in-lbf. See pp. 236-238 of
%Barlow et. al., 3rd ed.

m = Corrected_Data(3,i);
n = Corrected_Data(5,i);
l = Corrected_Data(4,i);

Moments_b(:,i) = [l; m; n];
```

```
%Second entry is the conversion from the "Balance Centeric" moments to the
%Wind Reference monments with respect to the Balance Center (bc)

Moments_w_bc = [Moments_b(1,:).*cos(theta').*cos(si')-
Moments_b(2,:).*sin(si')+Moments_b(3,:).*sin(theta').*cos(si');

Moments_b(1,:).*sin(si').*cos(theta')+Moments_b(2,:).*cos(si')+Moments_b(3,:).*sin(theta').*sin(si');
          -Moments_b(1,:).*sin(theta')+Moments_b(3,:).*cos(theta')];

%Finally, the balance centered moments are converted to moments about the
%Model's Center of Mass (cm) or Center of Gravity (CG)

cgdist=sqrt((X_cmb)^2+(Z_cmb)^2); %Obtaining the direct distance between the
                        %center of the balance and the center of mass
w=atan(-Z_cmb/X_cmb);  %Obtaining the angle between cgdist and the x axes at zero angle of attack

X_cm(i,:)= cos(theta(i,:)+w)*cos(si(i,:))*(cgdist);
Y_cm(i,:) = Y_cmb + X_cm(i,:)*tan(si(i,:));            % appropriate for very small y_cmb and reasonable si
Z_cm(i,:)= -sin(theta(i,:)+w)*(cgdist);


Moments_w_cg_u = [Moments_w_bc(1,:) + Z_cm(i,:)*Forces_w(2,:) + Forces_w(3,:)* Y_cm(i,:);
            Moments_w_bc(2,:) - Forces_w(3,:)* X_cm(i,:) + Forces_w(1,:)* Z_cm(i,:);
            Moments_w_bc(3,:) - Forces_w(1,:)* Y_cm(i,:) - Forces_w(2,:)* X_cm(i,:)];

%#########################################################################

%VIII.- Calculation of the actual Lift and Drage nondimensional Coefficients, uncorrected for tunnel
effects, (Cl
%       and Cd)
%#########################################################################

C_D_u = Forces_w(1,:) ./ (q_Corrected' .* Wing_Area);
C_Y_u = Forces_w(2,:) ./ (q_Corrected' .* Wing_Area);
C_L_u = Forces_w(3,:) ./ (q_Corrected' .* Wing_Area);              %Keuthe & Chow pg 178
Coefficients = [C_L_u; C_D_u; C_Y_u]';
 Ave_Cl = mean(Coefficients(:,1));
 Ave_Cd = mean(Coefficients(:,2));

end

%#########################################################################
%IX          Drag Coefficient Correction
%#########################################################################

C_D_o = min(Coefficients(:,2));
C_L_u_sqrd = Coefficients(:,1).^2;
Delta_C_D_w = ((delta * Wing_Area) / X_Section) .* C_L_u_sqrd;
C_D_Corrected = C_D_u' + Delta_C_D_w;
```

```
%###########################################################################
%X.-  Angle of Attack due to upwash Correction
%###########################################################################

alpha_before = sample_data(:,1);
alpha =[alpha_before]-[0]; %18APR05 change to 5 for sting block angle, then back to 0 for Aero 517 SU
2005 ************************************
Delta_alpha_w = ((delta * Wing_Area) / X_Section) .* (57.3 * C_L_u);
alpha_Corrected = alpha + Delta_alpha_w';

%###########################################################################
%XI.-  Pitching Moment Correction
%###########################################################################

% tau2 = 0.65;
 c_bar = c_bar;                          % ft = Mean Chord of wing
% V_bar =  0/ (Wing_Area * c_bar);            %  Horizontal tail volume ratio
% eta_t = 1.0;
% epsilon_o = 0;
% i_t = pi/4;                                          % radians
% i_w = 0;
% Aspect_Ratio_t = Span_t^2 / Tail_Area;
%
% D_epslion_D_alpha = ((2 .* C_L_u) ./ (pi* Aspect_Ratio))';
% epsilon = epsilon_o + (D_epslion_D_alpha .* alpha_Corrected );
% alpha_t = alpha_Corrected - i_w - epsilon + i_t;
% C_L_alpha_t = 0 %((0.1* Aspect_Ratio) / (Aspect_Ratio_t +2)) * 0.8;
% D_Cm_cg_t_D_alpha_t = -C_L_alpha_t* V_bar * eta_t;
% Delta_C_m_cg_t = ((D_Cm_cg_t_D_alpha_t) * (delta*tau2) * (Wing_Area / X_Section) .* (C_L_u *
57.3))';

Cl_w_cg =   Moments_w_cg_u(1,:) ./ (q_Corrected' .* (Wing_Area * Span*12));
Cm_w_cg_u = Moments_w_cg_u(2,:) ./ (q_Corrected' .* (Wing_Area * c_bar*12));
Cn_w_cg =   Moments_w_cg_u(3,:) ./ (q_Corrected' .* (Wing_Area * Span*12));

Cm_w_cg_corrected = Cm_w_cg_u %-Delta_C_m_cg_t';  %no tail
Corrected_Moment_Coefficients = [Cl_w_cg' Cm_w_cg_corrected' Cn_w_cg'];

%OBTAINING THE MOMENT COEFFICIENTS CORRECTED ABOUT THE CENTER OF THE
%BALANCE

Cl_w_bc =   Moments_w_bc(1,:) ./ (q_Corrected' .* (Wing_Area * Span*12));
Cm_w_bc_u = Moments_w_bc(2,:) ./ (q_Corrected' .* (Wing_Area * c_bar*12));
Cn_w_bc =   Moments_w_bc(3,:) ./ (q_Corrected' .* (Wing_Area * Span*12));

Cm_w_bc_corrected = Cm_w_bc_u ;  %no tail
Corrected_Moment_Coefficients_bc = [Cl_w_bc' Cm_w_bc_corrected' Cn_w_bc'];
```

```
%##########################################################################
%XII.- OUTPUT VARIABLES FORMATING
%##########################################################################

alpha = sample_data(:,1);

% fprintf('   Mach Number Reynolds Number Dynamic Pressure(Psf)\r')
% % Flight_Parameters
% fprintf(' \r');
% fprintf(' Loads are in lbf and arranged [D S L] across the top and increments of alpha down the side \r')
% Forces_w'
% fprintf(' \r')
% fprintf(' Moments are in in-lbf and arranged [L M N] down the side and increments of alpha along the
top \r')
% % Moments_w_cg_u
% fprintf(' \r')
% fprintf('      Cl_u          Cd_u           CY_u \r');
% % Coefficients
% fprintf(' \r')
% fprintf('    Del_CD_w       CD_u     CD_Corrected \r');
% Compare_CD = [Delta_C_D_w C_D_u' C_D_Corrected]
% fprintf(' \r')
% fprintf('    Del_alpha_w    alpha_g     alpha_Corrected \r');
% Compare_alpha = [Delta_alpha_w' alpha alpha_Corrected ]
% fprintf(' \r')
% fprintf('    Cl_cg_wind    Cm_cg_corrected_w     Cn_cg_wind \r');
% % Corrected_Moment_Coefficients
% fprintf(' \r')
% fprintf('      M#          Re#         q_c          Uoo       alpha_c       C_L       C_D_c      Cl_cg_w
Cm_cg_c_w    Cn_cg_w       C_Y\r');
YY=[Flight_Parameters (Wind_Speed_Corrected .* (3600/5280)) alpha_Corrected C_L_u' C_D_Corrected
Corrected_Moment_Coefficients C_Y_u' NF_resolved AF_resolved]
% XX=['M#', 'Re#', 'q_c',  'Uoo', 'alpha_c', 'C_L', 'C_D_c', 'Cl_cg_w', 'Cm_cg_c_w', 'Cn_cg_w', 'C_Y_u'];

% ZZ=[XX; YY];
% wk1write('output.xls',YY,2,1)

% Max_Cl = max(Coefficients(:,1))

% LET US SAVE TOTAL DATA IN A EXTERNAL FILE

dlmwrite('Houck_Orig_Nov_30mph_8to10',YY,'\t')
```

Appendix C: Low-Speed Wind Tunnel Test Results

The following data was taken in the AFIT low-speed wind tunnel using the 10lb balance and resolved using the *MATLAB* code found in Appendix B.

Table 15: Original Configuration at 20 mph: Alpha Sweep

Original Configuration at 20 mph: Alpha Sweep - 14 Nov. 2006, T_{room} = 74.6° F, P_{baro} = 28.8058 "Hg, S = 307 in^2												
α (°)	L/D	Re (-)	V (mph)	q (lbf/ft^2)	L (lbs)	D (lbs)	C_L (-)	C_D (-)	C_Y (-)	C_l (-)	C_m (-)	C_n (-)
-4.30	-3.31	81167	20.00	0.9555	-0.228	0.069	-0.1121	0.0338	-0.0050	0.0015	0.0201	0.0018
-3.27	-2.00	80772	19.90	0.9463	-0.128	0.064	-0.0636	0.0318	-0.0039	0.0015	0.0142	0.0018
-2.15	-0.41	80413	19.81	0.9379	-0.025	0.059	-0.0123	0.0297	-0.0032	0.0014	0.0080	0.0017
-1.03	1.42	80334	19.79	0.9360	0.080	0.056	0.0400	0.0282	-0.0015	0.0011	0.0008	0.0016
0.10	3.17	80308	19.78	0.9354	0.185	0.058	0.0925	0.0292	-0.0016	0.0011	-0.0057	0.0018
1.22	4.70	80852	19.92	0.9481	0.298	0.063	0.1476	0.0314	0.0003	0.0014	-0.0108	0.0015
2.35	5.79	81162	19.99	0.9554	0.407	0.070	0.1996	0.0344	0.0010	0.0015	-0.0141	0.0014
3.47	6.36	80946	19.94	0.9503	0.508	0.080	0.2508	0.0394	0.0036	0.0015	-0.0172	0.0012
4.59	6.48	81001	19.95	0.9516	0.609	0.094	0.3002	0.0463	0.0063	0.0012	-0.0217	0.0001
5.64	6.12	80462	19.82	0.9390	0.727	0.119	0.3629	0.0593	0.0086	0.0007	-0.0319	-0.0005
6.77	5.77	80059	19.72	0.9296	0.837	0.145	0.4225	0.0732	0.0104	0.0002	-0.0410	-0.0007
7.88	5.24	80308	19.78	0.9354	0.929	0.177	0.4656	0.0888	0.0118	-0.0004	-0.0477	-0.0010
8.96	4.65	80516	19.83	0.9403	0.984	0.212	0.4906	0.1056	0.0132	-0.0015	-0.0558	-0.0009
10.03	4.14	80343	19.79	0.9362	1.006	0.243	0.5040	0.1217	0.0151	-0.0020	-0.0664	-0.0008
11.09	3.80	80131	19.74	0.9313	1.027	0.270	0.5172	0.1361	0.0157	-0.0026	-0.0744	0.0000
12.13	3.52	80406	19.81	0.9377	1.031	0.293	0.5157	0.1466	0.0158	-0.0017	-0.0789	-0.0004
13.10	3.30	80108	19.73	0.9308	1.038	0.315	0.5233	0.1587	0.0156	-0.0021	-0.0803	-0.0001
14.14	3.12	80068	19.72	0.9298	1.041	0.334	0.5251	0.1684	0.0160	-0.0024	-0.0790	0.0003
15.19	2.95	79775	19.65	0.9230	1.030	0.349	0.5233	0.1775	0.0170	-0.0022	-0.0759	0.0002

Table 16: Original Configuration at 30 mph: Alpha Sweep

Original Configuration at 30 mph: Alpha Sweep - 14 Nov. 2006, T_{room} = 74.6° F, P_{baro} = 28.8058 "Hg, S = 307 in^2												
α (°)	L/D	Re (-)	V (mph)	q (lbf/ft^2)	L (lbs)	D (lbs)	C_L (-)	C_D (-)	C_Y (-)	C_l (-)	C_m (-)	C_n (-)
-4.28	-3.58	126230	31.10	2.3112	-0.496	0.139	-0.1007	0.0281	-0.0036	0.0017	0.0177	0.0011
-3.25	-1.98	125710	30.97	2.2922	-0.247	0.125	-0.0506	0.0256	-0.0028	0.0010	0.0098	0.0010
-2.13	-0.02	125670	30.96	2.2908	-0.003	0.117	-0.0006	0.0240	-0.0022	0.0008	0.0036	0.0012
-1.01	2.13	125910	31.02	2.2995	0.240	0.112	0.0489	0.0229	-0.0013	0.0007	-0.0020	0.0013
0.11	4.20	126110	31.07	2.3065	0.502	0.120	0.1022	0.0243	0.0007	0.0012	-0.0072	0.0006
1.25	5.94	126330	31.12	2.3149	0.813	0.137	0.1647	0.0277	0.0040	0.0012	-0.0129	0.0001
2.37	6.86	126610	31.19	2.3252	1.071	0.156	0.2161	0.0315	0.0070	0.0012	-0.0168	-0.0002
3.49	7.36	126520	31.17	2.3216	1.310	0.178	0.2647	0.0360	0.0071	0.0006	-0.0225	-0.0001
4.61	7.39	126510	31.16	2.3213	1.552	0.210	0.3137	0.0425	0.0081	0.0006	-0.0297	-0.0004
5.72	6.99	126580	31.18	2.3238	1.775	0.254	0.3584	0.0512	0.0090	0.0005	-0.0351	-0.0006
6.74	6.41	126600	31.19	2.3245	1.986	0.310	0.4007	0.0625	0.0107	0.0004	-0.0399	-0.0009
7.84	5.73	126160	31.08	2.3084	2.170	0.379	0.4410	0.0769	0.0111	-0.0003	-0.0458	-0.0011
8.92	5.04	126150	31.08	2.3083	2.295	0.455	0.4663	0.0925	0.0139	-0.0007	-0.0537	-0.0010
9.98	4.45	126320	31.12	2.3145	2.332	0.523	0.4725	0.1061	0.0114	-0.0023	-0.0626	-0.0007
11.03	4.06	126320	31.12	2.3144	2.363	0.582	0.4789	0.1179	0.0128	-0.0026	-0.0690	-0.0003
12.09	3.78	126050	31.05	2.3044	2.411	0.638	0.4907	0.1298	0.0125	-0.0035	-0.0733	0.0004
13.06	3.54	126050	31.05	2.3045	2.433	0.688	0.4952	0.1400	0.0132	-0.0030	-0.0750	0.0006
14.09	3.31	126030	31.05	2.3036	2.409	0.727	0.4906	0.1481	0.0119	-0.0022	-0.0741	0.0002
15.13	3.11	125990	31.04	2.3023	2.391	0.768	0.4871	0.1564	0.0112	-0.0023	-0.0708	0.0005

Table 17: Original Configuration at 40 mph: Alpha Sweep

Original Configuration at 40 mph: Alpha Sweep - 14 Nov. 2006, T_{room} = 74.6° F, P_{baro} = 28.8058 "Hg, S = 307 in^2												
α (°)	L/D	Re (-)	V (mph)	q (lbf/ft^2)	L (lbs)	D (lbs)	C_L (-)	C_D (-)	C_Y (-)	C_l (-)	C_m (-)	C_n (-)
-4.27	-3.53	169890	41.85	4.1865	-0.843	0.239	-0.0945	0.0268	-0.0060	0.0002	0.0148	0.0021
-3.25	-1.93	169730	41.81	4.1782	-0.418	0.217	-0.0469	0.0244	-0.0045	0.0002	0.0093	0.0020
-2.13	0.15	170040	41.89	4.1935	0.031	0.204	0.0035	0.0228	-0.0029	0.0003	0.0030	0.0017
-1.00	2.46	170210	41.93	4.2022	0.485	0.197	0.0541	0.0220	-0.0005	0.0006	-0.0025	0.0010
0.14	5.05	170140	41.91	4.1986	1.097	0.217	0.1225	0.0243	0.0051	0.0010	-0.0081	-0.0004
1.27	6.64	170280	41.95	4.2055	1.583	0.238	0.1766	0.0266	0.0069	0.0010	-0.0130	-0.0006
2.38	7.51	170620	42.03	4.2221	2.009	0.268	0.2232	0.0297	0.0071	0.0006	-0.0177	-0.0005
3.50	7.96	170410	41.98	4.2117	2.433	0.306	0.2710	0.0340	0.0076	0.0006	-0.0243	-0.0006
4.62	7.94	170140	41.91	4.1986	2.874	0.362	0.3211	0.0404	0.0089	0.0004	-0.0336	-0.0010
5.73	7.42	170280	41.95	4.2056	3.300	0.444	0.3680	0.0496	0.0105	0.0004	-0.0430	-0.0016
6.84	6.72	170610	42.03	4.2220	3.703	0.551	0.4114	0.0612	0.0122	0.0001	-0.0517	-0.0022
7.86	5.94	170160	41.92	4.1995	4.033	0.679	0.4504	0.0758	0.0139	-0.0003	-0.0594	-0.0024
8.93	5.16	170060	41.89	4.1944	4.220	0.817	0.4719	0.0914	0.0142	-0.0010	-0.0641	-0.0022
9.98	4.54	169990	41.88	4.1912	4.235	0.933	0.4740	0.1044	0.0139	-0.0020	-0.0663	-0.0013
11.04	4.18	169510	41.76	4.1673	4.316	1.033	0.4858	0.1163	0.0123	-0.0033	-0.0699	-0.0005
12.09	3.86	169270	41.70	4.1559	4.353	1.128	0.4913	0.1273	0.0125	-0.0036	-0.0730	0.0002
13.05	3.61	169610	41.78	4.1724	4.363	1.209	0.4904	0.1359	0.0131	-0.0031	-0.0742	0.0002

Table 18: Original Configuration at 20 mph: Beta Sweep

Original Configuration at 20 mph: Beta Sweep – 5 Sept. 2006, T_{room} = 74.1° F, P_{baro} = 29.0115 "Hg												
α (°)	L/D	Re (-)	V (mph)	Mach (-)	q (lbf/ft^2)	C_L (-)	C_D (-)	C_Y (-)	C_l (-)	C_m (-)	C_n (-)	β (°)
4.57	6.18	80901	19.93	0.025800	0.9493	0.290460	0.046966	-0.052480	-0.005044	-0.018732	0.002467	7.47
4.57	6.34	80885	19.93	0.025795	0.9489	0.291570	0.045988	-0.046026	-0.003727	-0.019586	0.002269	6.62
4.57	6.52	80945	19.94	0.025814	0.9503	0.292870	0.044901	-0.039004	-0.002356	-0.020270	0.002036	5.69
4.58	6.69	80964	19.95	0.025820	0.9508	0.293320	0.043877	-0.031098	-0.000922	-0.021331	0.001730	4.71
4.58	6.84	80864	19.92	0.025788	0.9484	0.297170	0.043440	-0.023673	0.000183	-0.022353	0.001387	3.74
4.59	6.95	80737	19.89	0.025748	0.9454	0.300750	0.043268	-0.015894	0.001369	-0.023086	0.001023	2.80
4.59	7.01	80719	19.88	0.025742	0.9450	0.305640	0.043606	-0.008510	0.002665	-0.023378	0.000692	1.83
4.60	7.09	80763	19.90	0.025756	0.9461	0.307940	0.043425	-0.000787	0.003483	-0.023953	0.000378	0.85
4.59	7.09	80826	19.91	0.025776	0.9475	0.305070	0.043031	0.009359	0.005095	-0.021742	-0.000809	-0.13
4.60	7.06	80815	19.91	0.025772	0.9473	0.307830	0.043624	0.016779	0.006265	-0.023127	-0.001317	-1.10
4.60	6.98	80855	19.92	0.025785	0.9482	0.310460	0.044461	0.024821	0.007300	-0.023928	-0.001726	-2.08
4.61	6.89	80804	19.91	0.025769	0.9470	0.313200	0.045465	0.032757	0.008612	-0.024420	-0.002222	-3.06
4.61	6.78	80815	19.91	0.025772	0.9473	0.315470	0.046512	0.040364	0.009714	-0.023674	-0.002607	-4.03
4.61	6.62	80915	19.93	0.025804	0.9496	0.317510	0.047944	0.047475	0.010945	-0.022907	-0.002922	-5.01
4.61	6.42	80914	19.93	0.025804	0.9496	0.315380	0.049126	0.054359	0.012035	-0.020038	-0.003175	-5.95
4.61	6.24	80842	19.92	0.025781	0.9479	0.316730	0.050797	0.061393	0.013293	-0.018864	-0.003426	-6.88
4.61	6.05	80693	19.88	0.025734	0.9444	0.317840	0.052572	0.068283	0.014783	-0.018662	-0.003790	-7.86

Table 19: Original Configuration at 30 mph: Beta Sweep

Original Configuration at 30 mph: Beta Sweep – 5 Sept. 2006, T_{room} = 74.1° F, P_{baro} = 29.0115 "Hg												
α (°)	L/D	Re (-)	V (mph)	Mach (-)	q (lbf/ft^2)	C_L (-)	C_D (-)	C_Y (-)	C_l (-)	C_m (-)	C_n (-)	β (°)
4.58	6.72	126360	31.13	0.040296	2.3158	0.294950	0.043921	-0.044189	-0.004460	-0.023816	0.001511	7.13
4.58	6.93	126420	31.14	0.040316	2.3180	0.297080	0.042889	-0.037971	-0.003299	-0.025226	0.001407	6.29
4.59	7.11	126480	31.16	0.040336	2.3203	0.300490	0.042280	-0.031226	-0.001991	-0.026825	0.001146	5.35
4.59	7.27	126470	31.15	0.040332	2.3198	0.302120	0.041565	-0.024284	-0.000637	-0.027722	0.000879	4.37
4.59	7.37	126420	31.14	0.040315	2.3179	0.303100	0.041123	-0.017448	0.000734	-0.027833	0.000585	3.40
4.60	7.49	126410	31.14	0.040312	2.3175	0.307250	0.040996	-0.010804	0.001537	-0.029864	0.000373	2.46
4.60	7.53	126330	31.12	0.040286	2.3146	0.308360	0.040975	-0.003938	0.002783	-0.029833	0.000056	1.49
4.60	7.58	126290	31.11	0.040274	2.3132	0.309620	0.040853	0.003185	0.003983	-0.029142	-0.000435	0.51
4.60	7.56	126340	31.12	0.040290	2.3151	0.310080	0.041030	0.010353	0.005037	-0.028748	-0.000966	-0.47
4.60	7.49	126420	31.14	0.040317	2.3181	0.310880	0.041518	0.017439	0.006287	-0.028947	-0.001304	-1.44
4.60	7.42	126420	31.14	0.040317	2.3181	0.312350	0.042115	0.024355	0.007489	-0.029015	-0.001650	-2.42
4.61	7.32	126410	31.14	0.040312	2.3176	0.315180	0.043039	0.031597	0.008767	-0.028998	-0.002105	-3.40
4.61	7.21	126390	31.14	0.040308	2.3171	0.317560	0.044039	0.038661	0.010240	-0.028769	-0.002394	-4.37
4.61	7.08	126320	31.12	0.040283	2.3142	0.319420	0.045147	0.045006	0.011547	-0.028484	-0.002572	-5.35
4.62	6.90	126200	31.09	0.040245	2.3099	0.321170	0.046530	0.051649	0.012880	-0.027680	-0.002771	-6.37
4.62	6.70	126140	31.07	0.040225	2.3076	0.320500	0.047823	0.057980	0.014186	-0.025956	-0.003016	-7.35
4.62	6.50	126100	31.06	0.040213	2.3062	0.320990	0.049356	0.064046	0.015501	-0.024691	-0.003172	-8.32

Table 20: September 2006 Alpha Sweep for Original Configuration at 30 mph

Original Configuration at 30 mph: Alpha Sweep - Re ~ 125K			
September 2006, S = 307 in^2			
α (°)	L/D (-)	V (mph)	q (lbf/ft^2)
-4.28	-3.58	30.94	2.3071
-3.25	-1.98	30.88	2.2975
-2.13	-0.02	30.88	2.2972
-1.01	2.13	30.87	2.2964
0.11	4.20	30.89	2.2996
1.25	5.94	30.95	2.3082
2.37	6.86	30.98	2.3118
3.49	7.36	30.99	2.3132
4.61	7.39	30.96	2.3101
5.72	6.99	30.94	2.3060
6.74	6.41	30.92	2.3035
7.84	5.73	30.91	2.3024
8.92	5.04	30.90	2.3002
9.98	4.45	30.88	2.2970
11.03	4.06	30.86	2.2946
12.09	3.78	30.83	2.2904
13.06	3.54	30.80	2.2852
14.09	3.31	30.76	2.2803
15.13	3.11	30.73	2.2752

Table 21: CFD Data for Original Configuration at 40 mph: Alpha Sweep

CFD - Original Configuration at 40 mph: Alpha Sweep in AVUS, S = 307 in^2							
α (°)	L/D (-)	$C_L^{(3/2)}/C_D$	Re (-)	V (mph)	C_L (-)	C_D (-)	C_m (-)
-5.40	-4.77	-	170000	40.00	-0.136553	0.028619	0.000716
-4.40	-3.68	-	170000	40.00	-0.093313	0.025381	0.004593
-3.40	-2.05	-	170000	40.00	-0.047277	0.023110	0.008391
-2.40	-0.22	-	170000	40.00	-0.004932	0.022081	0.012127
-1.40	1.70	0.33	170000	40.00	0.037907	0.022237	0.017271
-0.40	3.47	0.99	170000	40.00	0.080571	0.023187	0.021938
0.60	5.05	1.78	170000	40.00	0.123828	0.024505	0.026518
1.60	6.28	2.57	170000	40.00	0.167259	0.026646	0.030766
2.60	7.17	3.29	170000	40.00	0.210463	0.029333	0.034456
3.60	7.54	3.78	170000	40.00	0.250664	0.033237	0.039292
4.60	7.70	4.15	170000	40.00	0.290035	0.037662	0.043436
5.60	7.73	4.43	170000	40.00	0.329029	0.042588	0.046231
6.60	7.51	4.55	170000	40.00	0.366723	0.048823	0.049826
7.60	7.17	4.54	170000	40.00	0.401967	0.056098	0.051961
8.60	6.72	4.42	170000	40.00	0.433366	0.064488	0.053459
9.60	5.91	3.98	170000	40.00	0.454795	0.076982	0.052095
9.60	5.85	3.94	170000	40.00	0.453343	0.077555	0.050644
10.60	5.06	3.41	170000	40.00	0.453174	0.089500	0.042383

Table 22: USAFA 18" Configuration at M = 0.25, Re ≈ 545K: Beta Sweep

USAFA 18" Houck Configuration - Beta Sweeps, S = 189 in^2								
	α = 0°		α = 5°		α = 10°		α = 15°	
β (°)	C_l (-)	C_n (-)	C_l (-)	C_n (-)	C_l (-)	C_n (-)	C_l (-)	C_n (-)
-4.66	-0.006	-0.0004	0.008	0.0033	0.0175	0.0055	0.025	0.0061
-2.25	0.002	0.0015	0.006	0.0028	0.0096	0.0054	0.0125	0.0058
0.35	0.00275	0.00215	0.0035	0.00285	0.00275	0.00494	0.0013	0.00488
2.8	0.00333	0.0019	-0.002	0.0038	-0.0045	0.00433	-0.0099	0.0038
5.3	0.005	0.0031	-0.004	0.0029	-0.012	0.0035	-0.022	0.0018

Table 23: Ailerons 20° Down at 20 mph: Alpha Sweep

Ailerons 20º Down at 20 mph: Alpha Sweep - 14 Nov. 2006, T_{room} = 74.6º F, P_{baro} = 28.8058 "Hg, S = 307 in^2												
α (º)	L/D	Re (-)	V (mph)	q (lbf/ft^2)	L (lbs)	D (lbs)	C_L (-)	C_D (-)	C_Y (-)	C_l (-)	C_m (-)	C_n (-)
-4.08	1.00	80360	19.80	0.9366	0.070	0.069	0.0349	0.0348	0.0005	0.0042	-0.0629	0.0004
-3.05	2.33	80574	19.85	0.9416	0.162	0.070	0.0809	0.0347	0.0012	0.0042	-0.0680	0.0006
-1.93	3.81	80442	19.82	0.9385	0.264	0.069	0.1320	0.0347	0.0026	0.0039	-0.0738	0.0004
-0.81	4.98	80215	19.76	0.9333	0.361	0.072	0.1814	0.0364	0.0041	0.0033	-0.0793	0.0002
0.29	5.65	80567	19.85	0.9415	0.448	0.079	0.2230	0.0395	0.0048	0.0031	-0.0795	0.0003
1.41	6.13	80498	19.83	0.9398	0.547	0.089	0.2731	0.0445	0.0064	0.0041	-0.0807	0.0001
2.54	6.47	80388	19.80	0.9373	0.658	0.102	0.3293	0.0509	0.0080	0.0043	-0.0849	-0.0001
3.67	6.54	80604	19.86	0.9423	0.775	0.118	0.3857	0.0590	0.0106	0.0048	-0.0932	-0.0008
4.79	6.44	80888	19.93	0.9490	0.885	0.137	0.4374	0.0680	0.0106	0.0035	-0.1018	-0.0005
5.82	6.01	80603	19.86	0.9423	0.975	0.162	0.4851	0.0808	0.0137	0.0032	-0.1068	-0.0020
6.94	5.56	80102	19.73	0.9306	1.062	0.191	0.5355	0.0963	0.0166	0.0030	-0.1126	-0.0026
8.03	5.06	80117	19.74	0.9310	1.119	0.221	0.5637	0.1115	0.0158	0.0013	-0.1178	-0.0021
9.08	4.50	80366	19.80	0.9368	1.139	0.253	0.5704	0.1268	0.0205	-0.0010	-0.1255	-0.0022
10.13	4.10	80101	19.73	0.9306	1.135	0.277	0.5721	0.1397	0.0189	-0.0027	-0.1303	-0.0015
11.18	3.76	79723	19.64	0.9218	1.133	0.301	0.5766	0.1532	0.0183	-0.0015	-0.1331	-0.0016
12.22	3.52	79792	19.66	0.9234	1.127	0.320	0.5726	0.1628	0.0213	-0.0007	-0.1307	-0.0017
13.17	3.31	79819	19.66	0.9241	1.120	0.339	0.5685	0.1720	0.0179	-0.0014	-0.1249	-0.0017
14.20	3.12	79902	19.68	0.9260	1.110	0.356	0.5623	0.1801	0.0189	-0.0016	-0.1162	-0.0009
15.23	2.92	79487	19.58	0.9164	1.078	0.369	0.5516	0.1890	0.0174	-0.0023	-0.1073	0.0006

Table 24: Ailerons 20° Down at 30 mph: Alpha Sweep

Ailerons 20º Down at 30 mph: Alpha Sweep - Alpha Sweep - 14 Nov. 2006, T_{room} = 74.6º F, P_{baro} = 28.8058 "Hg, S = 307 in^2												
α (º)	L/D	Re (-)	V (mph)	q (lbf/ft^2)	L (lbs)	D (lbs)	C_L (-)	C_D (-)	C_Y (-)	C_l (-)	C_m (-)	C_n (-)
-4.08	1.07	126260	31.10	2.3121	0.155	0.145	0.0315	0.0294	0.0014	0.0042	-0.0574	-0.0002
-3.06	2.62	125750	30.98	2.2934	0.378	0.144	0.0773	0.0295	0.0020	0.0041	-0.0633	-0.0002
-1.94	4.25	125760	30.98	2.2940	0.621	0.146	0.1270	0.0299	0.0037	0.0041	-0.0696	-0.0004
-0.82	5.62	125980	31.03	2.3017	0.862	0.153	0.1756	0.0313	0.0048	0.0042	-0.0747	-0.0004
0.30	6.55	125990	31.04	2.3024	1.114	0.170	0.2270	0.0346	0.0068	0.0042	-0.0793	-0.0008
1.42	7.10	126570	31.18	2.3234	1.371	0.193	0.2769	0.0390	0.0086	0.0034	-0.0816	-0.0011
2.53	7.28	127220	31.34	2.3474	1.599	0.220	0.3196	0.0439	0.0108	0.0034	-0.0849	-0.0015
3.64	7.15	126960	31.28	2.3379	1.809	0.253	0.3629	0.0508	0.0106	0.0034	-0.0883	-0.0015
4.76	6.88	126620	31.19	2.3255	2.052	0.298	0.4139	0.0601	0.0128	0.0031	-0.0948	-0.0021
5.80	6.35	126210	31.09	2.3102	2.302	0.363	0.4675	0.0736	0.0164	0.0032	-0.0998	-0.0026
6.90	5.78	126320	31.12	2.3142	2.489	0.431	0.5045	0.0873	0.0173	0.0023	-0.1041	-0.0030
7.98	5.17	126330	31.12	2.3146	2.609	0.504	0.5287	0.1022	0.0190	0.0010	-0.1093	-0.0029
9.02	4.60	126190	31.09	2.3095	2.615	0.569	0.5312	0.1155	0.0181	-0.0010	-0.1153	-0.0023
10.07	4.18	125940	31.03	2.3006	2.616	0.625	0.5334	0.1275	0.0174	-0.0020	-0.1189	-0.0013
11.12	3.88	125530	30.92	2.2854	2.626	0.676	0.5390	0.1388	0.0163	-0.0019	-0.1196	-0.0007
12.17	3.64	125370	30.88	2.2798	2.634	0.724	0.5420	0.1489	0.0159	-0.0028	-0.1182	-0.0002
13.12	3.43	125610	30.94	2.2884	2.618	0.763	0.5367	0.1565	0.0164	-0.0026	-0.1129	0.0000
14.14	3.22	125720	30.97	2.2923	2.561	0.795	0.5239	0.1628	0.0157	-0.0019	-0.1049	0.0001
15.17	3.01	125400	30.89	2.2808	2.481	0.825	0.5102	0.1696	0.0152	-0.0019	-0.0967	0.0010

Table 25: Ailerons 20° Down at 40 mph: Alpha Sweep

Ailerons 20° Down at 40 mph: Alpha Sweep - 14 Nov. 2006, T_{room} = 74.6° F, P_{baro} = 28.8058 "Hg, S = 307 in^2												
α (°)	L/D	Re (-)	V (mph)	q (lbf/ft^2)	L (lbs)	D (lbs)	C_L (-)	C_D (-)	C_Y (-)	C_l (-)	C_m (-)	C_n (-)
-4.11	0.58	170650	42.04	4.2236	0.146	0.250	0.0162	0.0277	0.0027	0.0040	-0.0509	-0.0007
-3.08	2.27	170400	41.98	4.2115	0.555	0.245	0.0619	0.0273	0.0036	0.0041	-0.0562	-0.0007
-1.96	3.98	170640	42.04	4.2232	0.992	0.249	0.1102	0.0277	0.0051	0.0042	-0.0620	-0.0008
-0.84	5.56	170710	42.05	4.2267	1.441	0.259	0.1599	0.0288	0.0068	0.0042	-0.0675	-0.0011
0.27	6.60	170450	41.99	4.2137	1.885	0.286	0.2099	0.0318	0.0081	0.0045	-0.0712	-0.0014
1.40	7.26	170630	42.03	4.2226	2.359	0.325	0.2621	0.0361	0.0105	0.0038	-0.0738	-0.0017
2.52	7.65	170840	42.09	4.2333	2.833	0.370	0.3139	0.0410	0.0115	0.0027	-0.0806	-0.0018
3.64	7.63	171020	42.13	4.2420	3.310	0.434	0.3660	0.0480	0.0133	0.0030	-0.0853	-0.0020
4.75	7.29	171040	42.13	4.2429	3.684	0.505	0.4072	0.0558	0.0141	0.0030	-0.0887	-0.0022
5.86	6.77	170600	42.03	4.2211	4.053	0.599	0.4504	0.0665	0.0148	0.0028	-0.0933	-0.0023
6.87	6.15	170170	41.92	4.1998	4.379	0.712	0.4890	0.0795	0.0161	0.0022	-0.0975	-0.0025
7.96	5.49	169680	41.80	4.1757	4.619	0.841	0.5189	0.0944	0.0172	0.0011	-0.1025	-0.0026
9.02	4.87	169120	41.66	4.1484	4.702	0.966	0.5316	0.1092	0.0193	-0.0001	-0.1082	-0.0022
10.06	4.38	169540	41.77	4.1692	4.655	1.064	0.5237	0.1197	0.0151	-0.0020	-0.1113	-0.0010
11.11	4.07	169400	41.73	4.1619	4.715	1.159	0.5314	0.1306	0.0148	-0.0028	-0.1124	-0.0005
12.16	3.79	169260	41.70	4.1551	4.727	1.246	0.5336	0.1407	0.0148	-0.0029	-0.1115	0.0000
13.11	3.55	168610	41.54	4.1234	4.660	1.313	0.5301	0.1493	0.0144	-0.0028	-0.1087	0.0002

Table 26: Ailerons 20° Up at 20 mph: Alpha Sweep

Ailerons 20° Up at 20 mph: Alpha Sweep - 14 Nov. 2006, T_{room} = 74.6° F, P_{baro} = 28.8058 "Hg, S = 307 in^2												
α (°)	L/D	Re (-)	V (mph)	q (lbf/ft^2)	L (lbs)	D (lbs)	C_L (-)	C_D (-)	C_Y (-)	C_l (-)	C_m (-)	C_n (-)
-4.53	-4.43	80580	19.85	0.9418	-0.527	0.119	-0.2625	0.0593	-0.0060	0.0043	0.1077	0.0023
-3.49	-3.91	80638	19.86	0.9431	-0.419	0.107	-0.2082	0.0532	-0.0041	0.0039	0.1002	0.0020
-2.37	-3.22	80313	19.78	0.9355	-0.311	0.097	-0.1560	0.0485	-0.0025	0.0043	0.0943	0.0018
-1.24	-2.32	79929	19.69	0.9266	-0.204	0.088	-0.1034	0.0446	-0.0002	0.0046	0.0879	0.0016
-0.12	-1.11	80422	19.81	0.9381	-0.095	0.086	-0.0477	0.0430	0.0007	0.0045	0.0800	0.0016
1.02	0.23	80579	19.85	0.9418	0.020	0.088	0.0099	0.0439	0.0028	0.0046	0.0733	0.0012
2.15	1.56	80182	19.75	0.9325	0.143	0.092	0.0718	0.0461	0.0060	0.0041	0.0678	0.0008
3.28	2.53	80390	19.80	0.9373	0.249	0.099	0.1247	0.0494	0.0096	0.0033	0.0644	0.0002
4.39	3.28	80713	19.88	0.9449	0.349	0.106	0.1731	0.0527	0.0089	0.0029	0.0594	0.0005
5.42	3.67	80475	19.82	0.9393	0.441	0.120	0.2200	0.0599	0.0116	0.0032	0.0557	0.0002
6.54	3.96	80637	19.86	0.9431	0.540	0.136	0.2685	0.0678	0.0110	0.0031	0.0514	0.0001
7.65	4.03	80633	19.86	0.9430	0.632	0.157	0.3142	0.0780	0.0124	0.0029	0.0455	-0.0002
8.76	3.91	80412	19.81	0.9378	0.711	0.182	0.3555	0.0909	0.0144	0.0025	0.0393	-0.0004
9.85	3.66	80164	19.75	0.9321	0.766	0.209	0.3856	0.1054	0.0134	0.0016	0.0326	-0.0005
10.91	3.36	80178	19.75	0.9324	0.793	0.236	0.3989	0.1186	0.0166	0.0008	0.0243	-0.0003
11.97	3.16	80475	19.82	0.9393	0.823	0.261	0.4110	0.1302	0.0156	0.0001	0.0146	-0.0003
12.94	2.98	80773	19.90	0.9463	0.849	0.285	0.4206	0.1411	0.0222	0.0005	0.0052	0.0002
14.01	2.85	80071	19.73	0.9299	0.866	0.304	0.4371	0.1533	0.0183	0.0000	-0.0019	0.0004
15.07	2.74	79805	19.66	0.9237	0.882	0.322	0.4480	0.1635	0.0190	0.0005	-0.0080	0.0003

Table 27: Ailerons 20° Up at 30 mph: Alpha Sweep

Ailerons 20º Up at 30 mph: Alpha Sweep - 14 Nov. 2006, T_{room} = 74.6º F, P_{baro} = 28.8058 "Hg, S = 307 in^2												
α (º)	L/D	Re (-)	V (mph)	q (lbf/ft^2)	L (lbs)	D (lbs)	C_L (-)	C_D (-)	C_Y (-)	C_l (-)	C_m (-)	C_n (-)
-4.48	-4.38	125710	30.97	2.2921	-1.130	0.258	-0.2313	0.0528	-0.0041	0.0040	0.0993	0.0016
-3.45	-3.84	124900	30.77	2.2628	-0.890	0.232	-0.1844	0.0481	-0.0027	0.0038	0.0942	0.0016
-2.33	-3.07	125050	30.81	2.2681	-0.643	0.209	-0.1330	0.0433	-0.0011	0.0037	0.0877	0.0014
-1.21	-2.04	125540	30.93	2.2859	-0.389	0.190	-0.0798	0.0390	0.0005	0.0037	0.0787	0.0012
-0.08	-0.61	126050	31.05	2.3046	-0.111	0.182	-0.0225	0.0370	0.0022	0.0039	0.0653	0.0007
1.06	1.05	126060	31.05	2.3047	0.191	0.183	0.0390	0.0372	0.0050	0.0039	0.0519	-0.0001
2.19	2.56	126240	31.10	2.3116	0.490	0.191	0.0994	0.0389	0.0077	0.0035	0.0385	-0.0007
3.32	3.66	126380	31.13	2.3164	0.755	0.206	0.1530	0.0418	0.0084	0.0032	0.0268	-0.0009
4.44	4.42	126530	31.17	2.3220	1.001	0.226	0.2022	0.0457	0.0080	0.0029	0.0158	-0.0005
5.46	4.81	127340	31.37	2.3519	1.246	0.259	0.2486	0.0517	0.0098	0.0027	0.0053	-0.0011
6.59	4.91	126800	31.24	2.3318	1.494	0.304	0.3005	0.0612	0.0126	0.0027	-0.0050	-0.0022
7.71	4.81	125950	31.03	2.3009	1.726	0.359	0.3518	0.0732	0.0150	0.0022	-0.0150	-0.0030
8.81	4.49	126420	31.14	2.3181	1.927	0.429	0.3900	0.0868	0.0170	0.0016	-0.0238	-0.0033
9.88	4.11	126760	31.23	2.3306	2.040	0.496	0.4105	0.0998	0.0163	0.0011	-0.0291	-0.0030
10.95	3.75	126240	31.10	2.3115	2.091	0.557	0.4242	0.1130	0.0187	0.0008	-0.0329	-0.0030
12.01	3.48	125670	30.96	2.2904	2.121	0.609	0.4343	0.1248	0.0189	-0.0004	-0.0354	-0.0021
12.97	3.25	125680	30.96	2.2911	2.151	0.661	0.4404	0.1354	0.0184	-0.0007	-0.0374	-0.0016
14.02	3.07	125610	30.94	2.2884	2.158	0.702	0.4423	0.1439	0.0180	-0.0003	-0.0385	-0.0012
15.07	2.92	125480	30.91	2.2835	2.186	0.748	0.4490	0.1536	0.0173	0.0000	-0.0401	-0.0012

Table 28: Ailerons 20° Up at 40 mph: Alpha Sweep

Ailerons 20º Up at 40 mph: Alpha Sweep - 14 Nov. 2006, T_{room} = 74.6º F, P_{baro} = 28.8058 "Hg, S = 307 in^2												
α (º)	L/D	Re (-)	V (mph)	q (lbf/ft^2)	L (lbs)	D (lbs)	C_L (-)	C_D (-)	C_Y (-)	C_l (-)	C_m (-)	C_n (-)
-4.45	-4.38	169900	41.85	4.1865	-1.877	0.429	-0.2103	0.0480	-0.0021	0.0032	0.0849	0.0005
-3.41	-3.68	169950	41.87	4.1894	-1.388	0.377	-0.1554	0.0422	0.0001	0.0032	0.0713	0.0000
-2.28	-2.61	170110	41.91	4.1973	-0.883	0.338	-0.0987	0.0378	0.0017	0.0033	0.0571	-0.0003
-1.15	-1.23	169670	41.80	4.1755	-0.378	0.307	-0.0425	0.0345	0.0039	0.0037	0.0442	-0.0007
-0.02	0.48	170140	41.91	4.1985	0.144	0.299	0.0161	0.0334	0.0058	0.0040	0.0311	-0.0010
1.12	2.33	170240	41.94	4.2037	0.708	0.304	0.0790	0.0340	0.0077	0.0035	0.0178	-0.0015
2.25	3.73	170270	41.94	4.2048	1.202	0.322	0.1341	0.0359	0.0094	0.0030	0.0063	-0.0018
3.36	4.70	170500	42.00	4.2162	1.642	0.349	0.1827	0.0389	0.0096	0.0026	-0.0038	-0.0020
4.48	5.32	170460	41.99	4.2144	2.088	0.392	0.2324	0.0437	0.0105	0.0026	-0.0140	-0.0021
5.51	5.58	170790	42.07	4.2307	2.530	0.453	0.2805	0.0502	0.0113	0.0025	-0.0239	-0.0023
6.63	5.49	170820	42.08	4.2323	2.965	0.540	0.3286	0.0599	0.0127	0.0026	-0.0335	-0.0025
7.74	5.19	170510	42.00	4.2166	3.373	0.649	0.3752	0.0722	0.0139	0.0022	-0.0427	-0.0027
8.84	4.76	170320	41.96	4.2072	3.708	0.779	0.4134	0.0869	0.0160	0.0016	-0.0502	-0.0031
9.93	4.31	169960	41.87	4.1898	3.916	0.909	0.4384	0.1018	0.0178	0.0010	-0.0549	-0.0038
10.99	3.91	169910	41.86	4.1870	4.019	1.028	0.4503	0.1151	0.0200	0.0002	-0.0578	-0.0042
12.03	3.60	169930	41.86	4.1880	4.046	1.123	0.4531	0.1257	0.0198	-0.0010	-0.0589	-0.0032
13.00	3.39	169680	41.80	4.1757	4.089	1.206	0.4594	0.1355	0.0211	-0.0011	-0.0604	-0.0030

Table 29: 1" Cut in Flow Guides at 20 mph: Alpha Sweep

1" Cut in Flow Guides at 20 mph: Alpha Sweep - 1 Feb. 2007, T_{room} = 71.7° F, P_{baro} = 28.8197 "Hg, S = 307 in^2												
α (°)	L/D	Re (-)	V (mph)	q (lbf/ft^2)	L (lbs)	D (lbs)	C_L (-)	C_D (-)	C_Y (-)	C_l (-)	C_m (-)	C_n (-)
-4.37	-2.98	81979	20.08	0.9690	-0.201	0.067	-0.0972	0.0326	-0.0005	0.0051	0.0148	0.0005
-3.25	-1.56	79682	19.51	0.9154	-0.093	0.060	-0.0478	0.0306	0.0009	0.0046	0.0081	0.0005
-2.12	0.21	81659	20.00	0.9614	0.012	0.056	0.0058	0.0275	0.0013	0.0031	0.0002	0.0004
-1.01	1.89	82165	20.12	0.9734	0.104	0.055	0.0500	0.0265	0.0022	0.0038	-0.0062	0.0003
0.13	3.64	77814	19.06	0.8730	0.209	0.057	0.1124	0.0308	0.0021	0.0041	-0.0143	0.0004
1.26	5.23	77976	19.10	0.8767	0.325	0.062	0.1738	0.0332	0.0031	0.0034	-0.0209	0.0003
2.39	6.32	79393	19.44	0.9088	0.446	0.071	0.2301	0.0364	0.0040	0.0038	-0.0255	0.0003
3.51	6.77	80286	19.66	0.9294	0.549	0.081	0.2772	0.0410	0.0056	0.0035	-0.0296	-0.0003
4.56	6.67	79593	19.49	0.9134	0.657	0.099	0.3376	0.0506	0.0072	0.0033	-0.0403	-0.0003
5.70	6.48	77998	19.10	0.8772	0.758	0.117	0.4052	0.0625	0.0077	0.0026	-0.0497	-0.0005
6.82	6.10	78137	19.14	0.8803	0.853	0.140	0.4547	0.0746	0.0081	0.0024	-0.0563	-0.0006
7.84	5.59	82865	20.29	0.9901	0.929	0.166	0.4399	0.0787	0.0082	0.0009	-0.0555	-0.0007
8.92	5.01	82836	20.29	0.9894	0.975	0.195	0.4622	0.0922	0.0108	-0.0005	-0.0614	-0.0007
9.99	4.43	78001	19.10	0.8772	1.002	0.226	0.5356	0.1209	0.0130	-0.0022	-0.0776	-0.0001
11.01	4.05	79540	19.48	0.9122	1.016	0.251	0.5223	0.1290	0.0107	-0.0031	-0.0797	0.0002
12.01	3.75	82607	20.23	0.9839	1.034	0.276	0.4928	0.1315	0.0089	-0.0026	-0.0779	0.0006
13.11	3.49	79918	19.57	0.9209	1.042	0.298	0.5308	0.1519	0.0119	-0.0021	-0.0847	0.0007
14.16	3.30	79939	19.58	0.9214	1.056	0.320	0.5376	0.1629	0.0100	-0.0027	-0.0830	0.0012
15.21	3.10	79336	19.43	0.9075	1.048	0.338	0.5418	0.1746	0.0134	-0.0021	-0.0807	0.0010

Table 30: 1" Cut in Flow Guides at 30 mph: Alpha Sweep

1" Cut in Flow Guides at 30 mph: Alpha Sweep - 1 Feb. 2007, T_{room} = 71.7° F, P_{baro} = 28.8197 "Hg, S = 307 in^2												
α (°)	L/D	Re (-)	V (mph)	q (lbf/ft^2)	L (lbs)	D (lbs)	C_L (-)	C_D (-)	C_Y (-)	C_l (-)	C_m (-)	C_n (-)
-4.36	-3.08	125400	30.71	2.2673	-0.438	0.142	-0.0905	0.0294	-0.0007	0.0011	0.0116	0.0003
-3.23	-1.56	128700	31.52	2.3881	-0.199	0.127	-0.0390	0.0249	0.0006	0.0013	0.0047	0.0002
-2.12	0.40	129620	31.74	2.4224	0.047	0.120	0.0092	0.0232	0.0017	0.0010	-0.0020	0.0002
-1.00	2.54	127260	31.17	2.3352	0.297	0.117	0.0596	0.0235	0.0028	0.0013	-0.0081	0.0002
0.13	4.69	128670	31.51	2.3871	0.580	0.124	0.1141	0.0243	0.0038	0.0021	-0.0163	0.0001
1.26	6.25	127850	31.31	2.3568	0.852	0.136	0.1696	0.0271	0.0046	0.0028	-0.0233	-0.0001
2.37	7.01	127210	31.15	2.3334	1.086	0.155	0.2184	0.0312	0.0056	0.0021	-0.0273	0.0000
3.47	7.46	130640	31.99	2.4606	1.338	0.179	0.2550	0.0342	0.0059	0.0015	-0.0336	-0.0002
4.48	7.38	133470	32.69	2.5686	1.569	0.212	0.2865	0.0388	0.0061	0.0018	-0.0378	-0.0003
5.60	7.04	131570	32.22	2.4961	1.793	0.255	0.3369	0.0478	0.0068	0.0012	-0.0439	-0.0003
6.72	6.43	129330	31.67	2.4117	1.996	0.310	0.3881	0.0604	0.0081	0.0010	-0.0491	-0.0006
7.80	5.75	130920	32.06	2.4713	2.169	0.377	0.4116	0.0715	0.0086	0.0005	-0.0530	-0.0008
8.89	5.07	129280	31.66	2.4099	2.282	0.450	0.4442	0.0876	0.0114	-0.0006	-0.0609	-0.0009
9.87	4.51	128180	31.39	2.3691	2.325	0.516	0.4603	0.1022	0.0122	-0.0017	-0.0686	-0.0005
10.92	4.12	128710	31.52	2.3884	2.360	0.573	0.4635	0.1126	0.0126	-0.0022	-0.0729	0.0000
11.96	3.86	130750	32.02	2.4651	2.425	0.628	0.4615	0.1195	0.0104	-0.0035	-0.0728	0.0008
13.05	3.59	126770	31.05	2.3172	2.440	0.679	0.4940	0.1374	0.0123	-0.0029	-0.0784	0.0008
14.09	3.37	127520	31.23	2.3445	2.437	0.723	0.4876	0.1446	0.0130	-0.0018	-0.0760	0.0006
15.10	3.18	130070	31.85	2.4393	2.419	0.760	0.4651	0.1462	0.0123	-0.0014	-0.0694	0.0005

Table 31: 2" Cut in Flow Guides at 20 mph: Alpha Sweep

2" Cut in Flow Guides at 20 mph: Alpha Sweep - 1 Feb. 2007, T_{room} = 72.1° F, P_{baro} = 28.8188 "Hg, S = 307 in^2												
α (°)	L/D	Re (-)	V (mph)	q (lbf/ft^2)	L (lbs)	D (lbs)	C_L (-)	C_D (-)	C_Y (-)	C_l (-)	C_m (-)	C_n (-)
-4.37	-3.11	80938	19.84	0.9453	-0.201	0.065	-0.0999	0.0321	-0.0019	0.0053	0.0144	0.0009
-3.25	-1.63	79686	19.53	0.9163	-0.094	0.058	-0.0483	0.0297	0.0000	0.0060	0.0074	0.0008
-2.12	0.21	79100	19.39	0.9028	0.011	0.054	0.0059	0.0283	0.0009	0.0054	-0.0007	0.0008
-0.99	2.30	79038	19.37	0.9014	0.122	0.053	0.0633	0.0276	0.0027	0.0037	-0.0087	0.0005
0.12	3.95	81928	20.08	0.9685	0.218	0.055	0.1056	0.0267	0.0030	0.0032	-0.0142	0.0004
1.23	5.46	83475	20.46	1.0055	0.331	0.061	0.1546	0.0283	0.0031	0.0033	-0.0198	0.0003
2.38	6.51	81135	19.88	0.9499	0.449	0.069	0.2216	0.0341	0.0054	0.0036	-0.0257	0.0000
3.52	6.91	79583	19.50	0.9139	0.559	0.081	0.2869	0.0415	0.0097	0.0036	-0.0352	-0.0009
4.56	6.78	79314	19.44	0.9077	0.665	0.098	0.3439	0.0507	0.0108	0.0030	-0.0465	-0.0009
5.67	6.56	80845	19.81	0.9431	0.766	0.117	0.3808	0.0581	0.0115	0.0027	-0.0527	-0.0011
6.76	6.11	81510	19.98	0.9587	0.853	0.139	0.4173	0.0682	0.0129	0.0028	-0.0568	-0.0013
7.88	5.57	80542	19.74	0.9361	0.931	0.167	0.4663	0.0837	0.0139	0.0024	-0.0643	-0.0016
8.98	4.99	79542	19.49	0.9130	0.982	0.197	0.5045	0.1011	0.0157	0.0008	-0.0735	-0.0015
9.96	4.44	79611	19.51	0.9145	1.009	0.228	0.5177	0.1167	0.0163	-0.0016	-0.0817	-0.0007
11.01	4.07	80005	19.61	0.9236	1.032	0.253	0.5243	0.1287	0.0162	-0.0020	-0.0855	-0.0002
12.09	3.77	79242	19.42	0.9061	1.055	0.280	0.5459	0.1450	0.0168	-0.0014	-0.0915	0.0001
13.10	3.54	81279	19.92	0.9533	1.067	0.302	0.5248	0.1485	0.0161	-0.0016	-0.0890	0.0002
14.13	3.35	82201	20.15	0.9750	1.075	0.321	0.5172	0.1544	0.0161	-0.0017	-0.0843	0.0008
15.11	3.15	81014	19.86	0.9471	1.073	0.341	0.5315	0.1688	0.0157	-0.0020	-0.0825	0.0008

Table 32: 2" Cut in Flow Guides at 30 mph: Alpha Sweep

2" Cut in Flow Guides at 30 mph: Alpha Sweep - 1 Feb. 2007, T_{room} = 72.1° F, P_{baro} = 28.8188 "Hg, S = 307 in^2												
α (°)	L/D	Re (-)	V (mph)	q (lbf/ft^2)	L (lbs)	D (lbs)	C_L (-)	C_D (-)	C_Y (-)	C_l (-)	C_m (-)	C_n (-)
-4.34	-3.06	128410	31.47	2.3791	-0.415	0.136	-0.0819	0.0268	-0.0019	0.0013	0.0104	0.0007
-3.23	-1.48	126990	31.12	2.3271	-0.179	0.122	-0.0361	0.0245	-0.0005	0.0013	0.0034	0.0006
-2.11	0.58	126530	31.01	2.3102	0.066	0.114	0.0133	0.0232	0.0013	0.0015	-0.0032	0.0005
-0.99	2.88	126630	31.03	2.3138	0.320	0.111	0.0649	0.0225	0.0030	0.0019	-0.0114	0.0003
0.13	4.83	128080	31.39	2.3673	0.572	0.119	0.1134	0.0235	0.0039	0.0026	-0.0177	0.0001
1.26	6.58	129060	31.63	2.4036	0.862	0.131	0.1682	0.0256	0.0048	0.0027	-0.0249	-0.0001
2.36	7.42	130500	31.98	2.4575	1.110	0.150	0.2119	0.0286	0.0067	0.0018	-0.0294	-0.0002
3.40	7.67	129240	31.67	2.4100	1.360	0.177	0.2646	0.0345	0.0083	0.0017	-0.0379	-0.0006
4.54	7.57	125910	30.86	2.2876	1.598	0.211	0.3276	0.0433	0.0100	0.0016	-0.0475	-0.0007
5.65	7.14	126560	31.02	2.3111	1.816	0.254	0.3686	0.0516	0.0112	0.0015	-0.0518	-0.0009
6.74	6.50	127220	31.18	2.3354	2.013	0.310	0.4044	0.0622	0.0124	0.0014	-0.0557	-0.0012
7.83	5.81	128430	31.48	2.3802	2.182	0.375	0.4300	0.0740	0.0138	0.0009	-0.0602	-0.0014
8.90	5.12	128350	31.46	2.3773	2.295	0.448	0.4529	0.0884	0.0148	0.0001	-0.0673	-0.0013
9.87	4.56	128650	31.53	2.3881	2.343	0.514	0.4603	0.1010	0.0149	-0.0009	-0.0738	-0.0009
10.93	4.17	128930	31.60	2.3987	2.392	0.573	0.4678	0.1121	0.0140	-0.0013	-0.0781	-0.0005
12.01	3.89	127230	31.18	2.3359	2.469	0.634	0.4958	0.1273	0.0151	-0.0024	-0.0830	0.0002
13.05	3.64	128320	31.45	2.3758	2.497	0.686	0.4930	0.1353	0.0151	-0.0022	-0.0828	0.0005
14.13	3.42	125300	30.71	2.2653	2.503	0.732	0.5183	0.1517	0.0154	-0.0016	-0.0846	0.0005
15.07	3.22	126150	30.92	2.2963	2.469	0.767	0.5043	0.1568	0.0160	-0.0008	-0.0787	0.0001

Table 33: No Flow Guides at 20 mph: Alpha Sweep

No Flow Guides at 20 mph: Alpha Sweep - 1 Feb. 2007, T_{room} = 72.4° F, P_{baro} = 28.8110 "Hg, S = 254 in^2												
α (°)	L/D	Re (-)	V (mph)	q (lbf/ft^2)	L (lbs)	D (lbs)	C_L (-)	C_D (-)	C_Y (-)	C_l (-)	C_m (-)	C_n (-)
-4.35	-2.87	79423	19.48	0.9110	-0.164	0.057	-0.1018	0.0354	-0.0015	0.0037	0.0130	0.0010
-3.24	-1.61	77999	19.13	0.8786	-0.083	0.052	-0.0538	0.0333	-0.0006	0.0041	0.0063	0.0009
-2.12	0.33	79468	19.49	0.9120	0.016	0.049	0.0099	0.0303	0.0019	0.0038	-0.0023	0.0008
-1.01	2.05	79131	19.41	0.9043	0.097	0.047	0.0607	0.0297	0.0032	0.0049	-0.0083	0.0005
0.11	3.87	79155	19.42	0.9048	0.191	0.049	0.1199	0.0310	0.0035	0.0045	-0.0149	0.0005
1.22	5.30	80348	19.71	0.9323	0.285	0.054	0.1732	0.0327	0.0029	0.0036	-0.0217	0.0005
2.35	6.28	79221	19.43	0.9063	0.385	0.061	0.2409	0.0384	0.0051	0.0037	-0.0287	0.0002
3.40	6.53	77070	18.90	0.8578	0.485	0.074	0.3203	0.0490	0.0106	0.0031	-0.0418	-0.0012
4.53	6.66	77010	18.89	0.8565	0.586	0.088	0.3882	0.0583	0.0126	0.0024	-0.0561	-0.0013
5.64	6.48	78144	19.17	0.8819	0.682	0.105	0.4386	0.0677	0.0141	0.0024	-0.0649	-0.0015
6.74	6.05	78490	19.25	0.8897	0.762	0.126	0.4855	0.0803	0.0148	0.0023	-0.0714	-0.0016
7.79	5.53	80970	19.86	0.9468	0.826	0.149	0.4947	0.0894	0.0154	0.0016	-0.0743	-0.0017
8.86	5.01	82234	20.17	0.9766	0.887	0.177	0.5147	0.1028	0.0174	0.0000	-0.0815	-0.0017
9.83	4.46	83041	20.37	0.9959	0.913	0.205	0.5200	0.1165	0.0194	-0.0016	-0.0907	-0.0009
10.93	4.08	80682	19.79	0.9401	0.944	0.232	0.5696	0.1398	0.0205	-0.0022	-0.1040	-0.0007
12.02	3.77	78459	19.25	0.8890	0.952	0.253	0.6074	0.1612	0.0226	-0.0034	-0.1137	-0.0004
13.08	3.53	78588	19.28	0.8919	0.966	0.273	0.6141	0.1737	0.0228	-0.0030	-0.1152	-0.0007
14.16	3.34	76238	18.70	0.8394	0.953	0.286	0.6435	0.1929	0.0232	-0.0033	-0.1180	-0.0003
15.12	3.16	76297	18.71	0.8407	0.960	0.304	0.6473	0.2050	0.0219	-0.0026	-0.1120	-0.0001

Table 34: No Flow Guides at 30 mph: Alpha Sweep

No Flow Guides at 30 mph: Alpha Sweep - 1 Feb. 2007, T_{room} = 72.4° F, P_{baro} = 28.8110 "Hg, S = 254 in^2												
α (°)	L/D	Re (-)	V (mph)	q (lbf/ft^2)	L (lbs)	D (lbs)	C_L (-)	C_D (-)	C_Y (-)	C_l (-)	C_m (-)	C_n (-)
-4.32	-2.69	124860	30.63	2.2516	-0.321	0.119	-0.0807	0.0300	-0.0018	0.0004	0.0091	0.0007
-3.22	-1.22	125640	30.82	2.2797	-0.131	0.107	-0.0326	0.0267	-0.0003	0.0004	0.0016	0.0005
-2.11	0.64	128480	31.51	2.3839	0.065	0.101	0.0153	0.0241	0.0014	0.0004	-0.0042	0.0004
-1.00	2.88	125990	30.90	2.2924	0.285	0.099	0.0706	0.0245	0.0033	0.0012	-0.0130	0.0001
0.11	4.75	125030	30.67	2.2575	0.503	0.106	0.1263	0.0266	0.0043	0.0023	-0.0206	0.0000
1.22	6.34	127450	31.26	2.3458	0.739	0.116	0.1786	0.0281	0.0047	0.0019	-0.0266	0.0000
2.33	7.20	127360	31.24	2.3425	0.961	0.133	0.2325	0.0323	0.0080	0.0017	-0.0332	-0.0003
3.37	7.43	125750	30.85	2.2838	1.185	0.160	0.2942	0.0396	0.0104	0.0019	-0.0443	-0.0011
4.47	7.37	127680	31.32	2.3544	1.397	0.190	0.3365	0.0457	0.0113	0.0016	-0.0518	-0.0011
5.57	7.02	127970	31.39	2.3650	1.595	0.227	0.3823	0.0544	0.0127	0.0014	-0.0578	-0.0014
6.66	6.45	129210	31.69	2.4110	1.779	0.276	0.4182	0.0649	0.0141	0.0013	-0.0628	-0.0018
7.74	5.83	129910	31.87	2.4373	1.944	0.333	0.4521	0.0775	0.0160	0.0008	-0.0692	-0.0020
8.83	5.17	129390	31.74	2.4178	2.065	0.399	0.4843	0.0936	0.0184	0.0000	-0.0784	-0.0022
9.79	4.59	130380	31.98	2.4551	2.126	0.463	0.4909	0.1070	0.0187	-0.0018	-0.0872	-0.0013
10.87	4.17	127940	31.38	2.3638	2.182	0.523	0.5233	0.1254	0.0193	-0.0019	-0.0967	-0.0011
11.94	3.90	127340	31.23	2.3418	2.234	0.573	0.5409	0.1387	0.0201	-0.0032	-0.1001	-0.0005
12.99	3.66	127830	31.36	2.3600	2.258	0.617	0.5424	0.1482	0.0203	-0.0041	-0.1000	0.0001
14.03	3.44	126930	31.13	2.3267	2.239	0.650	0.5455	0.1584	0.0195	-0.0035	-0.0986	0.0003
14.99	3.25	126370	31.00	2.3061	2.209	0.681	0.5430	0.1673	0.0173	-0.0025	-0.0943	0.0009

Appendix D: Additional Hot-Wire Analysis Plots

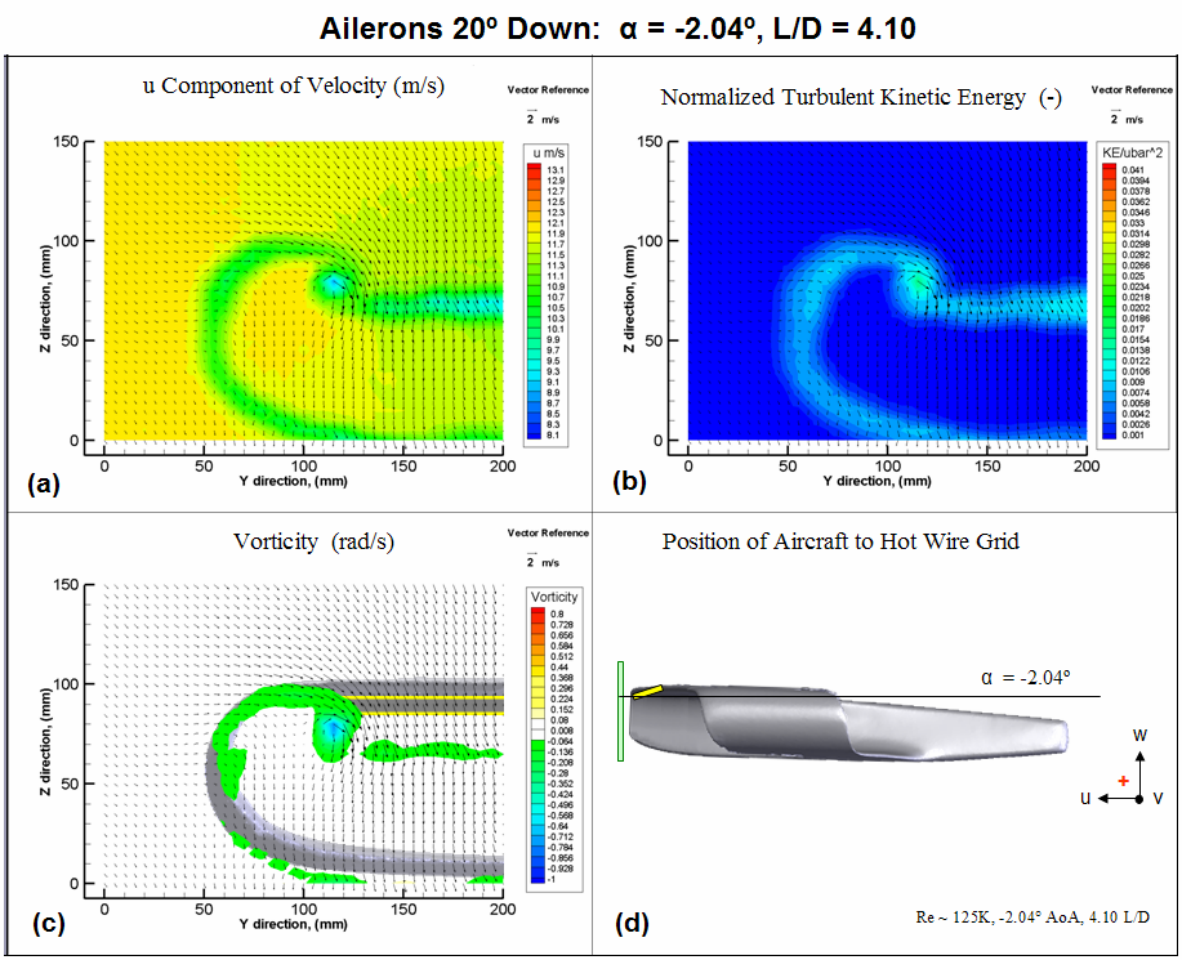

Figure 66: Hot-Wire Analysis of 24" Houck Configuration, δ = 20º down, α = -2.04º, L/D = 4.10

(a) *u*-component contours with *v* & *w* Vectors, (b) Non-dimensional turbulence contours with *v* & *w* vectors,
(c) Vorticity behind wing with *v* & *w* vectors, (d) Position of hot-wire grid with respect to the 24" Houck Configuration

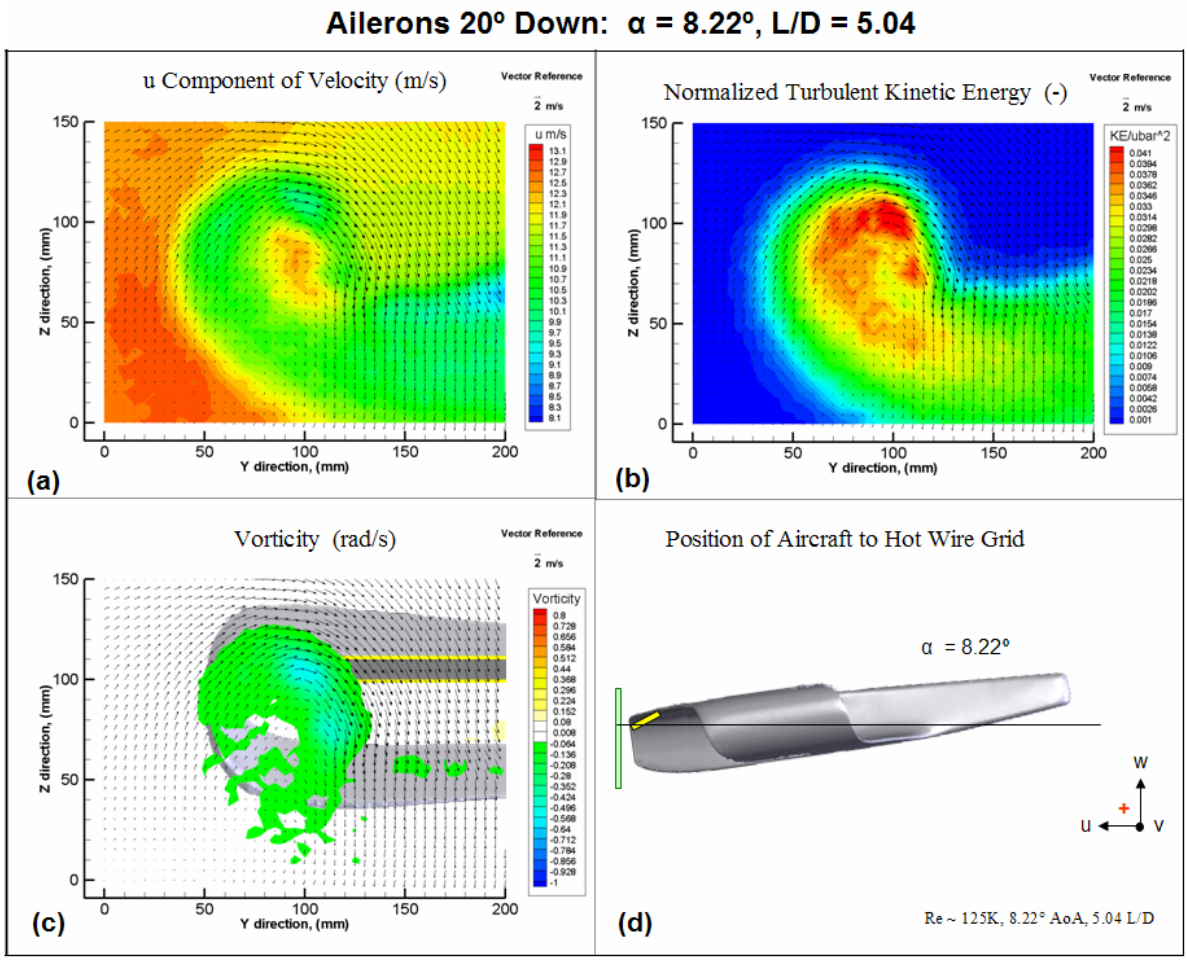

Figure 67: Hot-Wire Analysis of 24" Houck Configuration, δ = 20º down, α = 8.22º, L/D = 5.04

(a) *u*-component contours with *v* & *w* Vectors, (b) Non-dimensional turbulence contours with *v* & *w* vectors,
(c) Vorticity behind wing with *v* & *w* vectors, (d) Position of hot-wire grid with respect to the 24" Houck Configuration

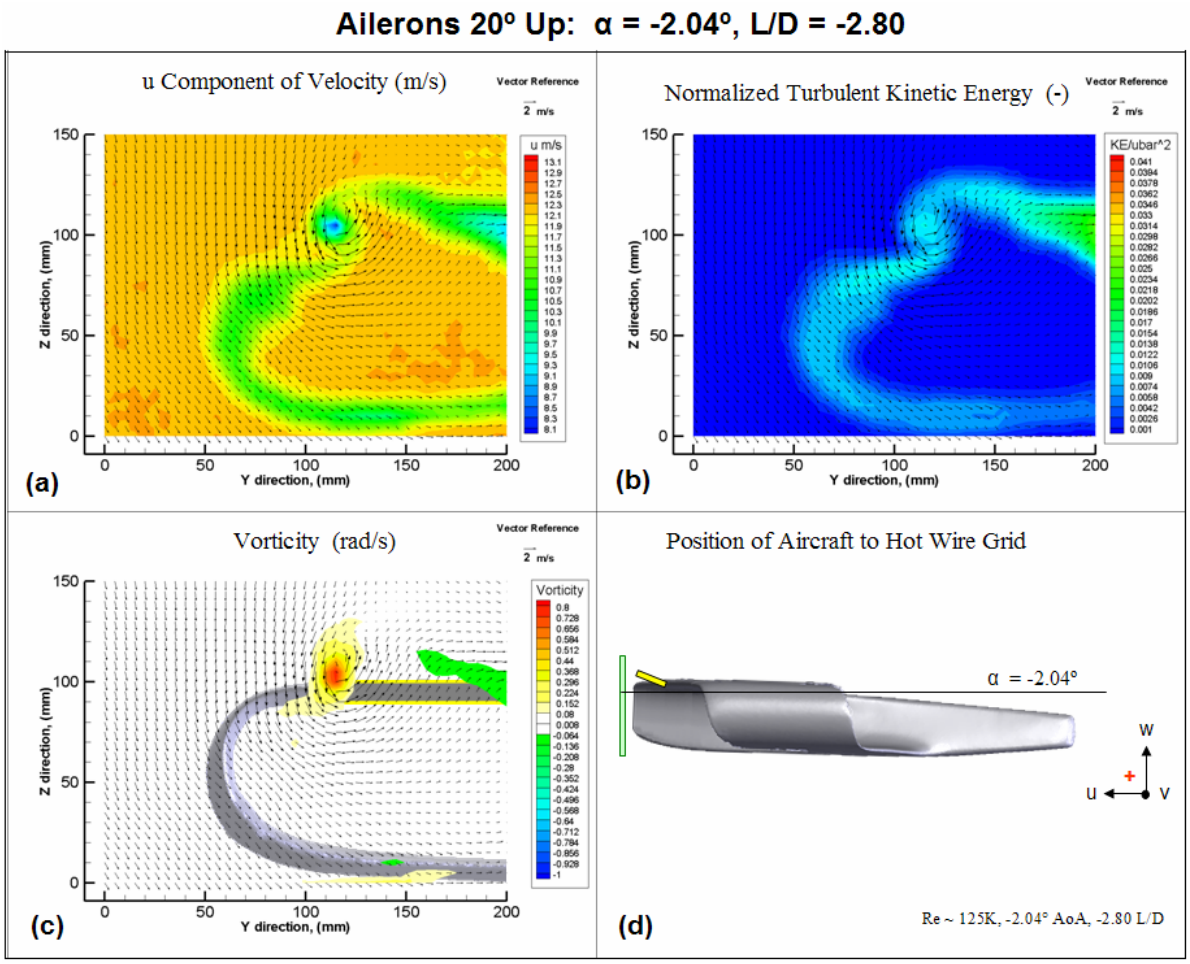

Figure 68: Hot-Wire Analysis of 24" Houck Configuration, δ = 20º up, α = -2.04º, L/D = -2.80

(a) *u*-component contours with *v* & *w* Vectors, (b) Non-dimensional turbulence contours with *v* & *w* vectors,
(c) Vorticity behind wing with *v* & *w* vectors, (d) Position of hot-wire grid with respect to the 24" Houck Configuration

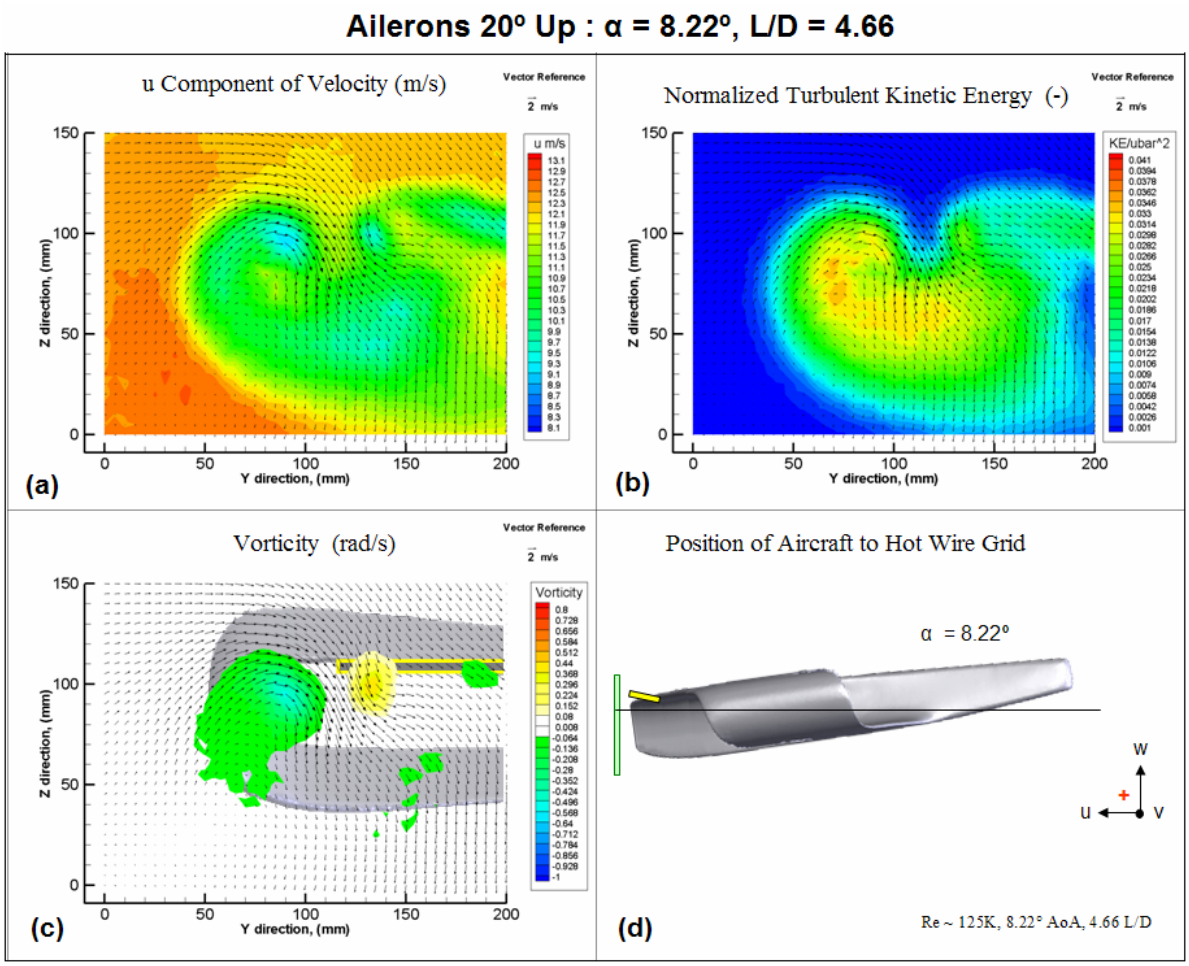

Figure 69: Hot-Wire Analysis of 24" Houck Configuration, δ = 20º up, α = 8.22°, L/D = 4.66

(a) *u*-component contours with *v* & *w* Vectors, (b) Non-dimensional turbulence contours with *v* & *w* vectors,
(c) Vorticity behind wing with *v* & *w* vectors, (d) Position of hot-wire grid with respect to the 24" Houck Configuration

Bibliography

1. Ahmed, N. A., and Archer, R. D. "Performance Improvements of a Biplane with Endplates." *Journal of Aircraft*, Vol. 38, No. 2, 2001. pp. 398-400.

2. Anderson, J. D. *Fundamentals of Aerodynamics, 2nd ed*. New York: McGraw-Hill, 1991. pp. 1-772.

3. Barlow, J. B., Rae, W. H., and Pope, A. *Low-Speed Wind Tunnel Testing, 3rd ed*. New York: John Wiley & Sons, 1999. pp. 1-713.

4. Bryant, E. M. "Unique Stealth UAV Houck Aircraft Design Program." Collaborative Project Order FA8650-05-3-9017. 6 November, 2006.

5. Cary, M. D. *A Parametric Analysis of Winglet Effects*. MS thesis, Air Force Institute of Technology (AU), Wright-Patterson AFB OH, December 1976. pp. 1-102.

6. Chattot, J. J. "Analysis and Design of Wings and Wing/Winglet Combinations at Low Speeds." AIAA 42nd Aerospace Sciences Meeting, 5-8 January 2004. AIAA Paper 2004-220.

7. Corneille, J., and Franke, M. E. "Wind Tunnel Tests of a Joined-Wing Missile Model." AIAA 38th Aerospace Sciences Meeting, 10-13 January, 2000. pp. 1-8.

8. DeLuca, A. M. *Experimental Investigation into the Aerodynamic Performance of both Rigid and Flexible Wing Structured Micro-Air-Vehicles*. Thesis, Air Force Institute of Technology, WPAFB OH, March 2004.

9. Filippone, A. "Lift-to-Drag Ratios." *Advanced Topics in Aerodynamics*. n. pag. http://www.aerodyn.org/HighLift/ld-tables.html. September 2006.

10. Filippone, A. "Wing Tip Devices." *Advanced Topics in Aerodynamics*. n. pag. http://www.aerodyn.org/Frames/1tunnel.html. September 2006.

11. Gall, P. D., and Smith, H. C. "Study of Winglets Applied to Biplanes," AIAA 23rd Aerospace Sciences Meeting, 14-17 January 1985. AIAA Paper 85-0279. pp. 1-6.

12. Houck, R. G. II. Lifting Foil. Patent 774,865. September 2006.

13. Loftin, L. K. Jr. "Maximum Lift-Drag Ratio." *Quest for Performance: The Evolution of Modern Aircraft*. n. pag. http://www.hq.nasa.gov/pao/History/SP-468/ch7-6.htm. August 2004.

14. Kroo, I. M., Gallman, J. W., and Smith, S. C. "Optimization of Joined-Wing Aircraft," *Journal of Aircraft*, Vol. 30, No. 6, 1993. pp. 897-905.

15. Kuethe, A. M., and Chow, C. Y. *Foundations of Aerodynamics: Bases of Aerodynamic Design*. New York: John Wiley & Sons, 1998. pp. 1-572.

16. Lin, C. S., Ng, T. T., and Skaff, A. "An Experimental Study of Wing Tips for Wing Performance Improvement," AIAA Paper 96-2413, 1996. pp. 304-314.

17. Masak, P. "Winglet Design for Sailplanes." *Schreder Sailplane Design*. n. pag. http://www.soaridaho.com/Schreder/Technical/Winglets/Masak.htm. January 2005.

18. Mathieu, J. and Scott, J. "*An Introduction to Turbulent Flow*." New York: Cambridge University Press, 2000. pp 51.

19. Maughmer, M. D. "About Winglets." M&H Soaring. pp. 1-11. http://www.mandhsoaring.com/articles/WL-Soaring.pdf. October 2002.

20. Maughmer, M. D. "The Design of Winglets for High-Performance Sailplanes." *Journal of Aircraft*, Vol. 40, No. 6, 2003. pp. 1099-1106.

21. Maughmer, M. D., Swan, T. S., and Willits, S. M. "The Design and Testing of a Winglet Airfoil for Low-Speed Aircraft." AIAA 19th Applied Aerodynamics Conference, 11-14 June, 2001. AIAA Paper 2001-2406.

22. Mock, R. M. "The Distribution of Loads Between the Wings of a Biplane Having Decalage," NACA-TN-269, 1927. pp. 1-47.

23. Nangia, R. K., Palmer, M. E., and Doe, R. H. "Aerodynamic Design Studies of Conventional & Unconventional Wings with Winglets." 25th Applied Aerodynamics Conference, 5-8 June. 2006. AIAA Paper 2006-3460. pp. 1-18.

24. Oligney, B., and Frash, M. *Aerodynamic and Stability Evaluation of the Houck Joined Wing Aircraf*. Senior Project, United States Air Force Academy, USAFA CO, January 2007. pp. 1-29.

25. Perry, A.E. *Hot-Wire Anemometry*. New York: Oxford University Press, 1982. pp. 1-176.

26. Rivera Parga, J. R. Wind Tunnel Investigation of the Static Stability and Control Effectiveness of a Rotary Tail in a Portable UAV. Thesis, Air Force Institute of Technolgoy, WPAFB OH, December 2004.

27. Talay, T. A. "Subsonic Flow Effects." *Introduction to the Aerodynamics of Flight*. n. pag. http://history.nasa.gov/SP-367/chapt4.htm#4.1. January 2005.

28. Traub, L. W. “Theoretical and Experimental Investigation of Biplane Delta Wings.” *Journal of Aircraft*, Vol. 38, No. 3, 2001. pp. 536-546.

29. White, F. M. Viscous Fluid Flow, 3rd ed. New York: McGraw-Hill, 2006. pp. 170-180, 473-479.

30. Wolkovitch, J. “The Joined Wing: An Overview”, AIAA 23rd Aerospace Sciences Meeting, 14-17 January 1985. AIAA Paper 85-0274. pp. 161-178.

31. Yechout, T. R., Morris, S. L., and Hallgren, W. F. *An Introduction to Aircraft Flight Mechanics: Performance and Static Stability*. United States Air Force Academy Draft Text, 2001. pp. 1-273.

Vita

Michael Walker was born in Columbus, Ohio. He graduated from Mount Vernon High School, in Mt Vernon, Ohio in 1999. He went on to earn a Bachelors degree in Aeronautical Engineering from the United States Air Force Academy in Colorado Springs, Colorado from 1999 to 2003. Following graduation, he was commissioned as an Officer in the United States Air Force and was stationed at Hanscom Air Force Base, Massachusetts. In the Fall of 2005 he began attending the Air Force Institute of Technology at Wright Patterson Air Force Base, Ohio for completion of his Masters Degree in Aeronautical Engineering. After graduation in Spring 2007, he will continue working at WPAFB in the National Air and Space Intelligence Center.

REPORT DOCUMENTATION PAGE

Form Approved
OMB No. 074-0188

1. REPORT DATE *(DD-MM-YYYY)*	2. REPORT TYPE	3. DATES COVERED *(From – To)*
22-03-2007	Master's Thesis	26-06-2006 – 22-03-2007

4. TITLE AND SUBTITLE

THE AERODYNAMIC PERFORMANCE OF THE 24 INCH HOUCK CONFIGURATION

5a. CONTRACT NUMBER
JON ENY 07-249

5b. GRANT NUMBER

5c. PROGRAM ELEMENT NUMBER

6. AUTHOR(S)

Walker, Michael M., 1st Lieutenant, USAF

5d. PROJECT NUMBER

5e. TASK NUMBER

5f. WORK UNIT NUMBER

7. PERFORMING ORGANIZATION NAMES(S) AND ADDRESS(S)
Air Force Institute of Technology
Graduate School of Engineering and Management (AFIT/EN)
2950 Hobson Way, Building 640
WPAFB OH 45433-8865

8. PERFORMING ORGANIZATION REPORT NUMBER
AFIT/GAE/ENY/03-M30

9. SPONSORING/MONITORING AGENCY NAME(S) AND ADDRESS(ES)
AFRL/VAAA
Attn: Capt Elaine Bryant or Mr. Cale Zeune
Building 45, 2130 8th St
WPAFB OH 45433

10. SPONSOR/MONITOR'S ACRONYM(S)

11. SPONSOR/MONITOR'S REPORT NUMBER(S)

12. DISTRIBUTION/AVAILABILITY STATEMENT

APPROVED FOR PUBLIC RELEASE; DISTRIBUTION UNLIMITED.

13. SUPPLEMENTARY NOTES

14. ABSTRACT

Fuel efficiency of aircraft is of great importance to the military and private sector. A more efficient wing design for UAVs would lead to improvements in mission support while reducing fuel costs for the Air Force. An experimental investigation of one candidate design, the Houck Aircraft Configuration, has been conducted in the AFIT low speed wind tunnel. This aircraft shares similarities to other joined-wing aircraft, but includes curved flow-guides of varying spanwise camber connecting the upper and lower wingtips. Experimental results that the addition of flow guides on the 24" Houck Configuration results in a 2.5% reduction in L/D_{max} at $Re \approx 80K$ and a 0.3% reduction in L/D_{max} at $Re \approx 125K$. This trend shows a decrease in the performance gap as the Reynolds number increases from 80K to 125K. It is recommended that additional testing at higher Reynolds numbers be performed to determine if an increase in performance can be shown. The designed flow guides proved to be successful in combining the upper and lower wing-tip vortices into a single vortex. The flow guides alter what would be two smaller compact vortices and instead produce a slightly larger, spread out vortex which follows the curve of the flow guide. Ultimately, evidence of improvements in aerodynamic efficiency will need to be shown before other claims of the design are demonstrated to be fully successful.

15. SUBJECT TERMS

Joined wing, Biplane, Lift-to-drag, Low-speed wind tunnel, Hot-wire analysis, Flow visualization, Flow guides, Winglets, Wing-tip vortices, Aerodynamic efficiency, Effective aspect ratio, Span efficiency factor

16. SECURITY CLASSIFICATION OF:			17. LIMITATION OF ABSTRACT	18. NUMBER OF PAGES	19a. NAME OF RESPONSIBLE PERSON
a. REPORT	b. ABSTRACT	c. THIS PAGE			Dr. Mark Reeder
U	U	U	UU	152	19b. TELEPHONE NUMBER *(Include area code)* (937) 255-6565, ext 4530; (mark.reeder@afit.edu)

Standard Form 298 (Rev. 8-98)
Prescribed by ANSI Std. Z39-18